

**U.S. Coast Guard Research and Development Center**  
1082 Shennecossett Road, Groton, CT 06340-6048

---

**Report No. CG-D-05-06**

**LEEWAY OF SUBMARINE ESCAPE RAFTS AND SUBMARINE  
EMERGENCY POSITIONING BEACONS**



**FINAL REPORT  
JULY 2006**

This document is available to the U.S. public through the  
National Technical Information Service, Springfield, VA 22161

Prepared for:

U.S. Navy  
Naval Submarine Medical Research Laboratory  
Naval Submarine Base New London  
Groton, CT 06349-5900

# NOTICE

This document is disseminated under the sponsorship of the Department of Homeland Security in the interest of information exchange. The United States Government assumes no liability for its contents or use thereof.

The United States Government does not endorse products or manufacturers. Trade or manufacturers' names appear herein solely because they are considered essential to the object of this report.

This report does not constitute a standard, specification, or regulation.



Marc B. Mandler, Ph.D.  
Technical Director  
United States Coast Guard  
Research & Development Center  
1082 Shennecossett Road  
Groton, CT 06340-6048

1. Report No. CG-D-05-06		2. Government Accession Number		3. Recipient's Catalog No.	
4. Title and Subtitle  LEEWAY OF SUBMARINE ESCAPE RAFTS AND SUBMARINE EMERGENCY POSITIONING BEACONS				5. Report Date July 2006	
				6. Performing Organization Code Project No. 7500	
7. Author(s) Chris Turner <sup>[1]</sup> , Thomas Waddington <sup>[2]</sup> , John Morris <sup>[2]</sup> , Vladimir Osychny <sup>[2]</sup> , and Pamela Luey <sup>[2]</sup>				8. Performing Organization Report No. R&DC 765	
9. Performing Organization Name and Address U.S. Coast Guard <sup>[1]</sup> Research and Development Center 1082 Shennecossett Road Groton, CT 06340-6048		SAIC <sup>[2]</sup> 23 Clara Drive Suite 206 Mystic, CT 06355		10. Work Unit No. (TRAIS)	
				11. Contract or Grant No. HSCG-32-05-D-R00010	
12. Sponsoring Organization Name and Address U.S. Navy Naval Submarine Medical Research Laboratory (NSMRL) Naval Submarine Base New London Groton, CT 06349-5900				13. Type of Report & Period Covered Final	
				14. Sponsoring Agency Code NSMRL Groton, CT, 06349-5900	
15. Supplementary Notes The R&D Center's technical point of contact is Mr. Chris Turner, 860-441- 2623, email: <a href="mailto:A.Chris.Turner@uscg.mil">A.Chris.Turner@uscg.mil</a> .					
16. Abstract  The leeway behavior of Submarine Emergency Position Indicating Radio Beacons (SEPIRBs) and Mark-10 Submarine Escape and Immersion Equipment (SEIE) life rafts was measured for use in search and rescue planning. SEIE and SEPIRB drift targets were outfitted with position tracking equipment, and one raft was also equipped with a current profiler. The targets were deployed and tracked along with Self-Locating Datum Marker Buoys (SLDMBs) under generally heavy wind and sea conditions during fall 2005 on the Atlantic Ocean off St. John's, Newfoundland, Canada. The duration of each test ranged from 24 hours to approximately 60 hours. Maximum wind speeds (5-minute averages) ranged from just under 20 knots to nearly 40 knots, with gust speeds to 43 knots.  SEIE and SEPIRB leeway speeds were determined either directly from the current profiler data or indirectly using the SLDMB data. Leeway coefficients for SAR planning use were calculated using the concurrent wind data. The leeway speed of the undrogued raft was greater than that of the drogued raft. The data indicate that SEPIRB leeway is zero. The study recommends that these coefficients be incorporated into submarine survivor search planning guidance. Problems with raft performance were encountered that were attributed to the installed instrument package, instrument mounting materials incompatibility and the absence of a human passenger in the high wind and wave environment. Issues with SEPIRB operation and performance are also noted.					
17. Key Words Submarine rescue, Leeway, SEIE raft, SEPIRB, SLDMB, ADCP, Optimal interpolation, SAR			18. Distribution Statement This document is available to the U.S. public through the National Technical Information Service, Springfield, VA 22161.		
19. Security Class (This Report) UNCLASSIFIED		20. Security Class (This Page) UNCLASSIFIED		21. No of Pages	
				22. Price	

Form DOT F 1700.7 (8/72) Reproduction of form and completed page is authorized.

## ACKNOWLEDGEMENTS

We would like to thank the Canadian Coast Guard, Newfoundland Region, for not only the use of the CCGS *Ann Harvey* for the field testing, but also their assistance in many other areas. We would like to specifically thank Brian Stone, Peter Fontaine, Grant Ivey, and Steve Sheppard. We would also like to thank Oceans, Ltd. of St. John's, Newfoundland for their assistance during the field program, as well as their willingness to openly share their extensive leeway knowledge and useful local resources. In particular, we would like to thank Reg Fitzgerald, Duncan Finlayson, and Andrew Cook. Finally, we would like to thank the officers and crew of the CCGS *Ann Harvey* for providing both an exceptional work platform and comfortable accommodations while at sea.

Mr. Gary Reas and Tim Norton of Anteon Corporation who maintain the equipment inventory at the Research and Development Center were very helpful in locating and configuring equipment for the study. We are also grateful to Mr. Art Allen of G-RPR, who provided guidance on the development of a leeway analysis approach, along with MATLAB routines.

## EXECUTIVE SUMMARY

Leeway, defined as the movement of the search object through water caused by the action of wind on the exposed surfaces of the object, is fundamental to search planning. Over the past several years, the U.S. Coast Guard (CG) Research and Development Center (R&DC) and the Canadian Coast Guard (CCG) have participated in leeway studies of various drift targets such as life rafts, evacuation vessels, sailboats, and other targets of interest. The leeway coefficients computed for each drift target generated from these leeway studies are used in Search and Rescue (SAR) planning software to define potential search areas during SAR operations.

Between late-October through mid-November 2005, the R&DC conducted tests of two drift objects for the U.S. Navy, the Mark-10 Submarine Escape and Immersion Equipment (SEIE) life raft, and the Submarine Emergency Position Indicating Radio Beacon (SEPIRB). The SEIE is a one-person survival raft incorporating a weather-tight hood that is used following evacuation from a sunken submarine. The SEPIRB is an emergency signaling device that can be activated to broadcast the location of a submarine in distress. Instrumented SEIE training rafts and SEPIRBs were deployed by the R&DC and tracked as they drifted on the open ocean off of St. John's, Newfoundland, Canada under various wind and sea conditions. These drift targets contained equipment on board to track their movements including satellite transmitters that would periodically broadcast recent positions of the drift targets. Meteorological data, including wind speed and direction were collected by a monitoring buoy moored in the study area. To provide a direct measure of leeway motion, one of the deployed rafts was equipped with an acoustic Doppler current profiler (ADCP). The motion of the drift target relative to local surface currents (i.e. leeway) was measured directly by the profiler. In other cases, indirect estimates of the near-surface currents at the drift targets were provided by self-locating datum marker buoys (SLDMBs) in the vicinity of the drift targets during each deployment. The drift target leeway motion was then derived as the difference between the target's movement over the ground and the estimated local sea surface current calculated from the motions of adjacent SLDMBs. This array of instrumentation provided all of the data required to evaluate the relationship between wind speed and direction and the leeway motion of both the SEIE rafts and the SEPIRBs.

Following an initial preliminary drift run to check the performance of the targets and equipment on 29 and 30 October, five drift tests (drifts one through five) were conducted from 31 October until 19 November. The duration of each test ranged from 24 hours to approximately 60 hours. Maximum wind speeds (5-minute averages) ranged from just under 20 knots to nearly 40 knots, with gust speeds as high as 43 knots.

The ADCP data from drifts two and four were used to calculate downwind and crosswind leeway coefficients for the drogued SEIE raft. Because no ADCP data were available for calculating leeway of the undrogued SEIEs and SEPIRBs, a statistical interpolation technique was used to estimate the surface current field around each drifter. The motions of nearby (within a 10 km radius) SLDMBs were used in an objective spatial interpolation technique to derive the local surface current field. Leeway was calculated as the difference between the total drift target motion and the surface current. As would be expected, the leeway of the undrogued raft was greater than that of the drogued raft.

Indirect leeway computations for the SEPIRBs based on two separate drifts showed that the SEPIRBs exhibited little leeway motion in either the downwind or crosswind direction. The leeway of the SEPIRB is therefore set as zero. The SEPIRB is basically a long vertical cylinder extending into the water column with little above-water surface representation. Its motion was therefore defined by the surface current field.

Some problems with the SEIE rafts were noted during the study. The Velcro® seal on the canopy flap failed in high winds, so intervention by a human passenger would be needed to keep the flap closed. Air leaks occurred in the buoyancy bladder and through the threaded CO2 canister connection. Opened flaps and buoyancy loss due to air leaks resulted in raft flooding and some loss of data. The flap closure problem and the air leaks were corrected by field modifications. An examination of the rafts after the end of the study concluded that abrasion from our instrument packs and ballast caused the air leaks from the buoyancy bladder.

SEPIRBs are designed to repeatedly transmit only the initial position that is recorded when the unit is first deployed. As the SEPIRB is moved away from the initial deployment location by local currents and winds, it would be helpful to searchers if the present position for the SEPIRB location were also transmitted. This information would be particularly useful in the event that personnel have evacuated the submarine and are adrift in the ocean (perhaps in a SEIE raft). The data return from the SEPIRBs was also relatively low. This may have been caused by the relatively low above-surface profile of the SEPIRB. The low data return may also have been exacerbated by the weather conditions that were encountered.

The leeway coefficients developed from this study are recommended for incorporation by the U.S. Navy into its search planning tools for recovering the crew of a disabled submarine on the ocean floor. This same information should also be incorporated by the CG into its current and next generation tools for search planning.

## TABLE OF CONTENTS

<b>ACKNOWLEDGEMENTS .....</b>	<b>iv</b>
<b>EXECUTIVE SUMMARY .....</b>	<b>v</b>
<b>LIST OF ACRONYMS, ABBREVIATIONS, AND SYMBOLS.....</b>	<b>xii</b>
<b>1.0 INTRODUCTION.....</b>	<b>1</b>
<b>2.0 METHODS.....</b>	<b>3</b>
2.1 Field Program.....	3
2.1.1 Pre-Field Study Mobilization.....	3
2.1.2 On-Site Mobilization .....	8
2.1.3 Drift Target Deployment, Tracking and Recovery .....	14
2.1.4 Demobilization.....	15
2.2 Data Reduction/Filtering.....	16
2.3 Data Analysis .....	17
<b>3.0 EXPERIMENTAL RESULTS.....</b>	<b>21</b>
3.1 Monitoring Buoy Data Results .....	21
3.1.1 Coastal Monitoring Buoy.....	21
3.1.2 Waverider Buoy .....	26
3.2 SEIE Life Raft and SEPIRB Drift Results.....	29
3.2.1 Drift One .....	38
3.2.2 Drift Two .....	38
3.2.3 Drift Three .....	39
3.2.4 Drift Four .....	39
3.2.5 Drift Five.....	40
<b>4.0 LEEWAY DATA ANALYSIS .....</b>	<b>41</b>
4.1 Trajectory Analyses .....	41
4.2 Surface Current Field Resolution.....	43
4.2.1 Direct Current Field Calculations .....	43
4.2.2 Indirect Current Field Calculations.....	45
4.3 Leeway Calculations.....	56
4.3.1 Leeway of Drogued SEIE Rafts.....	56
4.3.2 Leeway of Undrogued SEIE Rafts.....	59
4.3.3 SEPIRB Leeway .....	62
<b>5.0 CONCLUSIONS.....</b>	<b>67</b>
<b>6.0 RECOMMENDATIONS.....</b>	<b>70</b>
<b>7.0 REFERENCES.....</b>	<b>71</b>
<b>APPENDIX A – SUPPORTING DRIFT TARGET RESULTS .....</b>	<b>A-1</b>

## LIST OF FIGURES

Figure 1.	The primary operations area for the Leeway Study showing locations of the Coastal Monitoring Buoy (CMB) and the Waverider buoy.....	5
Figure 2.	Overview of SEIE Rafts, SEPIRBs, and SLDMBs deployed during the Leeway Study.....	6
Figure 3.	Overview of the Canadian Coast Guard Ship <i>Ann Harvey</i> that was used to support the Leeway Study.....	11
Figure 4.	Overview of the Coastal Monitoring Buoy deployment for the Leeway Study and a description of the parameters measured during the deployment.....	13
Figure 5.	Times-series views of the uncorrected CMB wind data relative to the St. John's airport observations and Oceans, Ltd. model prediction for the location of the CMB.....	22
Figure 6.	Detailed view of the two primary measurements that were used to compute the wind speed direction for the CMB data. ....	24
Figure 7.	Time-series views of the CMB wind data after corrections were made to direction and speed. ....	25
Figure 8.	Complete time-series view of the CMB data, reflecting both the wind direction offset and the 10-m reference height adjustment. ....	27
Figure 9.	Time-series view of the Waverider data over the complete deployment period. ....	28
Figure 10.	Trajectories of SEIE raft and SLDMBs for Drift One from 31 October to 2 November.....	30
Figure 11.	Trajectories of SEIE rafts and SLDMBs for Drift Two from deployment on 9 November to recovery on 10 November.....	31
Figure 12.	Trajectories of SEIE raft and SLDMBs for Drift Three from deployment on 10 November to recovery on 14 November.....	32
Figure 13.	Trajectories of SEIE rafts and SLDMBs for Drift Four from deployment on 14 November to recovery on 16 November.....	33
Figure 14.	Trajectories of SEIE rafts and SLDMBs for Drift Five from deployment on 17 November to recovery on 19 November.....	34
Figure 15.	Trajectories of SEPIRBs from ARGOS-calculated positions from Drifts One through Five. ....	35
Figure 16.	Trajectories of SEPIRBs from GPS-calculated positions during Drifts One and Four. ....	36
Figure 17.	Time-series trajectory plot of the drogued SEIE raft and the SLDMBs during Drift Two. ....	42
Figure 18.	Time-series trajectory plot of the movement of the drogued SEIE raft and SLDMBs relative to the near-surface water and motions of nearby SLDMBs over ground during Drift Two.....	44
Figure 19.	Time-series views of the near-surface current field from drogued raft and SLDMB data during Drift Two.....	46
Figure 20.	Time-series of the eastward components for SLDMBs deployed during the first 8 days of the field study, as well as the low-pass, band-pass, and high-pass components of the original data.....	47



Figure 21.	Time-series of the northward components for SLDMBs deployed during the first 8 days of the field study, as well as the low-pass, band-pass, and high-pass components of the original data.....	48
Figure 22.	The computed spatial mean current field and spatial correlation functions for each of the three frequency bands derived from the SLDMB data. ....	49
Figure 23.	The computed direct and indirect near-surface current field at the drogued raft during Drift Two. ....	52
Figure 24.	Time-series of the vector components of the computed direct and indirect near-surface current field at the drogued raft during Drift Four. ....	53
Figure 25.	Time-series of the vector components of the computed near-surface current field (bounded by $\pm 1$ standard deviation of the error) at the undrogued raft during Drift Two. ....	54
Figure 26.	Time-series of the vector components of the computed near-surface current field (bounded by $\pm 1$ standard deviation of the error) at the undrogued raft during Drift One.....	55
Figure 27.	Progressive vector diagrams and leeway angle scatter plots for the drogued rafts from Drifts Two and Four.....	58
Figure 28.	Unconstrained downwind and crosswind (positive and negative) leeway components computed for the drogued rafts from Drifts Two and Four.....	60
Figure 29.	Progressive vector diagrams and leeway angle scatter plots for the undrogued rafts from Drifts One and Two. ....	61
Figure 30.	The constrained and unconstrained downwind and crosswind (positive and negative) leeway components computed for the undrogued rafts from Drifts One and Two.....	63
Figure 31.	Progressive vector and leeway angle scatter plots for the SEPIRBs from Drifts One and Four. ....	65
Figure 32.	The constrained and unconstrained downwind and crosswind (positive and negative) leeway components computed for the SEPIRBs from Drifts One and Four. ....	66
Figure A-1.	Time-series vector plot of the movement of the drogued SEIE raft over the ground and also the computed direct current field during Drift Two. ....	A-2
Figure A-2.	Progressive vector diagrams and constrained and unconstrained downwind and crosswind (positive and negative) leeway components computed for the drogued raft from Drift Two. ....	A-3
Figure A-3.	Time-series vector plot of the movement of the drogued SEIE raft over the ground and also the computed direct current field during Drift Four.....	A-4
Figure A-4.	Progressive vector diagrams and constrained and unconstrained downwind and crosswind (positive and negative) leeway components computed for the drogued raft from Drift Four.....	A-5
Figure A-5.	Time-series vector plot of the movement of the undrogued SEIE raft over the ground and also the computed indirect current field during Drift One.....	A-6
Figure A-6.	Progressive vector diagrams and constrained and unconstrained downwind and crosswind (positive and negative) leeway components computed for the undrogued raft from Drift One.....	A-7
Figure A-7.	Time-series vector plot of the movement of the undrogued SEIE raft over the ground and also the computed indirect current field during Drift Two.....	A-8

Figure A-8.	Progressive vector diagrams and constrained and unconstrained downwind and crosswind (positive and negative) leeway components computed for the undrogued raft from Drift Two. ....	A-9
Figure A-9.	Time-series vector plot of the movement of SEPIRB 53241 over the ground and also the computed indirect current field during the course of the drift from 31 October through 15 November.....	A-10
Figure A-10.	Progressive vector diagrams and constrained and unconstrained downwind and crosswind (positive and negative) leeway components computed for SEPIRB 53241.....	A-11
Figure A-11.	Time-series vector plot of the movement of SEPIRB 53243 over the ground and also the computed indirect current field during the course of the drift from 14 November through 16 November.....	A-12
Figure A-12.	Progressive vector diagrams and constrained and unconstrained downwind and crosswind (positive and negative) leeway components computed for SEPIRB 53243.....	A-13

## LIST OF TABLES

Table 1. Daily summary of activities during the field portions of the Leeway Study. ....	4
Table 2. Planned ARGOS PTT use during the Leeway Study. ....	10
Table 3. Drift target deployment and recovery information for each of the five primary drift runs. ....	37
Table 4. Summary of the calculated leeway coefficients and relevant statistics. ....	57

## LIST OF ACRONYMS, ABBREVIATIONS, AND SYMBOLS

ADCP	Acoustic Doppler Current Profiler
AI	Aanderaa Instruments A/S
ALP	Auxiliary Location Processing
CANSARP	Canadian Search and Rescue Planning
CCG	Canadian Coast Guard
CCGS	Canadian Coast Guard Ship
CG	U.S. Coast Guard
cm	centimeter
cm/sec	centimeters per second
CMB	Coastal Monitoring Buoy
COSPAS	Space system for search and rescue of distressed vessels
DFO	Department of Fisheries and Oceans
DND	Department of National Defense
e.g.	<i>exempli gratia</i> (For example)
et al.	<i>et alia</i> (And others)
FTP	File transfer protocol
GIS	Geographical information system
G-RPR	U.S. Coast Guard Office of Search and Rescue
GPS	Global Positioning System
km	kilometers
m	meter
m/s	meters per second
MHz	megahertz
nmi	nautical mile
NSMRL	Naval Submarine Medical Research Laboratory
QA	Quality Assurance
QC	Quality Control
PTT	Platform Transmitter Terminal
R&DC	Research and Development Center
SAIC	Science Applications International Corporation

SAR	Search and Rescue
SARSAT	Search And Rescue Satellite Aided Tracking System
SEIE	Submarine Escape and Immersion Equipment
SEPIRB	Submarine Emergency Position Indicating Radio Beacon
SI	Statistical Interpolation
SLDMB	Self-Locating Datum Marker Buoy
SOLAS	Safety of Life at Sea
VHF	Very High Frequency

(This page intentionally left blank.)

## 1.0 INTRODUCTION

The U. S. Coast Guard (CG) Research and Development Center (R&DC) has participated in joint leeway studies with the Canadian Coast Guard (CCG) in the waters off St. John's, Newfoundland since the early 1990's. These studies have provided much of the empirical data that the CG uses in Search and Rescue (SAR) planning and have employed consistent data collection and analysis methods that provide the desired, internally consistent coefficients to the CG for its SAR planning software. As a continuation of this program, a leeway study was conducted off St. John's from mid-October through mid-November 2005. Science Applications International Corporation (SAIC) served as the support contractor for the CG, and Oceans, Ltd. served as the support contractor for the CCG.

During the past several years, the R&DC, with support from the CCG, has conducted a number of leeway experiments using common SAR objects in environmental conditions typically encountered on the east coast of Canada and the United States. The SAR objects investigated included 4-, 6- and 20-person inflatable life rafts, persons-in-water, sea kayaks, wharf boxes, small open plank boats, and a 22-person Safety of Life at Sea (SOLAS) approved fiberglass life capsule, in various configurations (e.g., Fitzgerald et al., 1993 and 1994, Allen et al., 1999). The leeway parameters of the common SAR objects have been incorporated in the U.S. National SAR Supplement (National Search and Rescue Committee, 2000) and the Canadian Search and Rescue Planning (CANSARP) program (DFO, 1998). The primary objective of the previous work was to evaluate the relationship between wind velocity and SAR object leeway in wind speeds up to 50 knots.

The U.S. National SAR Supplement, consistent with an earlier edition, defines leeway as "the movement of the search object through water caused by the action of wind on the exposed surfaces of the object" (DND and CCG, 1985). To standardize leeway field measurements, Fitzgerald et al. (1993) refined the definition to read: "leeway is the velocity vector relative to the downwind direction at the search object as it moves relative to the surface current, as measured between 0.3 m and 1.0 m depth, caused by the winds (adjusted to a reference height of 10 m) and waves." For consistency with the earlier work, including more recent work by the CG (e.g. Allen et al., 1999), this working definition was used in 2005 field experiments.

For the 2005 Leeway Study, the Naval Submarine Medical Research Laboratory (NSMRL) provided funding to the R&DC to determine the leeway of Submarine Emergency Position Indicating Radio Beacons (SEPIRB) and Mark-10 Submarine Escape and Immersion (SEIE) life rafts used by Navy submariners. NSMRL conducts research and development, as well as testing and evaluation of technology related to submarine and diving operations, with applications to other military operations. NSMRL was mandated by Congress to accelerate identification and rescue of survivors in naval SAR environments. The primary intent of the program is to reduce the time required to find survivors at sea including, specifically, escapees from a sunken submarine who are using the SEIE life raft. This report documents one component of this project, quantifying the leeway of survivors that have reached the ocean surface and are drifting in the SEIE raft. This project also describes how the SEIE raft will move relative to the SEPIRB drifter.

The CCG commissioned Oceans, Ltd. of St. John's, Newfoundland for phase I of a leeway study for the 4- and 7- person Ovatek rigid life rafts that was conducted in September 2004. To take advantage of this ongoing work, the R&DC issued a task order to Oceans, Ltd. to conduct leeway field tests of the SEPIRB. The 2004 SEPIRB study was postponed due to logistical constraints until October 2005, when phase II of the Canadian tests was scheduled to be conducted. During the winter of 2004, the R&DC and NSMRL also decided that concurrent tests of the SEIE life raft should be added to the SEPIRB study.

To conduct the 2005 field study, instrumented drift targets (e.g., SEIE rafts and SEPIRBs) were deployed and tracked as they drifted on the open ocean off St. John's, Newfoundland under carefully observed environmental conditions from late October through mid-November 2005. In addition to various forms of radio and visual devices to aid in target recovery, the drift targets were also equipped with on-board GPS data-logging equipment to accurately track the movement of the target over time. To provide data backup, and assist with target tracking and recovery, ARGOS platform transmitter terminals (PTTs) were also included with the drift target instrument package to periodically transmit drift target position data that could be accessed in near real-time. To provide a direct measure of near-surface currents, some of the deployed rafts were equipped with an Acoustic Doppler Current Profiler (ADCP) to measure the raft motion relative to the water. In other cases, an indirect estimate of the near-surface currents at the drift targets was provided by self-locating datum marker buoys (SLDMBs) that were released in the vicinity of the drift targets during each deployment. Meteorological data (e.g., wind direction and speed, air and water surface temperature), along with Eulerian measurements of near-surface current speed and direction, were provided by an Aanderaa Coastal Monitoring Buoy (CMB) that was deployed in a central location in the primary operations area. This array of instrumentation provided all of the data that were required to evaluate the relationship between wind direction and velocity and the leeway for each target type. A more thorough discussion of the methods employed for both the field study and the subsequent data analyses is provided in Section 2.0.

This report documents the results of the effort to develop leeway coefficients for the SEIE rafts and SEPIRBs. It outlines the field procedures used for collecting the necessary data, as well as the data processing and analysis procedures used for developing the required leeway coefficients for the SEIE rafts and the SEPIRBs. Based on the extensive data reduction and analyses that were conducted, this report presents the average leeway coefficients computed for the SEIE rafts and SEPIRBs, as well as an assessment of the variability of leeway in the downwind and crosswind directions, and the functional relationship between wind velocity and leeway for these same targets.



## **2.0 METHODS**

The following sections will provide an overview of the methods employed during the three main elements of the 2005 Leeway Study: the Field Program; Data Reduction; and Data Analyses. The observed results from the field program will be presented in Section 3 and the results of the data analyses will be presented in Section 4.

### **2.1 Field Program**

The field portions of this study were conducted over approximately a one-month period from mid-October through late November 2005 (Table 1). Prior to the start of the field program, SAIC developed a Test Plan (SAIC, 2005) that outlined the planned procedures for assembling and testing the drift targets (SEIE life rafts and SEPIRBs) and collecting the necessary leeway data during the field study conducted off St. John's (Figure 1). The following sections will cover some of the same material presented in the Test Plan, and provide a more detailed discussion of the methods employed during the actual field portions of this study. Because the Test Plan was written prior to the start of this logistically complex field program, changes to some elements of the plan were not unexpected. These changes will be addressed in the following sections.

#### **2.1.1 Pre-Field Study Mobilization**

Over a three-week period immediately following contract award and prior to the start of the field study, extensive testing of government-furnished and contractor electronics equipment was conducted at the contractor facilities in Rhode Island. Drifter design, assembly, and testing operations were conducted during this same period. In addition, a new ARGOS service account was established in order to place all of the PTTs that would be employed in this study under a single dedicated ARGOS service account. Finally, all of the required equipment had to be packed and then shipped to the CCG facility in St. John's.

#### **Drift Target Configuration**

Figure 2 provides an overview of the drift targets used in this study. More detailed information on these targets and their development can be found in the Test Plan. The NSMRL provided SEIE training rafts for the study. These rafts are identical to those deployed aboard submarines with the exception that the training rafts have an over-inflation protection relief valve and are of more durable construction to support repeated use during training. The SEIE raft is a one-person survival raft incorporating a weathertight canopy and a sea drogue. For this study, the target rafts were shaped and ballasted with concrete paving blocks to simulate a 200-lb occupant, and instrumented to provide for tracking and visual recovery in both upright and inverted positions. A mannequin torso was placed in each of the test rafts to better represent the true shape of the raft during use. Instrumentation installed onboard the SEIE life rafts included a Garmin GPS (GPSMap 76) receiver, a GeoStats GPS data logger, an external battery pack, an external GPS antenna, and an ARGOS PTT, all enclosed within a watertight case. A SmartCat ARGOS PTT unit was also fastened within a ballast pocket on the underside of the raft in the event that the raft was overturned for any reason. An upward-facing Novatech RF-700C1 combination VHF (154.585 – 160.785 MHz) radio beacon/xenon flasher was attached to the mannequin to

Table 1. Daily summary of activities during the field portions of the Leeway Study.

Date (2005)	Activity Type	At Sea (Y/N)	Overview
22-Oct	Travel		John Morris (Field Program Lead) and Pamela Luey (Field Technician) arrive at St. John's.
23-Oct	Mobilization		Learn area, locate Oceans, LTD and visit Coast Guard station, tour CCG Ann Harvey.
24-Oct	Mobilization		Meet with Oceans, LTD employees set up office area. Truck and Jim Singer (CMB operator) arrive in St. John's.
25-Oct	Mobilization		Mobilize equipment from truck.
26-Oct	Mobilization		Aanderaa buoy shipped from MA. FedEx arrives.
27-Oct	Mobilization		Mobilize electronic equipment (SEPIRBs)
28-Oct	Mobilization		Mobilize vessel and Preliminary drift targets.
29-Oct	Deploy	Y	Deploy Preliminary Drift targets - 2 rafts, 1 SEPIRB, 3 SLDMBs. Mobilize Aanderaa buoy.
30-Oct	Recover / Deploy	Y	Deploy CMB; Recover Preliminary Drift targets. Mobilize for Drift 1.
31-Oct	Deploy	Y	Deploy Drift 1 targets - 2 rafts, 1 SEPIRB, 4 SLDMBs.
1-Nov	Mobilization	Y	Mobilize targets for next deployment. Jim Singer (CMB operator) departs St. John's.
2-Nov	Recover	Y	Attempt ARGOS antenna installation on CMB - buoy locked up.
			Recover Drift 1 targets. Respond to SAR call.
3-Nov	Mobilization		Float test newly assembled SEPIRB. Tom Waddington (Assistant Field Program Lead) arrives in St. John's.
4-Nov	Search	Y	Search for Ovatek life rafts with Oceans.
5-Nov	Mobilization		Mobilize targets for next deployment.
6-Nov	Mobilization/SAR	Y	Recover Aanderaa buoy and redeploy without ARGOS antenna; Drift 2 deployment delayed due to SAR call.
7-Nov	SAR	Y	SAR call continues.
8-Nov	Mobilization		John Morris (Field Program Lead) departs St. John's and Kate Montgomery (Field Technician) arrives in St. John's.
			Attempt to patch and reconfigure remaining SEIE rafts.
9-Nov	Deploy	Y	Deploy Drift 2 targets - 2 rafts, 1 SEPIRB, 4 SLDMBs
10-Nov	Recover / Deploy	Y	Search for and recover Ovateks offshore; Recover Drift 2 Targets
			Redeploy for Drift 3 - 1 raft, 3 SLDMBs
11-Nov	Mobilization	Y	Assemble new SEIE rafts.
12-Nov	Mobilization		Demobilize gear from ship to truck due to fisheries patrol assignment; continue bale and raft configuration
13-Nov	Mobilization		Remobilize. Tom Waddington (Assistant Field Program Lead) departs; John Morris (Field Program Lead) returns.
14-Nov	Recover / Deploy	Y	Recover Drift 3, deploy Drift 4 - 2 rafts, 2 SEPIRBs and 5 SLDMBs.
15-Nov	Recover	Y	Search and site on all targets from Drift 4 and recover targets from previous Drifts.
16-Nov	Recover	Y	Recover Drift 4 targets.
17-Nov	Deploy	Y	Deploy Drift 5 - 2 rafts, 2 SEPIRBs, and 5 SLDMBs.
18-Nov	Demobilization		Begin to organize and demobilize
19-Nov	Recover	Y	Recover Drift 5 targets and CMB
20-Nov	Demobilization		Demobilize vessel.
21-Nov	Demobilization		Demobilize Oceans, LTD office. Organize and itemize in truck.
22-Nov	Demobilization		Kate Montgomery (Field Technician) and Pamela Luey (Field Technician) depart St. John's.
23-Nov	Demobilization		Prepare items for shipping
24-Nov	Demobilization		Prepare items for shipping
25-Nov	Demobilization		Prepare items for shipping
26-Nov	Demobilization		Truck departs St. John's
27-Nov	Demobilization		John Morris (Field Program Lead) departs St. John's.

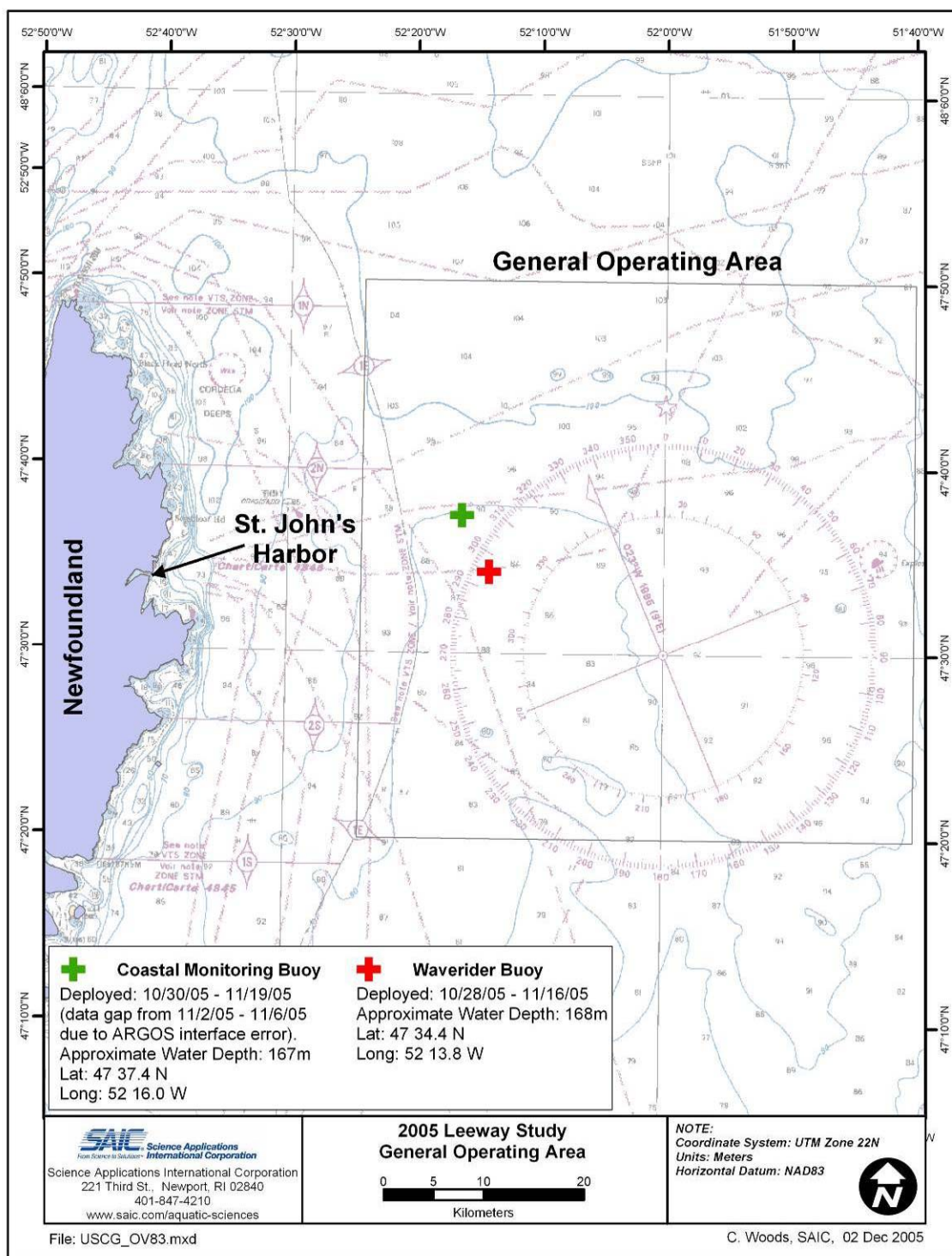


Figure 1. The primary operations area for the Leeway Study showing locations of the Coastal Monitoring Buoy (CMB) and the Waverider buoy.

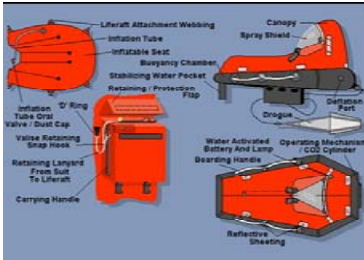



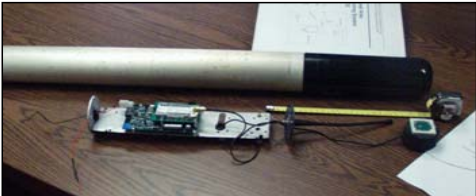


Drifter Type (Number Available)	Configuration Details	Images	
<b>Submarine Escape and Immersion Equipment Life Raft (SEIE)</b>  (4)	4 SEIE rafts 5 Garmin GPS units 5 Geostats GPS data loggers 3 SmartCat ARGOS beacons 3 ADISS ARGOS beacons 3 Novatech RF-700C1 radio beacons 1 RDI Workhorse Monitor 1200 kHz ADCP with a gimbaled mount	  	
<b>Submarine Emergency Position Indicating Radio Beacon (SEPIRB)</b>  (5)	3 Clearwater GPS / ARGOS SEPIRBs with no internal data logging 2 SEPIRB enclosures with GPS, ARGOS, and internal data logging	 	
<b>Self - Locating Datum Marker Buoy (SLDMB)</b>  (22)	22 SLDMBs No internal GPS logging GPS transmitted by ARGOS 30 minute position update Approximate 30 day battery life	 	

Figure 2. Overview of SEIE Rafts, SEPIRBs, and SLDMBs deployed during the Leeway Study.

facilitate recovery. The range of the radio beacon was three to six nautical miles, and its battery life was estimated at eight days in 4 °C water.

Initial comparisons of draft and trim of the raft containing a live crew member and with the raft containing the instrument package were made prior to the study on the ocean in Rhode Island. The test resulted in the shifting of ballast aft in the raft to reduce its forward draft (i.e. at the occupant's feet).

One of the SEIE rafts was additionally equipped with a downward-looking RD Instruments, Workhorse Monitor Acoustic Doppler Current Profiler (ADCP). The ADCP provided information on current velocity within the surface waters, between 75- to 100-cm water depths. The ADCP was equipped with a 1200 kHz Zedhead® transducer, which sub-divided the upper 10 m of the water column into 39 individual 25 cm layers or bins. The ADCP was set up to “blank” or ignore data from the first 25 cm bin to provide the necessary time delay between transmitting and receiving acoustic pulse. Therefore, the first valid current data were captured 75 cm below the water's surface. To improve data quality, the ADCP was attached to the underside of the raft on a gimbaled mount that was designed to minimize the effects of heave, pitch and roll associated with heavy seas.

The SEPIRB used for the study (Figure 2) is a replica of the Model T-1630/SRT Buoy manufactured by Ultra Electronics Ocean Systems for the U.S. Navy. The SEPIRB was developed as an emergency signaling device for submarines in distress. SEPIRBs are stored in an emergency escape trunk and launched from a submarine when needed. When launched, the SEPIRB ascends to the water's surface to obtain a geodetic position using an integrated GPS receiver that transmits an emergency message. Upon activation, a typical Model T-1630/SRT buoy transmits positioning information at a frequency of 406 MHz using the COSPAS-SARSAT satellite network. The transmitted message includes the time, initial GPS location and a unique SEPIRB ID. If the initial GPS position cannot be obtained immediately, the SEPIRB records the elapsed time between activation and GPS signal lock. Using this elapsed time, the initial point of activation can be calculated to locate the distressed submarine. Six hours after activation, the standard SEPIRB broadcasts a 121.5 MHz homing radio-beacon signal to aid in recovery. The 121.5 MHz signal also functions as a backup system in the event that the GPS system does not operate properly, permitting satellites to resolve a geodetic position within a 2-nmi radius.

For this study, several 3-inch diameter, 39-inch long, empty SEPIRB pressure hulls were acquired from Ultra Electronics Oceans Systems. The SEPIRBs were fitted with 401 MHz ARGOS PTTs, instead of the typical 406 and 121.5 MHz electronics found in the U.S. Navy SEPIRBs. The SEPIRBs used for the study were configured with Garmin18 GPS receivers and GeoStats data loggers to internally log GPS data. Three other SEPIRBs were provided by Clearwater Oceanographic Instruments, of Watertown, Massachusetts. These SEPIRBs were equipped with onboard GPS receivers that provided the latitude and longitude of the SEPIRB to the ARGOS PTT for transmission with each message (i.e., no data logger installed).

An ARGOS service account was established to provide data back-up for onboard data-logging systems, to assist with tracking and recovery of all the deployed drifters, and to provide periodic assurance that the moored weather buoy was operating properly. The “program” (or Systems

Use Agreement) was prepared by SAIC and submitted by the R&DC to Service ARGOS in early October 2005. Details for this program are provided in the Test Plan (SAIC, 2005).

SLDMBs covered under an existing CG program (2311) with Service ARGOS were deployed along with the drift targets to provide a measure of the surface current field within the study area. PTTs installed on all of the remaining drifters deployed in this program were included within the new ARGOS Program 3194 (Table 2). Through an external link to the CG FTP server, SAIC obtained remote access to the SLDMB data, which was uploaded, processed, and posted hourly by the CG Operations Systems Center (OSC) located in Martinsburg, WV. On the FTP server, SLDMB data were maintained in two separate data files – a master data file that contained all recorded SLDMB position data over the course of the program, and a second file that contained only the most recent two hours of data for the deployed SLDMBs. This second smaller file enabled more efficient remote access (from the recovery ship) to key position data during drifter recovery options.

The PTTs highlighted in yellow in Table 2 provided ARGOS position only and were used primarily to assist in drifter recovery operations. PTTs highlighted in blue provided a GPS position that was updated in 30-minute intervals. Because these GPS-enabled PTTs transmitted at a 200-second interval (instead of an ARGOS-recommended 90-second rate), the ability of the ARGOS system to compute their position by the conventional Doppler shift technique was limited. For these PTTs, Auxiliary Location Processing (ALP) was requested to enable an ARGOS position to be computed based on only two or three transmissions (instead of the standard four).

### **2.1.2 On-Site Mobilization**

All of the required equipment, with the exception of the SAIC-owned Aanderaa Instruments (AI) Coastal Monitoring Buoy (CMB), were shipped from SAIC on 21 October and arrived in St. John's on 24 October. The CMB required additional mobilization and testing at the AI facilities in Massachusetts and was shipped at a later date via special carrier. SAIC personnel arrived in St. John's on 22 October and began the extensive local mobilization in advance of the field study (Table 1). Mobilization activities included unloading the truck and mobilizing gear aboard the CCG Ship (CCGS) *Ann Harvey*, establishing a temporary office space at Oceans, Ltd., and beginning to assemble and test all of the drifters required for this study. Concurrently with the SAIC efforts, Oceans, Ltd. personnel were also mobilizing for their concurrent Ovatek life capsule drift study.

#### Coordination with CCG and Oceans, Ltd.

The Newfoundland Region of the CCG provided the services of a multi-task ice-strengthened vessel, the CCGS *Ann Harvey*, for the 2005 field trials. The CCGS *Ann Harvey* is 83 m in length, with a beam of 16.2 m and a draft of 6.2 m (Figure 3). The *Ann Harvey* sails with a complement of a captain, 9 officers and 16 crew members who work on 28-day shifts; during this study, a crew change occurred on 9 November. Because the *Ann Harvey* is a multi-task vessel, she was also required to provide sporadic SAR and fisheries support during the 2005 Leeway Study. Though these ancillary requirements did have some impact on the planned

Leeway operations, the overall extent of these disruptions was minimal over the course of the study.

The *Ann Harvey* provided equipment, instrumentation, and personnel to support the deployment and recovery of the Waverider and Coastal Monitoring Buoys, as well as all of the drift targets. The forward hold of the *Ann Harvey* was also used extensively for equipment storage and as a staging area. In addition, the *Ann Harvey* provided access to their VHF direction finder and weather facsimile, as well as necessary communications links to contact the shore base. The ship also supplied Internet access while at sea via the Globalstar® packet modem that was used to obtain periodic ARGOS position updates for drift targets. The *Ann Harvey* also provided meals and accommodations for up to seven support personnel from SAIC, Oceans, Ltd., and the CG.



Table 2. Planned ARGOS PTT use during the Leeway Study.

Planned Use of ARGOS PTT Platform IDs for the CG R&D Center 2005 Leeway Experiment					
No	Planned Platform IDs	Prior Use	Other Information HEX IDs	Serial No.	ARGOS Program
<b>CG MetOcean SLDMBs</b>					
1	38712	Unused	2ABA98B		CG Program 2311 / SAIC
2	43394	Unused	09BE626		CG Program 2311 / SAIC
3	43446	Unused	10FEF6A		CG Program 2311 / SAIC
4	38763	Unused	1BCC5BE		CG Program 2311 / SAIC
5	43358	Unused	029D3E1		CG Program 2311 / SAIC
6	38851	Unused	2AF7335		CG Program 2311 / SAIC
7	43381	Unused	078185F		CG Program 2311 / SAIC
8	43444	Unused	10FEF4C		CG Program 2311 / SAIC
9	43442	Unused	10FEF26		CG Program 2311 / SAIC
10	43448	Unused	10FEF8B		CG Program 2311 / SAIC
11	43430	Unused	0CA2D6A		CG Program 2311 / SAIC
12	43155	Unused	37CBA35		CG Program 2311 / SAIC
13	43087	Unused	378C6F2		CG Program 2311 / SAIC
14	38908	Unused	2B126C7		CG Program 2311 / SAIC
15	38639	Unused	2A87DF2		CG Program 2311 / SAIC
16	38991	Unused	2B68EF2		CG Program 2311 / SAIC
17	38952	Unused	2B1D38B		CG Program 2311 / SAIC
18	38648	Unused	2AA108B		CG Program 2311 / SAIC
19	38651	Unused	2AA10BE		CG Program 2311 / SAIC
20	38669	Unused	2AA43D4		CG Program 2311 / SAIC
21	38948	Unused	2B1D34C		CG Program 2311 / SAIC
22	38946	Unused	2B1D326		CG Program 2311 / SAIC
23	43038	Unused	3755DE1		CG Program 2311 / Oceans
24	32781	Unused	13F67D4		CG Program 2311 / Oceans
25	38863	Unused	2AF73F2		CG Program 2311 / Oceans
<b>SEIE Life rafts</b>					
1*	12020	> 3 years	BBD20	s/n - 24242	CG Program 3194 / SAIC
2*	12021	> 3 years	BBD73	s/n - 24243	CG Program 3194 / SAIC
3*	12022	> 3 years	BBD86	s/n - 24248	CG Program 3194 / SAIC
<b>Aanderaa CMB Buoy</b>					
1	21267	2-3 years	4C4C2		CG Program 3194 / SAIC
<b>CG SmartCat IDs (Back-up ARGOS &amp; Ovatek Life rafts)</b>					
1	4509	?	46765		CG Program 3194 / Oceans
2	4510	?	46790		CG Program 3194 / Oceans
3	4514	?	46893	s/n - 11790	CG Program 3194 / SAIC
4	4513	?	46866	s/n - 11789	CG Program 3194 / SAIC
5	4512	?	46835		CG Program 3194 / Oceans
<b>CG SEPIRB IDs</b>					
1	53241	> 3 years	7886798		CG Program 3194 / Oceans
2	53242	> 3 years	78867AD		CG Program 3194 / Oceans
3	53243	> 3 years	78867BE		CG Program 3194 / SAIC
4*	27956	> 3 years	B4D21		CG Program 3194 /
5*	27965	> 3 years	B4F4C		CG Program 3194 /
6*	27975	> 3 years	B51EC		CG Program 3194 /
7*	27980	> 3 years	B5327		CG Program 3194 /

\* GPS collected with an independent system

**Highlighting Key**

	GPS Data Transmission
	ARGOS Position Only
	Met Data Transmission



### Canadian Coast Guard Ship *Ann Harvey*

**Type:** Light Icebreaker - Major Nav aids Tender   **Home Port:** St. John's, Newfoundland, Canada

**Length:** 83 m   **Beam:** 16.2 m   **Draft:** 6.2 m   **Freeboard:** 1.8 m

**Gross Tonnage:** 3854 tons   **Net Tonnage:** 1534 tons

**Cruising Speed:** 12 knots   **Maximum Speed:** 16.5 knots

**Main Deck Area:** 210 m<sup>2</sup>   **Boat Deck Area:** 168 m<sup>2</sup>   **Fore Deck Area:** 108 m<sup>2</sup>

**Complement:** Officers - 10   Crew - 16   Available Berths - 23

**Communications Equipment:** VHF Radios, HF Radios, SatComm, WeatherFax, GlobalStar

**Electronics Equipment:** GPS Receivers, Gyro Compass, Radars, Autopilot, Speed Logs, Depth Sounder

**Deck Support Gear:** Deck Cranes, Winch, Forward Hold, FRC Small Boat and Davit

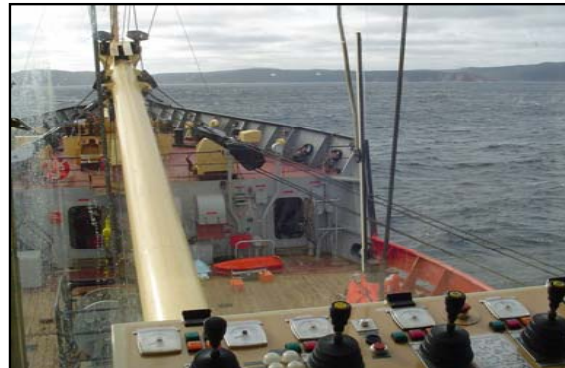


Figure 3. Overview of the Canadian Coast Guard Ship *Ann Harvey* that was used to support the Leeway Study.

Oceans, Ltd. supplied and archived weather forecasts, relevant weather charts, and data to support the leeway data analysis. The weather office provided a daily forecast to support daily and long-range planning of field operations. Prior to each field day, personnel of all parties, CG, CCG, Oceans, Ltd., and SAIC, would meet to discuss operating procedures, weather impacts, as well as objectives which had to be met for the day.

#### Deployment of Meteorological Buoy and Waverider Buoy

The 0.9-m Datawell® Directional Waverider buoy was deployed on 28 October within the primary operations area to acquire time-series data on wave direction, period, and height (Figure 1). The directional wave receiving system was set up at the Oceans, Ltd. office in St. John's. Wave data were collected continuously and transmitted to a receiving station at this site. The telemetered wave data were of value on marginal weather days by allowing the project manager to determine whether sea conditions were beyond operational limits before the ship left the pier. The Waverider buoy was recovered on 16 November, after the leeway studies were completed.

The CMB mooring was intended to provide the critical meteorological data (e.g., wind direction/speed, air/water surface temperature), along with Eulerian measurements of near-surface current speed and direction, necessary to support the development of leeway coefficients for the various drift targets (Figure 4). Due to delays in its final preparation, the CMB was not shipped from Attleboro, Massachusetts until 27 October and arrived in St. John's on 28 October. The ARGOS transmitter for the CMB was shipped separately by AI and arrived in St. John's on 30 October. The CMB was initially deployed, without the ARGOS transmitter installed, on 30 October from the CCGS *Ann Harvey* in the northern portion of the primary operations area and collected data for the preliminary drift and Drift One (Figures 1 and 4). On 2 November, when the ARGOS transmitter was connected to the CMB while still deployed, the buoy stopped recording data due to problems with the ARGOS transmitter interface. After a delay due to rough weather and sea conditions, the CMB buoy was recovered and then redeployed without the ARGOS transmitter, on 6 November and successfully recorded data from that point until its final recovery on 19 November (drifts two through five). No data were recorded by the CMB between 2 and 6 November. Fortunately, no drifts took place during this time. An overview of the CMB data return is provided in Section 3.1.

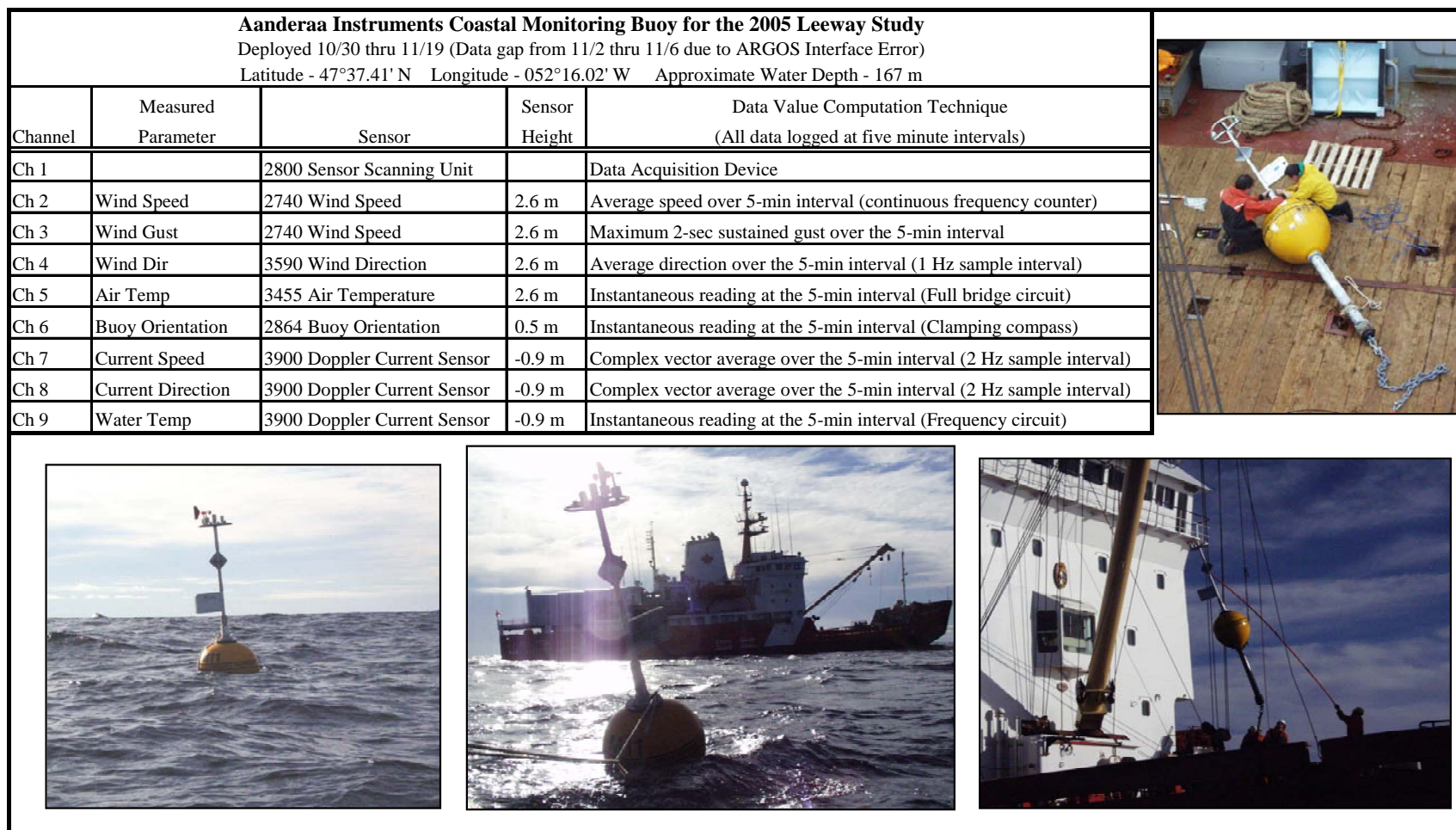


Figure 4. Overview of the Coastal Monitoring Buoy deployment for the Leeway Study and a description of the parameters measured during the deployment.

## Preliminary Drift and Drift Target Modifications

All SEIE life rafts and SEPIRBs were tested prior to deployment. The SEIE life-raft tracking equipment and SEPIRBs were positioned so that ARGOS and GPS positions would be received. Tests were conducted on the roof of Oceans Ltd. building to maximize access to the satellites, or on deck of the CCGS *Ann Harvey*. SEIE life rafts and SEPIRBs were tested for at least 12 hours prior to deployment. An initial preliminary drift run was conducted on 29 and 30 October to test the performance of the targets and electronic equipment under realistic conditions, to gather preliminary information on relative target drift rates, and to test deployment and recovery techniques. The preliminary drift was completed prior to deployment of the CMB buoy. Two rafts, one SEPIRB and three SLDMBs were deployed off the CCGS *Ann Harvey* for slightly over 24 hours.

At the end of the preliminary drift, both SEIE rafts were partially filled with seawater and the Velcro® seals had been torn open. SAIC made modifications to the rafts to address these problems. A layer of two-inch thick closed-cell foam was added to the underside of the equipment mounting base inside each raft to displace seawater. Grommets were also added to both sides of the enclosure flap so that this flap would remain sealed and more effectively shed seawater. In addition, a small electric submersible bilge pump was installed in the SEIE life raft that housed the ADCP current meter. Finally, an external bridle and lifting harness that better supported the raft during deployment and recovery was added to each of the rafts to minimize the likelihood of damage to the air bladder.

Despite careful handling, the SEIE life rafts still leaked air on a number of occasions. SAIC responded by patching the obvious leaks and by obtaining additional rafts from the R&DC. Because the SEIE rafts had only a single, continuous air bladder, any loss of air affected their buoyancy and performance. The two-inch thick closed cell flotation sheet minimized changes to the rafts' displacement and trim that resulted from subsequent flotation bladder leaks, as well as water entry through the canopy and through holes in the floor of the raft. In spite of these measures, the ocean exploited any weaknesses in the raft and installed instrument packs. During Drift Four, an undrogued raft operated for about a day before transmissions ended and it was lost at sea. At the end of Drift Five, a drogued raft was recovered partially deflated and upside down.

Due to their relatively straightforward design, no major modifications were required to the SEPIRBs during the course of the field study. One of the SEPIRBs was missing the lower lead coil attachment, so the ballasting of this unit had to be modified with the addition of some extra weight to the lower end. Due to their size and somewhat intermittent ARGOS transmission, the tracking of the SEPIRBs was not that reliable after they had been deployed. During the course of this study, five of the six SEPIRBs were lost at sea after deployment, though sufficient data were obtained from these units.

### **2.1.3 Drift Target Deployment, Tracking and Recovery**

The drift targets were deployed in the open ocean off St. John's under a variety of wind and sea conditions. The Oceans, Ltd. Weather Forecast office provided relevant weather forecast charts and data to help plan the field operations. In addition to various forms of radio and visual devices to aid in target recovery, all but one SEIE life raft, and all SAIC-modified SEPIRBs were

equipped with onboard GPS data-logging equipment to record accurate position data during drift periods. To provide data backup and to assist with target relocation and recovery, ARGOS PTTs were used to transmit periodic position data that could be accessed in near real-time. Currents in the upper 1 m of the water column were obtained from trajectories of SLDMBs that were typically deployed at each cardinal point of the compass around the primary drifter deployment location. The SLDMB separation distance was 1 km for Drift One and was increased to 5 km for the subsequent drift runs because the dispersion of the leeway drift target field was large.

To prepare for a drift scenario, project personnel typically began final pre-deployment mobilization and testing while docked in St. John's. Every effort was made to ensure that these pre-deployment system checks were completed while in transit to the deployment area so that all targets were ready for deployment when the ship had reached the designated area. The exact location of deployment was determined in discussions between the field team and the vessel captain to try to maximize the time that the targets remained near the CMB array. The SEIE rafts, SEPIRBs, and SLDMBs were then deployed based on the specific deployment scenario that had been developed.

At the end of a particular "drift run" (typically one to two days), an attempt was made to locate and recover all of the drift targets. During the target recovery phase, the near-real-time positioning data that were provided through the ARGOS updates obtained through the Globalstar access were used to identify a primary search area for all of the deployed drifters. After the primary search areas were identified through ARGOS, a 401 MHz Gonio® Radio Direction Finder (RDF) and VHF Novatech® RDFs supplied by the CG, along with visual observations, were used to locate the drifters. After the targets were identified visually, they were recovered under the direction of the captain and the assistance of the deck crew. Once the targets were recovered, they were secured on-deck or in the hold for the transit back to St. John's. In some instances, targets were turned around quickly for another deployment immediately after recovery. In these instances, the data were downloaded, batteries were replaced, and the target was quickly repackaged for deployment. Once the vessel arrived in St. John's, all data were downloaded to an onboard computer and eventually transferred to an external file transfer protocol (FTP) site established for the project. The first official drift (Drift One) for the field study began with target deployment on 31 October, and the final drift (Drift Five) for the field study concluded with target recovery on 19 November (Table 1). Results for each of these five drift runs are provided in Section 3.2.

#### **2.1.4 Demobilization**

Following the completion of the field studies and recovery of the CMB, final demobilization was completed in St. John's. Demobilization activities included offloading the ship, breaking down the temporary office space at Oceans, Ltd., appropriate cleaning of the instruments, removal of batteries, disassembly of arrays, and packing the truck for shipment back to Rhode Island. During the packing of the truck, a detailed inventory of gear was conducted to meet United States Custom requirements. When the truck arrived at SAIC facilities, further demobilization and cataloging continued. An inventory was created to provide an overview of the equipment that was lost or damaged and the present status of all of the equipment that was shipped back to Rhode Island. A more detailed itemized list of all equipment was prepared and provided with the equipment delivered back to the CG facility in Groton, CT.

## 2.2 Data Reduction/Filtering

The initial data reduction occurred while the field activities were still underway to facilitate timely assessment of data quality and support “on-the-fly” modifications to the field program or drift targets. The SEIE life rafts, SEPIRBs and SLDMBs, typically provided both GPS and ARGOS data positions. Though the ARGOS positions were useful for real-time tracking and recovery of drift targets, the ARGOS position quality was generally inconsistent, and the data interval was highly variable. When GPS data were available, those positions were used as the primary source for generating initial track plots and assessing data quality. In some cases, GPS positions were not available because of problems with the GPS receiver or the data logger. In these cases, the ARGOS position data were used to generate the initial drift target track plots. GPS data for the Clearwater SEPIRBs was encoded within the raw ARGOS messages which had to be parsed by Oceans, Ltd. well after the completion of the field program. These SEPIRB GPS data were provided to SAIC as electronic files in mid-January 2006.

The majority of the data reduction and analyses were conducted using specialized scripts written for the MATLAB® (v7.01) software package. These routines were initially used to edit, filter, interpolate, and visualize all of the position data files (for the SEIE rafts, the SEPIRBs, and the SLDMBs). These routines were also employed to create the standard time-series position data files that were then used to prepare the GIS track plots that summarized each of the main drifts. These time-series drift target position data files also served as the initial version of the comprehensive leeway analysis data files that were created for each successful drift target deployment.

In addition to examining the drift target and SLDMB position data, the data reduction phase also included initial processing of the CMB data. After completion of the field study, the raw data from the CMB were converted into the proper engineering units by applying the applicable calibration coefficients to each of the raw data fields. MATLAB routines were then used to generate time-series views of the CMB data over the deployment period. For quality assurance/quality control (QA/QC) of the CMB data, the wind magnitude and direction results from the CMB were compared to the hourly wind speed and direction data that were recorded at the St. John’s airport over the same period. In addition, modeled wind data from the Oceans, Ltd. weather forecast office were used as another QA/QC data source. MATLAB routines were used to conduct this QA/QC analysis and to make any necessary adjustments based on the comparisons.

The final wind data file was then run through a public domain MATLAB routine (CDNTC) to adjust the wind magnitude from the 2.6-m sensor height up to the 10-m reference height. The CDNTC routine was obtained via an open source web link that includes a variety of MATLAB routines for oceanographic applications (<http://woodshole.er.usgs.gov/operations/sea-mat/>). Based on Smith (1988), this routine computes the neutral drag coefficient and wind speed at a 10-m height given the wind speed and air temperature at a known sensor height. Finally, the adjusted wind data were run through either a 20-minute or 1-hour infinite impulse response Chebychev low-pass filter to smooth the data and prepare it for incorporation into the leeway analyses.



## 2.3 Data Analysis

Data analysis entailed three primary phases that were completed in sequential order as described below. Because the ARGOS-calculated position data were not equally spaced in time, all of the analyses described below were conducted only on the drift targets that had provided reliable GPS-calculated position data. The first phase was the refinement of the drift target and SLDMB motion over the ground for each of the five main drifts. Initially, time-series U (east-west) and V (north-south) vector components were computed from successive GPS positions for each drift target and SLDMB. (By convention, eastward and northward vector components were represented as positive values and westward and southward vector components were represented as negative values.) In some cases, anomalous spikes in these vector time-series helped to highlight small-scale position errors relative to the large and obvious position jumps detected during the initial review and reduction of the position data. Although they only produced small changes in position, these jumps still had an impact on the consistency of the corresponding velocity time-series. To automate detection and editing of the velocity outliers, each velocity time-series was first split into high- and low-frequency portions by application of a Chebychev 3-hour high-pass filter. Next, a time-series estimate of the standard deviation was obtained for the high-frequency portion by computing the running mean of the high frequency variance over the time-series. If the observed magnitude of the high-frequency portion of the velocity deviated from the running mean by more than three standard deviations at a given instant, then the identified outlier was replaced with the low-frequency velocity estimate. After a final smoothing of all of the velocity data based on the vector motion review, a final vector motion time-series plot was generated for each drift. Along with the drift target and SLDMB trajectories, these plots provided a view of the CMB wind speed and direction data over the course of the drift. These final time-series vector motion plots were useful for illustrating how the drift targets and SLDMBs moved relative to one another, and also how their motion may have been impacted by winds over the course of the drift.

The second analysis phase was the resolution of the leeway time-series for each drift target. Leeway was either directly measured by an on-board current meter (direct method), or based on the observed motion of the drift target relative to the surface current field (indirect method). The direct method was applied in those cases when a raft-mounted downward-looking ADCP was available to provide a direct measurement of the drift target's motion relative to the sea surface. The indirect method was applied in all other cases when a collective analysis of the SLDMB motion data was required to compute the current field at the location of each drift target. The drift target leeway was then calculated from the difference between the refined time-series vector data derived from the first phase and the surface current motion. Based on the data-logging intervals employed for the required data, the direct method resulted in 10-minute current field data, and the indirect method resulted in 30-minute current field data; this would also be the data interval carried through for the subsequent leeway analyses.

The calculation of leeway in the direct case was relatively straightforward because the ADCP measured leeway directly. ADCP data obtained from Drifts Two and Four were used. The raw, 2-second, time-series ADCP data were first averaged over a five-minute interval to remove high-frequency interferences caused by waves, roll, pitch and yaw of the raft, and ocean surface turbulence. The raw ADCP data were originally acquired in 25-cm depth bins; the initial averaging maintained data within these same bins. The first useable data bin began at a depth of

approximately 75 cm because returns closer to the transducer are affected by acoustic noise and are blanked out. By convention, ADCP current measurements are associated with the vertical center of each data bin, so in this case the observed currents in the first bin were associated with 25-cm-thick bin centered at a depth of approximately 87.5 cm. The ADCP raft movement data were finally run through a 20-minute low-pass filter to generate the 10-minute current field data that would be used for the subsequent direct leeway calculations. To confirm the consistency of the results, the ADCP current vector data were compared to adjacent SLDMB vector data for the same period. Because the rafts were moving relative to the sea surface current, this (ADCP-measured) motion was removed from the raft motion over the ground to obtain an estimate of the current over the ground.

The indirect method was computationally complex and was affected by a variety of factors (e.g., individual SLDMB motions, distance between the SLDMBs, and location of the drift target relative to nearby SLDMBs). The indirect surface current estimate at each drift target was derived from the low-frequency, band-pass, and high-frequency components of the movements of nearby SLDMBs in the study area. The contributions from SLDMB motions in each frequency band consisted of a time-varying spatial average for that frequency band derived from all SLDMBs, and a spatially-varying correction to the spatial average that was based on individual SLDMB motions and distances separating the applicable SLDMBs. The spatially-varying correction term was obtained by the Statistical Interpolation (SI) technique, which is also known as the Objective Analysis procedure (Bretherton et al. 1986, Emery and Thompson 2004). The SI functions as a distance-weighted interpolation technique that calculates the surface current field at each point in space and each time step within each frequency band. Specifically, the SI, like weighted averaging, estimates a value of deviation from the spatial average at each location as a sum of the products of measured deviations at adjacent points and weighting corrections. In this case, the measured values were deviations of the velocity of each applicable SLDMB (in the applicable frequency band) from the spatial average (also in the applicable frequency band). The SI weighting correction applied to each SLDMB velocity deviation was the magnitude of the spatial correlation function corresponding to the separation distance between the drift target and the SLDMB for the applicable frequency band. The weight of each SLDMB deviation vector was also influenced by correlations between all SLDMBs that were taken into account in a calculation for the applicable time step. In addition to providing a velocity estimate at the drift target, the SI also produced an estimate of the portion of spatial variance that was not recovered by the calculation; this is referred to as the error variance. Because the SI was performed separately for each frequency band, the overall error variance of a velocity estimate was the sum of error variances associated with each frequency band. The square root of this sum, in units of velocity, is typically accepted as a measure of error of a statistically interpolated velocity value. This error estimate was included with each indirect current field computation to provide a statistical indication of the quality of the estimated current velocities.

The first step in the indirect current field analysis was to decompose the vector motion of each SLDMB into eastward and northward components. Each vector series was then filtered to extract its low, high, and band-pass frequency components. Within each frequency band, the velocity component time-series from all SLDMBs were combined to create three spatial average surface current time-series over the study period. When summed, these three frequency band spatial averages (low, high, and band-pass frequency) created a spatially-uniform, time-varying



estimate of the sea surface current field. The three components of this spatially uniform series formed the basis for the spatially-varying current field estimate by the indirect method needed for each of the drift targets.

Once the mean surface current field was determined, spatial correlation functions were calculated for each of the three frequency bands. Separation distances were calculated between each combination of SLDMB pairs as a function of time over the course of the study. The eastward and northward velocity vector components in the three frequency bands at each time interval were compared for each of the SLDMB pairs to generate correlation data points that were then grouped into 1-km bins based on the concurrent distance between the SLDMB pairs. All SLDMB correlation pairs within each of the separation distance bins were then used to compute a correlation function for the eastward and northward components for each of the three frequency bands. Ultimately, the current field measurements for a drift target were based on the computed spatial mean that was then adjusted based on the instantaneous deviation from the spatial mean associated with the low-pass, band-pass, and high-pass contribution from each of the applicable SLDMBs. An estimate of the SLDMB variance contribution for each frequency band was computed from the distance-based correlation function, the SLDMB distance from the drift target, and the SLDMB's concurrent velocity deviation from the spatial average at each step along the time-series.

The third phase of the analysis process was to develop the downwind and crosswind leeway coefficients for each drift target configuration. Separate and comprehensive data files were developed for each drift target using the valid GPS data from each drift. The primary elements of these data files were the filtered GPS time and position data for the drift target, the computed vector motion of the drift target, the applicable wind speed and direction data from the CMB, the computed surface current vector, and the leeway vector. Data files based on direct current measurements provided by the ADCP were spaced at 10-minute intervals and those based on indirect current estimated derived from the SI technique were spaced at 30-minute intervals. The computed leeway movement data was examined relative to the recorded wind speed and direction data to obtain the downwind and crosswind leeway coefficients for each drift target from each drift. Progressive vector diagrams were also generated to reveal trends in the downwind and crosswind motions of the targets over time relative to the local wind. Because the estimated error of the current field measurements varied between drifts, each drift target was initially analyzed individually. After the individual leeway coefficients were computed, the data were grouped by drift target type (e.g., drogued SEIE raft, undrogued SEIE raft, and SEPIRB) so that average results could be computed and the consistency of the results could be evaluated.

The goal of the analysis was to derive coefficients for leeway velocity models. Past studies have modeled the relationship between wind speed and leeway speed as linear (Fitzgerald et al., 1993). For this study, both constrained and unconstrained linear regressions were used to describe both the downwind and crosswind leeway speeds relative to the 10-m wind speed. The simple linear regression model is of the form:

$$V_L = Y + \text{slope} * V_{10}$$

where:

$V_L$  is the leeway speed in knots;

Y is the y-intercept in knots;  
slope is the slope of the regression line; and  
 $V_{10}$  is the wind speed at 10 m above the sea surface in knots.

For the constrained regression model, the y-axis intercept value, Y, is fixed at zero. To assist in evaluating the quality of the regression model, the following statistics were computed as part of the analyses:

- Number of sample points included in the regression model (n)
- Standard error of the estimate computed from the scatter of the data about the regression line ( $Sy/x$ )
- Correlation coefficient of the regression (r)
- The measure of the linearity of the data ( $r^2$ )
- Measure of the bias introduced by the constrained estimate (Bias)

When evaluating the “quality” of the regression estimate, several factors need to be considered, including the bias, the standard error of the estimated regression, and the correlation coefficient. The bias between the measured data and the estimated regression is the difference between the average of the measured data (leeway downwind and crosswind values) and the average of the values computed from the estimated regression for the same wind speeds. It can be shown theoretically, that the unconstrained linear regression is an unbiased estimate of the data, while the constrained linear regression is a biased estimate. The correlation coefficient of the regression (r) measures the statistical strength of the linear dependence between the measured leeway speed (downwind and crosswind) and that estimated from the regression. Because both the constrained and unconstrained regressions are linearly dependent on the wind speed, the correlation coefficient also measures the statistical strength of linear dependence between the measured leeway speed and the wind speed. The correlation coefficients for the constrained and unconstrained regressions are identical because calculation of the correlation coefficient in both cases effectively involves the same data. A negative correlation coefficient between the measured leeway values and the regressed leeway values indicates that the regression does not provide a reasonable physical description of the data. The squared correlation coefficient ( $r^2$ ) measures the portion of variance in the data which is explained by the regression model; the larger the value of  $r^2$ , the better the regression model. While this holds true for comparison of the same models for different data (e.g., comparison of the quality of unconstrained regressions for the downwind and crosswind leeway speed), it does not apply when evaluating the “goodness” of fit of different models to the same data (because both the unconstrained and constrained regression models have the same  $r^2$ ). In these cases, the bias and the standard error of the estimated regression ( $Sy/x$ ) must be considered when evaluating the “quality” of the regression.

### **3.0 EXPERIMENTAL RESULTS**

The following sections provide an overview of the data provided by the CMB, as well as a summary of the drift target data obtained during each of the drift deployments. An initial preliminary drift run was conducted on 29 and 30 October 2005 to check the performance of the targets and electronic equipment under realistic conditions, to gather preliminary information on relative target drift rates, and to test deployment and recovery techniques. The first drift (Drift One) for the field study began with target deployment on 31 October, and the final drift (Drift Five) for the field study concluded with target recovery on 19 November.

#### **3.1 Monitoring Buoy Data Results**

##### **3.1.1 Coastal Monitoring Buoy**

As discussed in Section 2.1.2, the CMB mooring was initially deployed on 30 October and recovered for the final time on 19 November. Due to problems associated with connection of the ARGOS transmitter onto the buoy platform, there was a gap in the meteorological data from 2 November until 6 November. Due to the timing of the drift target deployments, the CMB data gap impacted only the last few hours of the Drift One target run. After the end of the field study, the raw data from the initial (30 October) and second deployment (6 November) periods were converted into the proper engineering units by applying calibration coefficients to each of the raw data fields. A local magnetic variation of  $20.3^{\circ}$  W was then applied to the wind and current direction data to obtain true directions. An initial time-series view of the processed CMB data showed that, with the exception of the gap between deployments, the CMB provided full data return for each of the eight measured parameters throughout the measurement period. Though the wind and current data were initially processed and stored as U (east-west) and V (north-south) vector components, these data were also converted to magnitude and direction to assist with the evaluation of wind speed during the various drift runs and with comparisons to other meteorological data. The preliminary CMB average wind-speed and wind-gust data were used to help characterize each of the various drift runs within the planned wind-speed categories.

During QA/QC of the CMB data, the wind speed and direction results from the CMB were compared to the hourly wind speed and direction data at St. John's International Airport over the same period. Though the St. John's airport wind data were from a shore station located more than 20 miles from the CMB mooring location, the airport data still provided a reasonable comparison data set. Oceans, Ltd. also provided model-derived wind direction and magnitude data for the CMB mooring location. The results of this comparison to these other data sources clearly showed a significant offset in the CMB wind direction during the second deployment period (Figure 5, panel (a)). For the shorter first deployment period, the wind directions compared well. The wind magnitudes generally agreed well for both deployments, except during periods of northerly winds when the St. John's airport winds were noticeably weaker (probably due to elevated topography north of the airport; Figure 5, panel (b)).

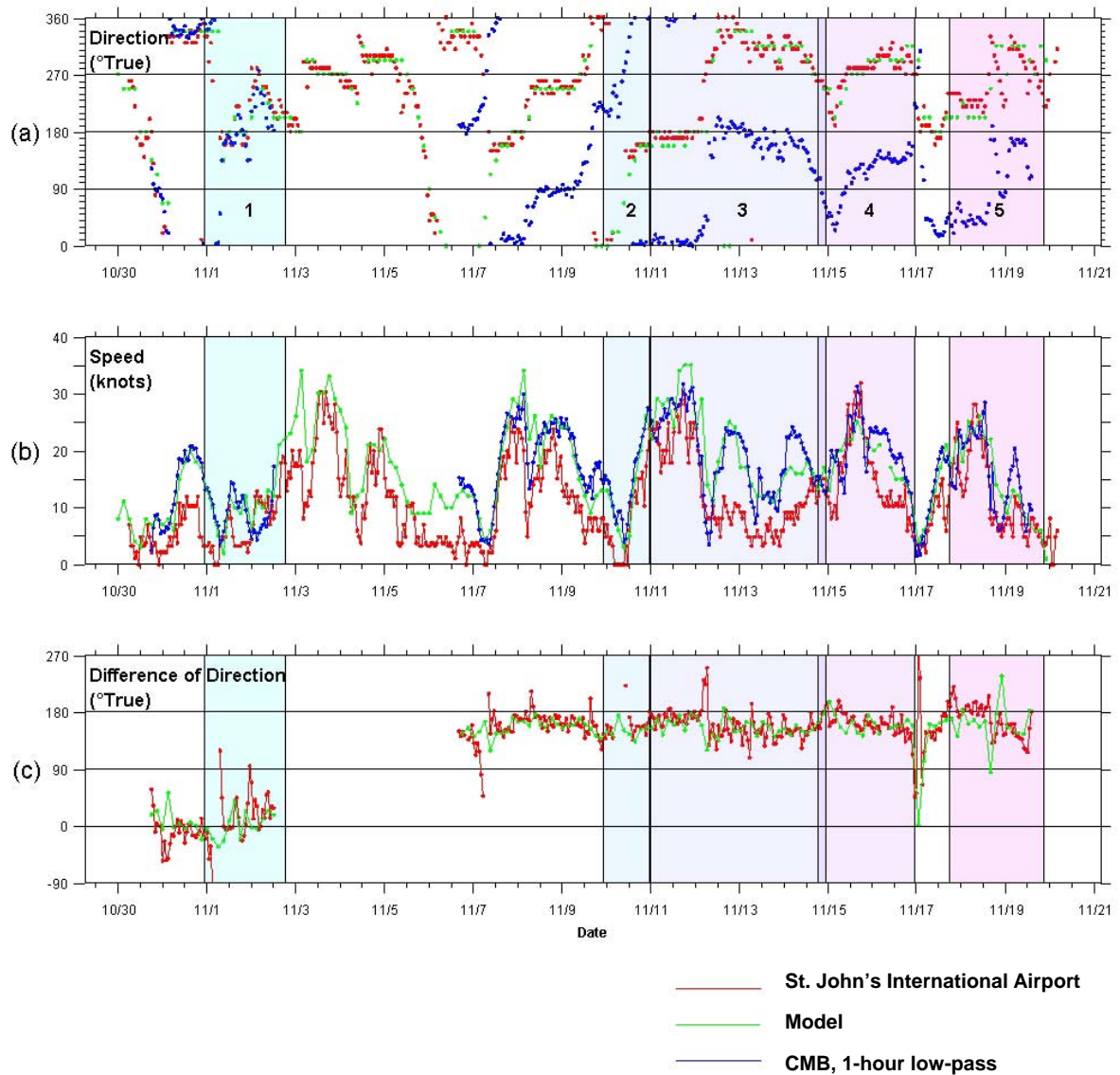


Figure 5. Times-series views of the uncorrected CMB wind data relative to the St. John's airport observations and Oceans, Ltd. model prediction for the location of the CMB. Panel (a) shows wind direction data. Panel (b) shows the wind speed data. Panel (c) shows the magnitude of the offset between the CMB direction and St. John's airport and Oceans, Ltd. wind direction.

Based on an initial review of the wind direction offset for the second deployment, it appeared that the CMB wind direction was 180 degrees out of phase with the airport wind direction. It was speculated that this may have been an artifact associated with the buoy power failure that occurred during the attempt to install the ARGOS transmitter. However, upon a closer review of the CMB data, it became apparent that the magnitude of the direction offset was not 180 degrees (Figure 5, panel (c)). The reported CMB wind direction is based upon a buoy orientation sensor (an internal clamping compass) and a wind direction sensor that measures the angular offset between the wind vane and heading of the buoy's reference axis. Because the buoy itself tends to align with the predominant wind direction (particularly in stronger wind conditions), the buoy orientation data provide a useable indication of the wind direction. When operating properly, the wind direction sensor will normally provide small angular offsets that are applied to the buoy orientation data to compute the instantaneous wind direction.

During the first deployment, the wind direction data appeared as expected and the computed wind direction data matched well with St. John's airport. For the second deployment, the buoy orientation data still appeared valid based on the strong correlation with the St. John's airport data (Figure 6). However, the angular offsets from the wind direction sensor were not focused around 0 degrees as would have been expected, but instead appeared clustered around 215 degrees (Figure 6, panel (b)). Panel (b) of Figure 6 shows the wind direction sensor data versus the buoy orientation sensor data for both deployments. Data points are color-coded by wind speed into three ranges. This figure shows that during the windier periods of the first deployment (red and green points at the lower left of the figure), the wind direction sensor values were clustered around 0 degrees; the computed average offset during this period was 0.7 degrees. During the windier periods of the second deployment (magenta and blue points), the wind direction sensor values were strongly clustered around 215 degrees; the computed average offset during this period was 215.1 degrees.

The wind vane sensor ring for the CMB is mechanically keyed and can only be installed in a single configuration aligned with the buoy's heads-up position. A male orientation pin of the upper cone is connected to the lower cone via a matching reference hole. After close inspection and re-testing at SAIC's Newport facility after the field study, it was determined that the pin and lock system of the buoy broke loose during the deployment, likely accounting for the offset in wind direction. A visual inspection showed that reference marks generated by SAIC personnel prior to initial deployment did not line up during re-testing and that the internal connection terminal was not fully secure. Because the extent of the offset was variable and dependent on how the locking connection was mechanically secured prior to deployment, there was no way to precisely measure this offset after the buoy had been recovered and disassembled.

Results of the correction for wind direction are shown in Figure 7. In order to make the CMB wind direction data useable for the subsequent leeway analyses, the observed wind direction offset for the second deployment had to be quantified and then removed. Because the observed bias (or offset) was not completely consistent across the full range of observed buoy orientation headings, an offset correlation curve was generated across the full range of buoy orientation headings based on all measured wind direction values when wind speeds were above 10 m/s. This offset correlation curve was then adjusted based on the observed offset between the first and second deployments during those periods when the buoy orientation heading was similar. This reduced the recorded wind direction offset values to near 0 degrees. Adjusted wind direction

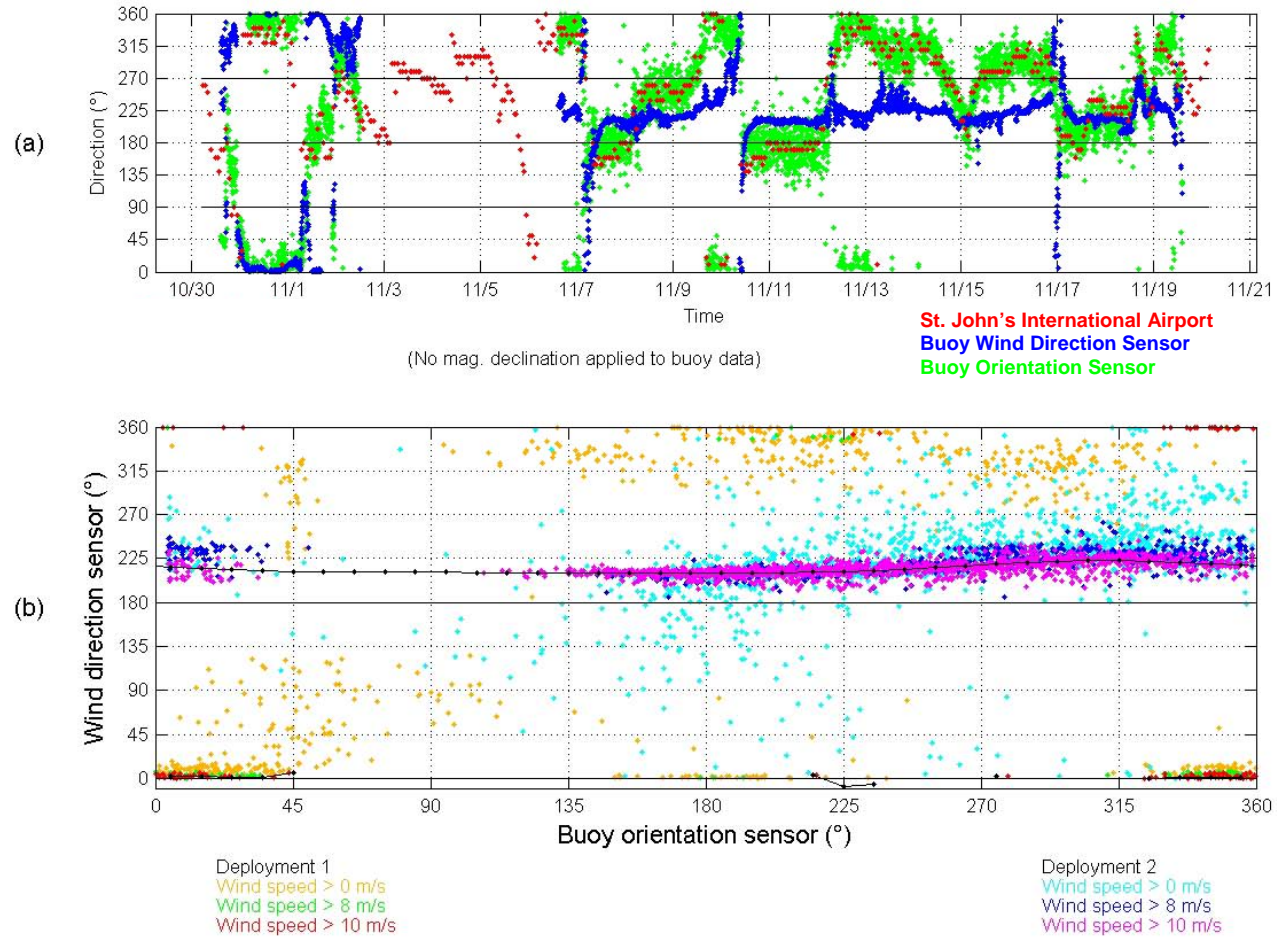
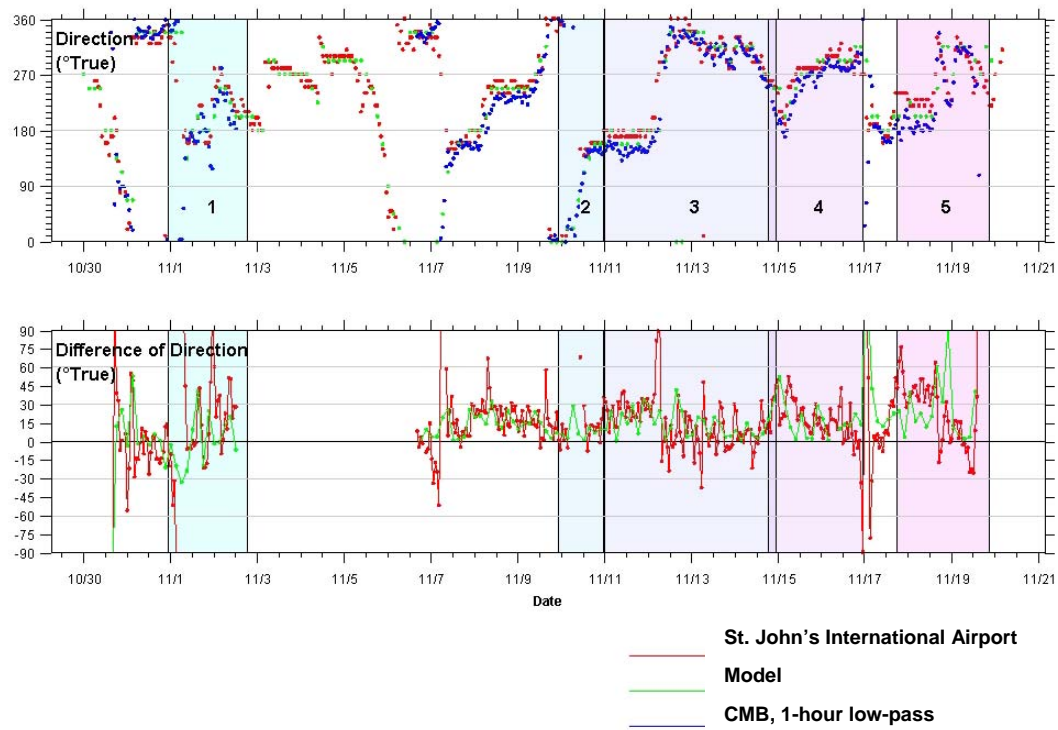


Figure 6. Detailed view of the two primary measurements that were used to compute the wind speed direction for the CMB data. Panel (a) shows the raw measurements for the buoy orientation sensor and the wind direction sensor, as well as the St. John's wind direction. Panel (b) shows the distribution of the wind direction sensor values based upon the heading of the buoy orientation sensor. The values are color-coded by wind speed to help illustrate the consistency of the wind direction sensor measurements during higher wind speed periods.

a)



b)

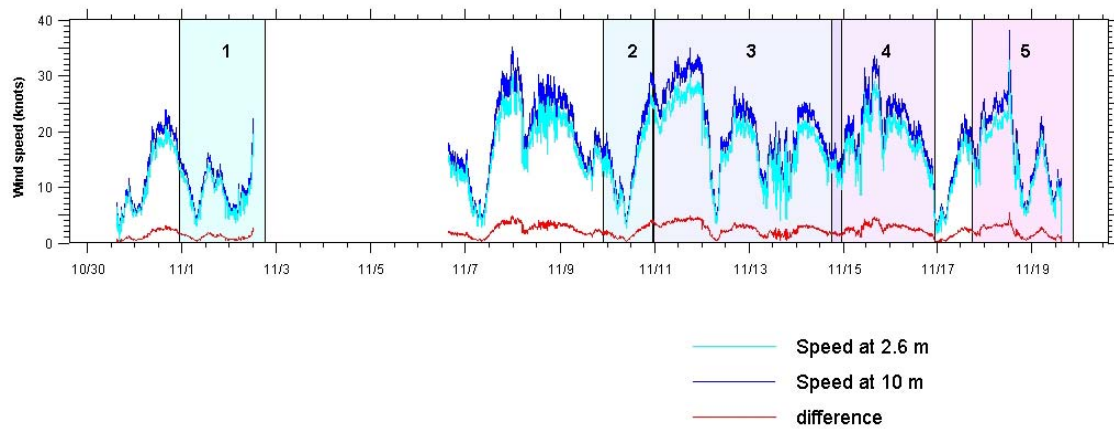


Figure 7. Time-series views of the CMB wind data after corrections were made to direction and speed. Panel (a) shows the revised CMB wind direction ( $^{\circ}\text{T}$ ) in blue, and observed differences with the St. John's airport (red) and modeled wind (green) direction data. Panel (b) shows the time-series view of the effect of the 10-m reference height adjustment to the computed CMB wind magnitude data.



offset values were then combined with the buoy orientation data to compute the adjusted true wind-direction data, shown as the blue series in Figure 7. As this figure shows, the recomputed CMB direction data for the second deployment generally agreed well with the St. John's airport data. Agreement was poorer at times when wind speed and direction were changing and during periods of northerly winds when the St. John's airport winds were noticeably weaker, perhaps a result of topography north of the airport.

The CMB wind speed data were then run through a MATLAB routine to adjust speed from the 2.6-m sensor height up to the 10-m reference height (panel (a) in Figure 8). This reference height adjustment resulted in an increase in the wind speed that varied from 1 to 5 knots, depending on the original value. Finally, these adjusted winds were run through both 20-minute and 1-hour Chebychev low-pass filters to prepare them for eventual incorporation into the leeway analyses data files (panel (b) in Figure 8). The filtering process produced wind direction and speed data at either 10-minute (direct) or 30-minute (indirect) time steps.

### **3.1.2 Waverider Buoy**

The 0.9-m Datawell Directional Waverider buoy was deployed on 28 October within the primary operations area and recovered on 16 November. Waverider data were telemetered to a receiving system at the Oceans, Ltd. office in St. John's and data were recorded at either hourly or half-hourly intervals throughout the deployment period. Some intermittent gaps in the record were caused by loss of the communication link between the buoy and the receiving station. Waverider data were processed and analyzed by Oceans, Ltd. Final Waverider data files were provided electronically to SAIC in late January 2006. In addition to date and time, the final Waverider data files included the following measured parameters: significant wave height, mean zero crossing period, peak frequency, peak period, ratio of peak period to mean zero crossing period, mean direction of spectral peak, and sea surface temperature. A time-series view of the Waverider data show the buoy results over the course of the deployment (Figure 9).

The Waverider data were intended to be used to compute the correlation between wave height and downwind and crosswind leeway components, and also to assess the impacts of building and decaying wave fields on drift target trajectories. However, the largest significant wave heights and also the two main periods of building and decaying wave fields occurred during times when useable drift target data were not acquired. The most prominent building and decaying wave field period occurred from 3 November through 9 November. This coincided with the period when the CMB was disabled and no drift target deployments were conducted. The other main period of building and decaying wave fields occurred from 11 November through 14 November. Though Drift Three did occur within this time-frame, the drift targets recovered from this period provided ARGOS-derived position data only and were not included in the subsequent leeway analysis. Most of the useable drift target data for the leeway analyses came from Drifts Two, Four, and Five. There was relatively little change in the recorded significant wave height during Drifts Two and Four, and the Waverider buoy had already been retrieved prior to the start of Drift Five. Because of the lack of sufficient and meaningful wave height data during the primary drift target periods, no further analyses were conducted with these data.



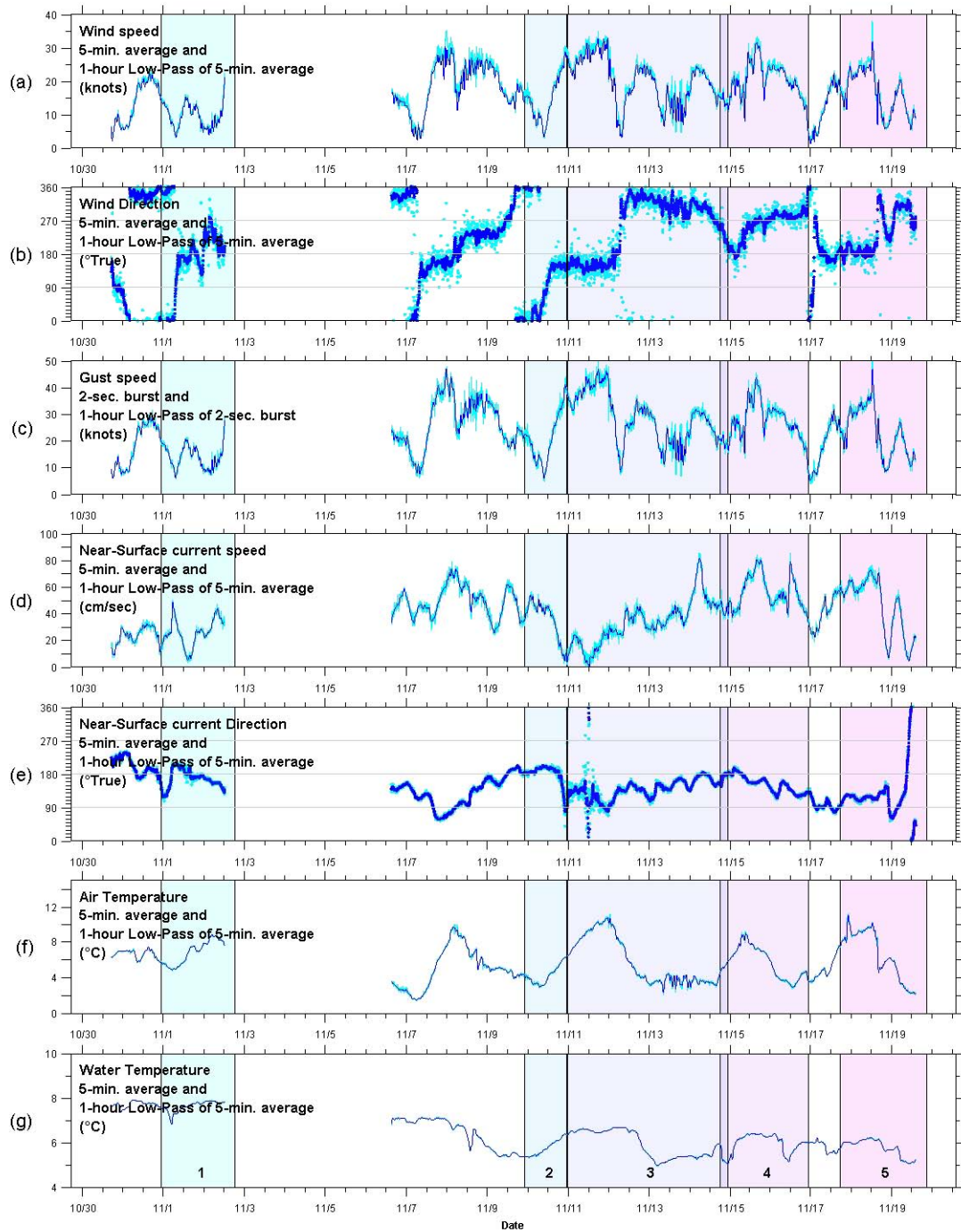


Figure 8. Complete time-series view of the CMB data, reflecting both the wind direction offset and the 10-m reference height adjustment. Shaded areas indicate time frame of primary drift runs. Drift numbers appear on the bottom panel (g).

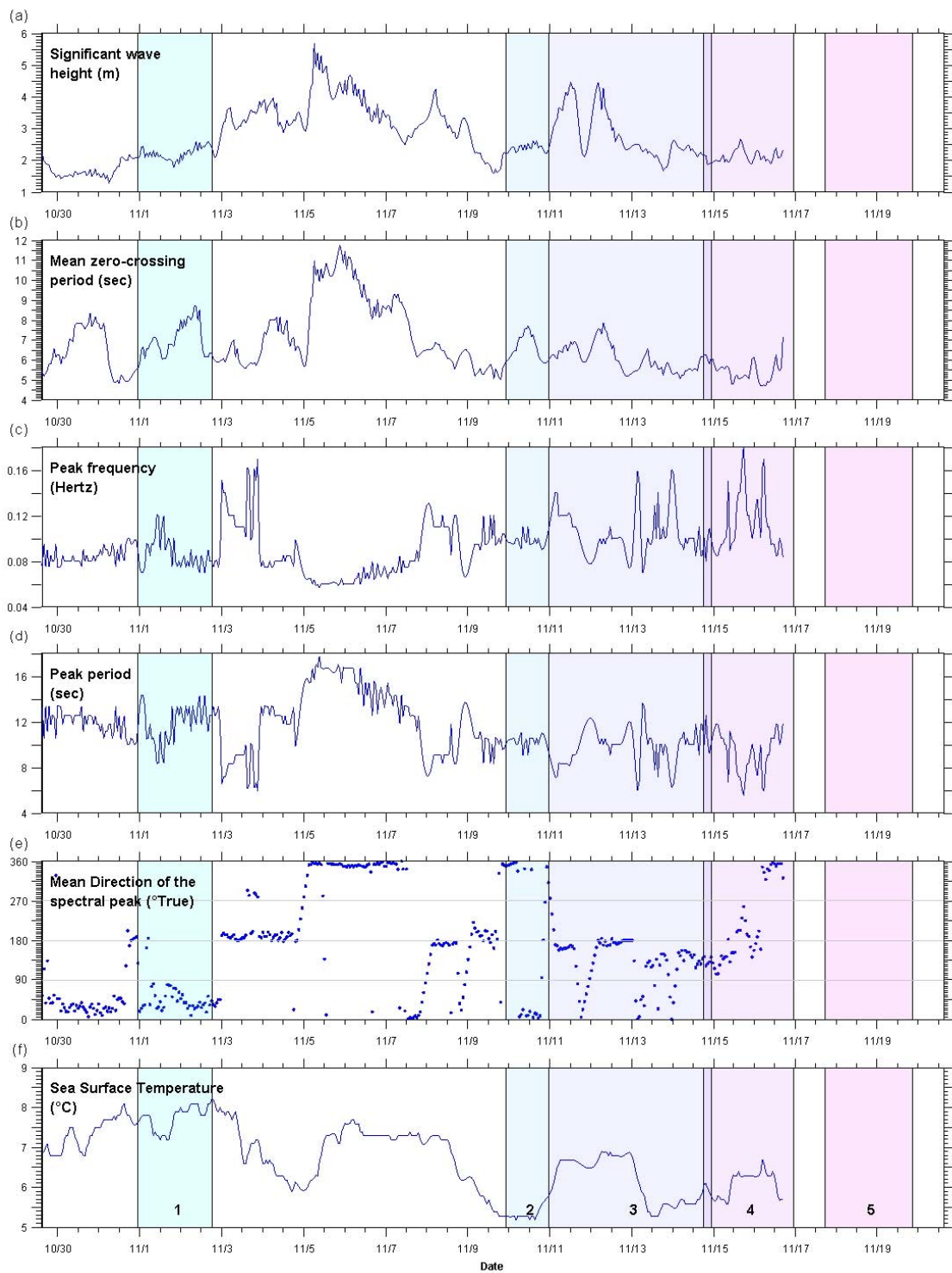


Figure 9. Time-series view of the Waverider data over the complete deployment period. Shaded areas indicate the time frame of primary drift runs; drift numbers are shown on the bottom panel (f).

### 3.2 SEIE Life Raft and SEPIRB Drift Results

The primary goal of the field program was to deploy and track SEIE life rafts and SEPIRBs, under varying wind conditions, for durations of approximately two days per deployment. The deployment pattern was fairly similar for all five drifts, in that a cluster of drift targets (e.g., SEIE rafts, SEPIRBs) were released at a central deployment location. The SLDMBs were released at a nominal distance of 1 km (Drift One) and 5 km (Drifts Two through Five) in each cardinal direction (i.e., 000, 090, 180, and 270 degrees True) around the central location. Deployment and recovery information, and the data return for each target for each drift run is summarized in Table 3. Figures 10 through 14 show the trajectories of targets deployed during each drift run. SEPIRB data are shown when data concurrent with the other drifters was returned; however, because the SEPIRBs were typically deployed over a much longer time-scale and covered much greater distances, their trajectories are also shown in separately (Figures 15 and 16).

In Table 3, the “Deployment” and “Recovery” columns indicate the dates and times that each drift target was deployed and recovered. Drift target deployment times were generally consistent within a drift run, but the recovery times showed more variation because recovery was sequential in nature. In some instances, targets that were “Not Recovered” would provide useful data via ARGOS before they were ultimately lost. The “Position Data Return” columns are intended to provide an overview of the data return associated with each of the deployed drift targets. The “Duration” field indicates the duration of the data set, the “Interval” field indicates the time step of the data obtained, and the “Type” field indicates whether the position data were derived using the internal GPS or were calculated by the ARGOS system. In most cases, the duration of each data set was consistent with length of time between deployment and recovery; however, for some cases, data were acquired for only a portion of the time that a target was deployed. The data return frequency of the various ARGOS-calculated data sets was highly variable, particularly for the SEPIRBs. The data calculated by the ARGOS system have not been used in the leeway analyses.

The position data used to generate the track plots shown in Figures 10 through 16 have been filtered to remove obvious positioning errors. Due to the much larger volume of SLDMB data (relative to the other data sets), the initial filtering of these data represented a proportionately larger effort. The recorded GPS data that were downloaded from the recovered SEIE rafts were of generally high quality and required only minimal smoothing or editing. There were a few SEIE raft deployments (Drift Three and Drift Five) that occurred without the GPS data loggers installed on the rafts due to concerns about recovery (associated related to raft integrity and rough weather). In Drift One and Drift Four, the onboard GPS data loggers failed due to flooding or loss of the raft; in both of these cases, transmitted ARGOS data were available over some or all of the deployment period. The transmitted ARGOS data from these various raft deployments were intermittent and somewhat noisier than the recorded GPS data. Again, the ARGOS-calculated position data were not used in the leeway analyses.

Most of the initial SEPIRB position data were based only on the GPS positions transmitted by ARGOS provided through the Clearwater SEPIRB units (PTTs 53241, 53242, and 53243; Figure 15).

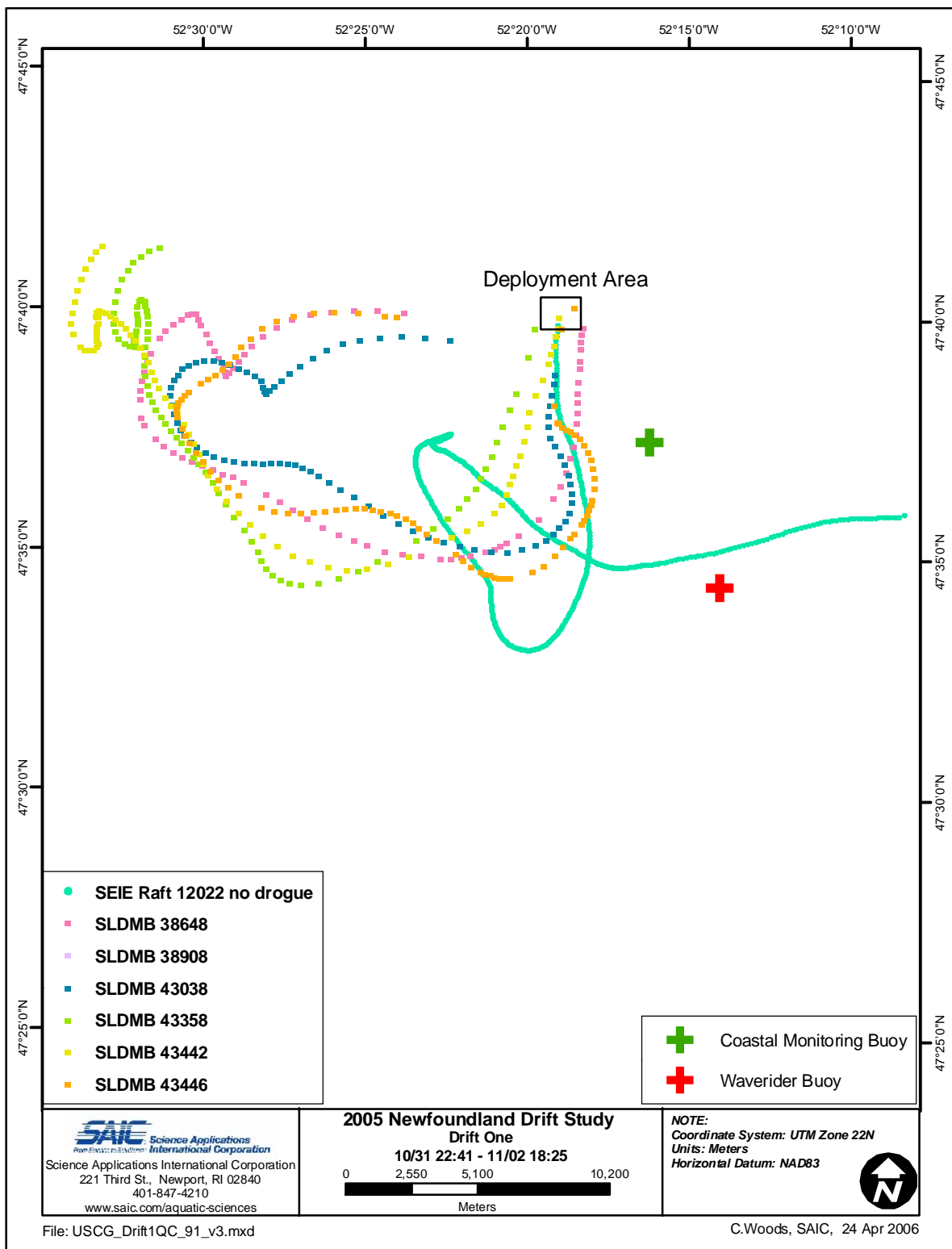


Figure 10. Trajectories of SEIE raft and SLDMBs for Drift One from 31 October to 2 November.

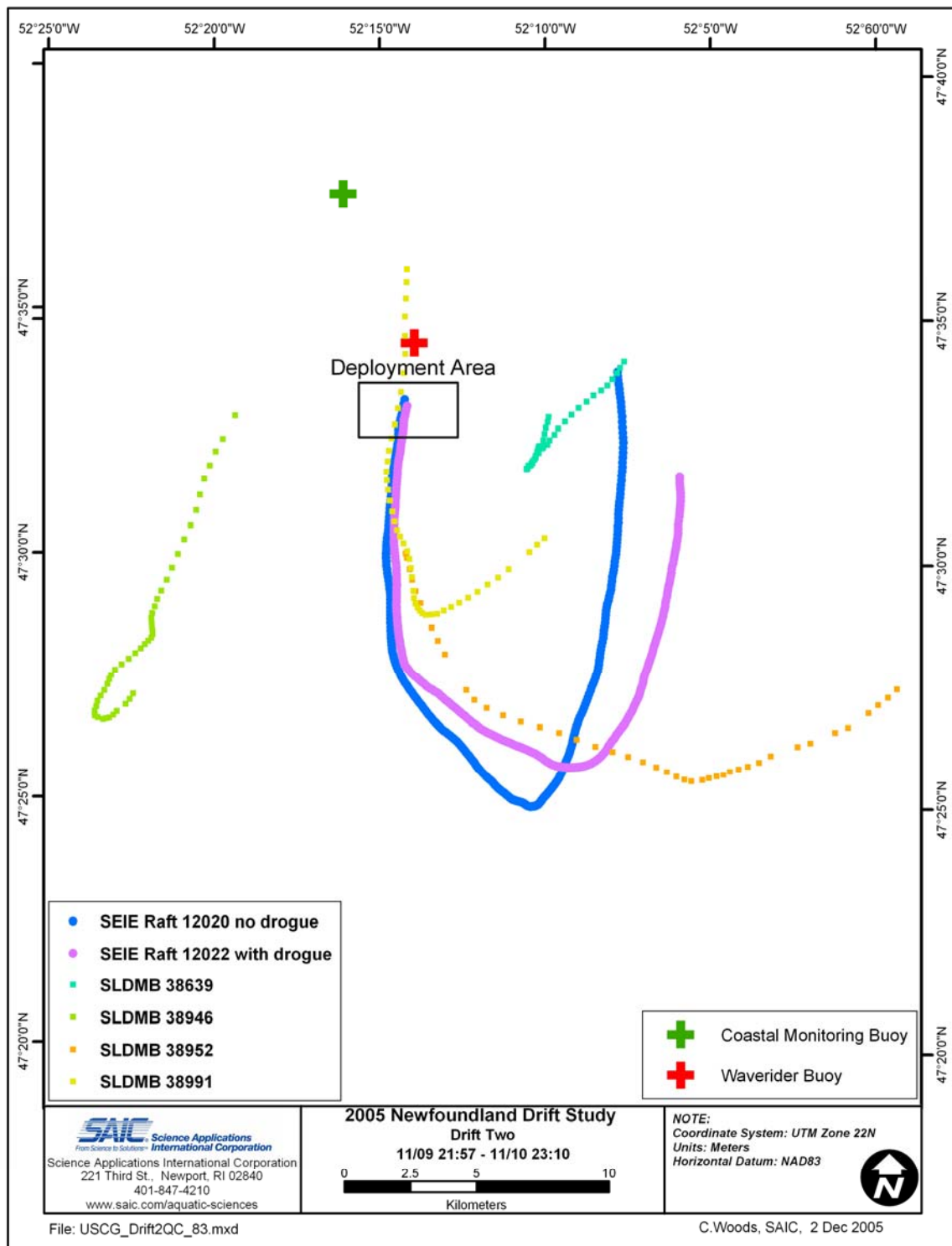


Figure 11. Trajectories of SEIE rafts and SLDMBs for Drift Two from deployment on 9 November to recovery on 10 November.

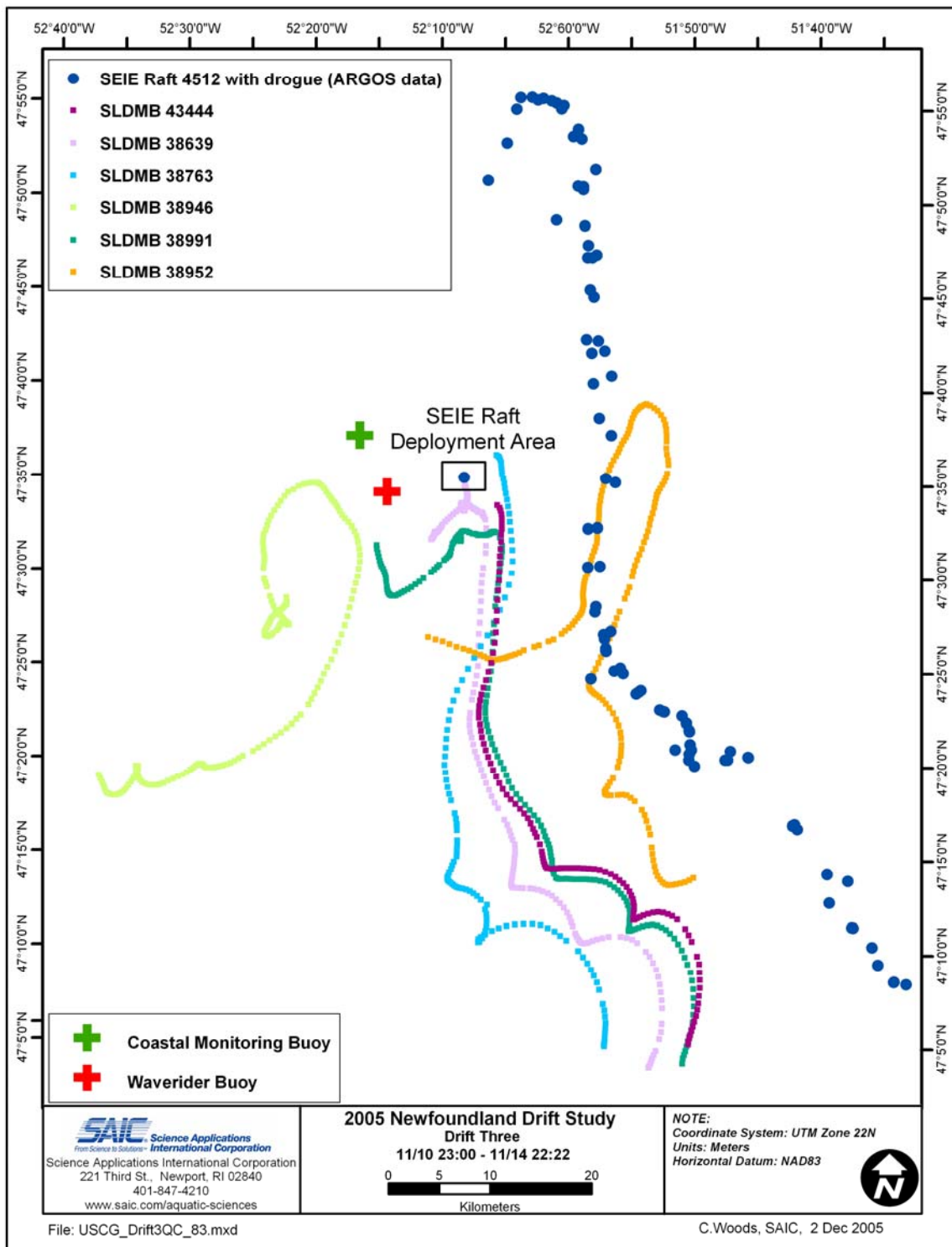


Figure 12. Trajectories of SEIE raft and SLDMBs for Drift Three from deployment on 10 November to recovery on 14 November.

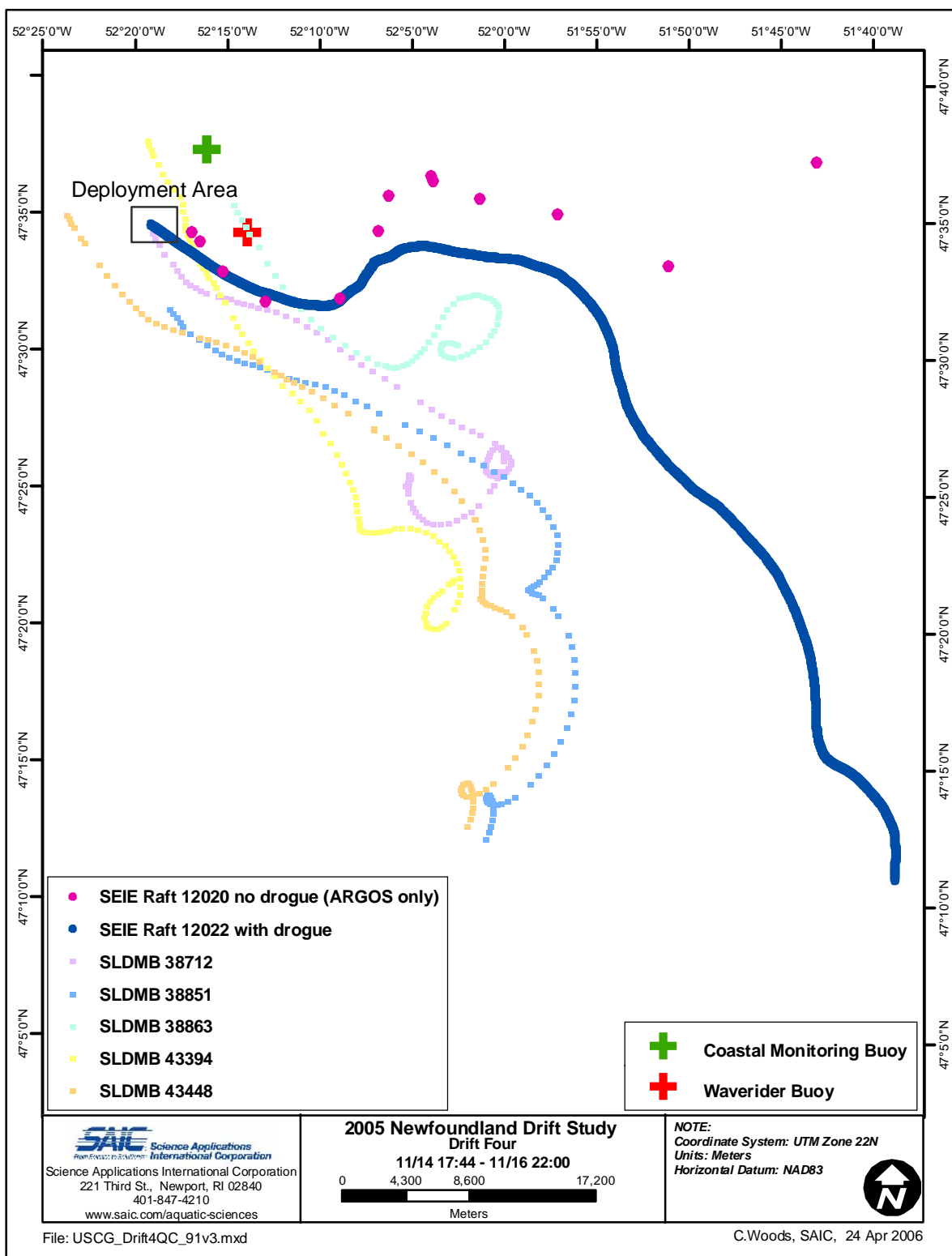


Figure 13. Trajectories of SEIE rafts and SLDMBs for Drift Four from deployment on 14 November to recovery on 16 November.







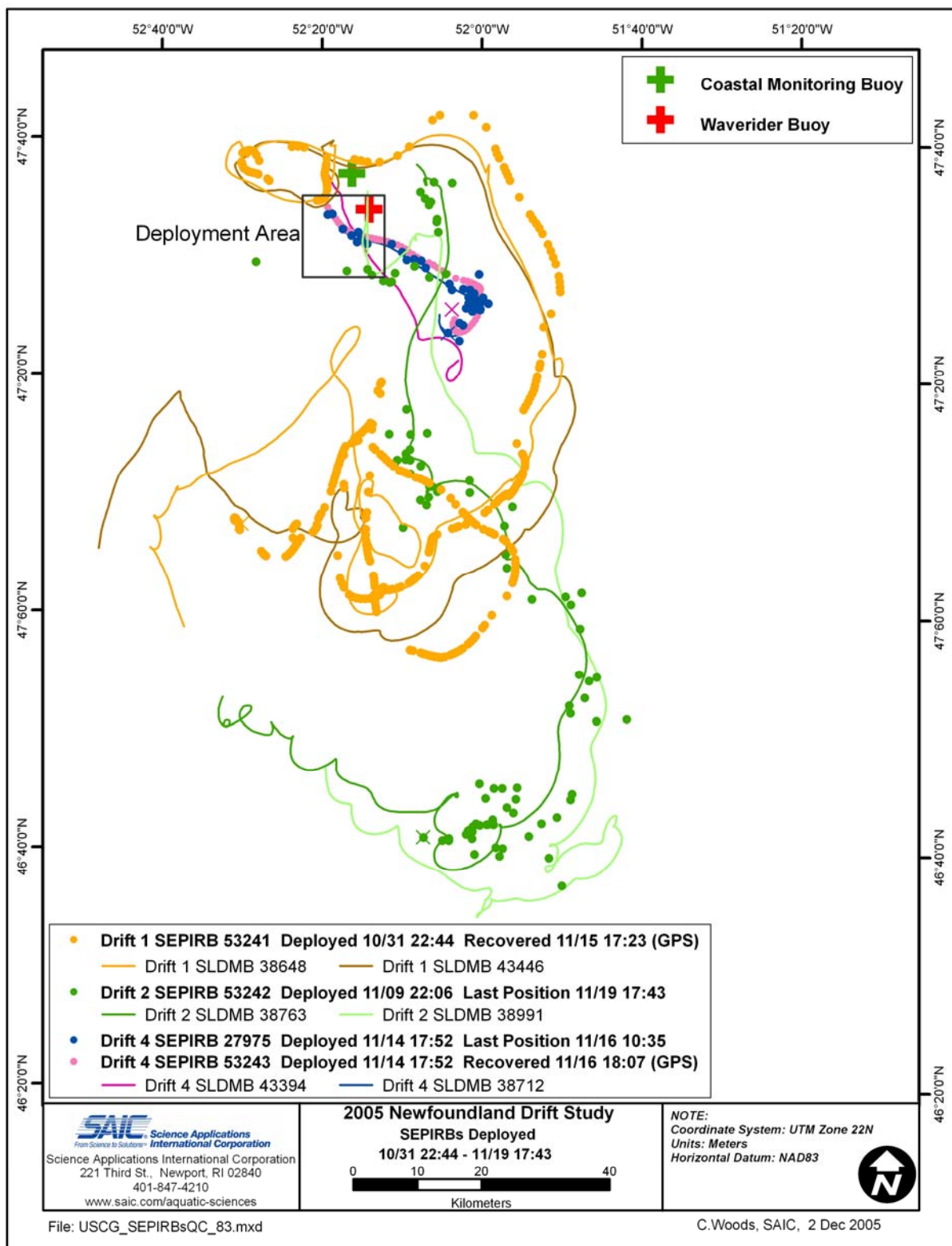


Figure 15. Trajectories of SEPIRBs from ARGOS-calculated positions from Drifts One through Five.

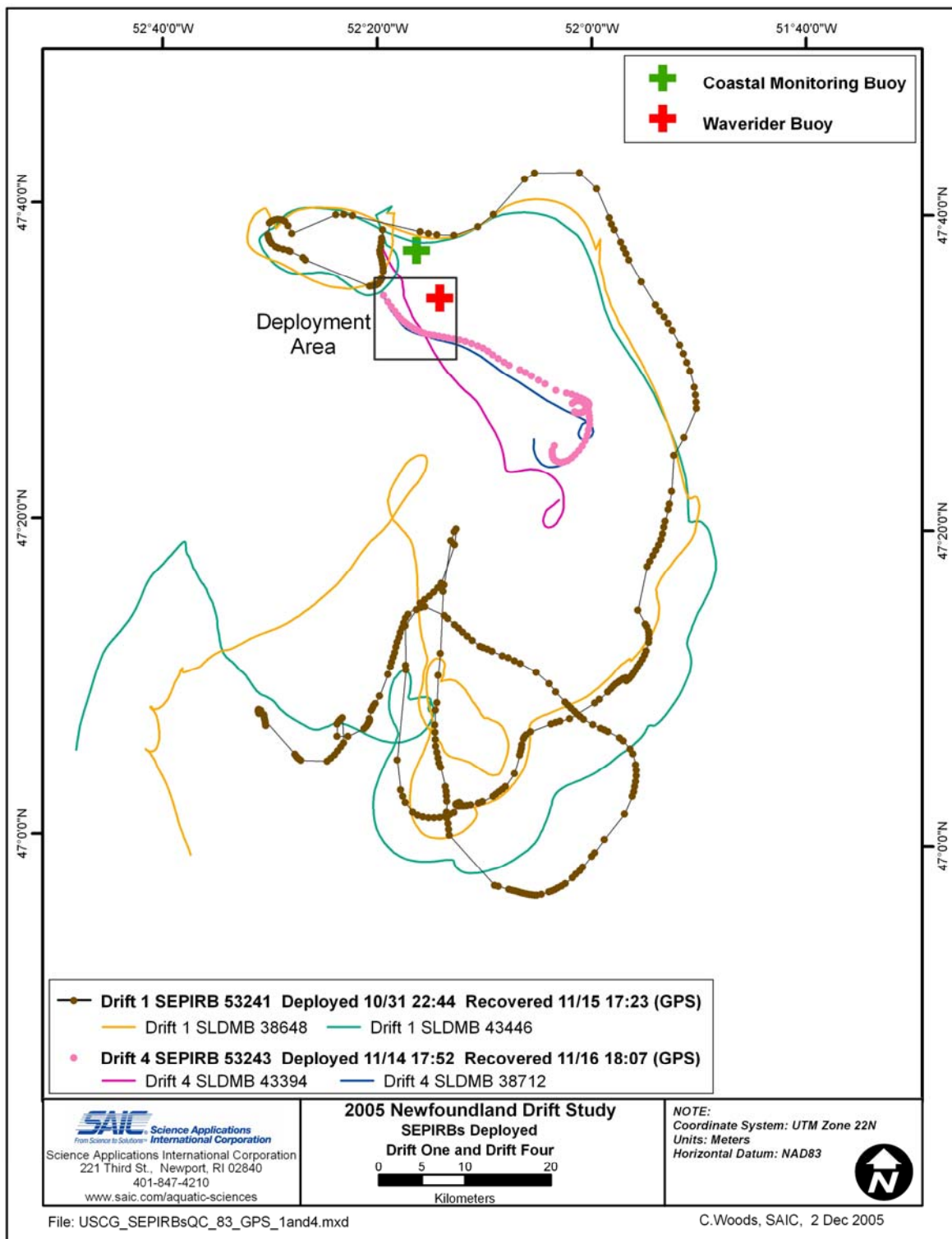


Figure 16. Trajectories of SEPIRBs from GPS-calculated positions during Drifts One and Four.

Table 3. Drift target deployment and recovery information for each of the five primary drift runs.

Drift	Drifter	PTT	Deployment Date / Time	Recovery Date / Time	Position Data Return			Max Wind Speed (knots)			Notes
					Duration (hrs)	Interval	Type	5-min Raw		30-min	
								Avg	Gust	Low-pass	
One	SEIE Raft w/ drogue	12021	10/31/05 22:37	11/2/05 15:10	40.4	Sporadic	ARGOS	19.6	22.9	18.5	Deflated and flooded on recovery; ARGOS data available
	SEIE Raft	12022	10/31/05 22:39	11/2/05 18:25	43.7	5 min	GPS				Flooded and partially submerged on recovery
	SEPIRB	53241	10/31/05 22:44	11/15/05 17:23	347.3	Sporadic	ARGOS	38.6	41.1	32.8	Transmitted until recovered on 11-15 / GPS data message
	SLDMBs					30 min	GPS				38648, 43442, 43358, 43038, 43446
Two	SEIE Raft	12020	11/9/05 21:57	11/10/05 23:10	25.2	5 min	GPS	32.5	36.7	28.4	SmartCat 4512
	SEIE Raft w/ drogue	12022	11/9/05 22:03	11/10/05 22:48	24.6	5 min	GPS				ADCP data acquired, SmartCat 4514, Backfloat
	SEPIRB	53242	11/9/05 22:06	Not Recovered	240.3	Sporadic	ARGOS	32.5	36.7	28.4	Transmitted until 11-23 use until 11-19 / GPS data message
	SLDMBs					30 min	GPS				38952, 38639, 38946, 38991
Three	SEIE Raft w/ drogue	4512	11/10/05 23:53	11/14/05 22:22	61.3	Sporadic	ARGOS	38.6	41.1	32.8	Deployed with SmartCat (4512) only / no GPS
	SEPIRB	27980	11/10/05 23:49	Not Recovered	None	N/A	N/A				Lost at sea - possibly during deployment
	SLDMBs		11/10/05 23:48	11/14/05 1:49		30 min	GPS	38.6	41.1	32.8	43444, 38763, 43087
Four	SEIE Raft	12020	11/14/05 17:44	Not Recovered	21.2	Sporadic	ARGOS	34.6	38.7	31.9	Lost at sea / ARGOS data until 11/15 at 1503
	SEIE Raft w/ drogue	12022	11/14/05 17:46	11/16/05 21:51	52.1	5 min	GPS				ADCP data acquired, Backfloat
	SEPIRB	53243	11/14/05 17:52	11/16/05 18:07	49.3	Sporadic	ARGOS	34.6	38.7	31.9	GPS data message
	SEPIRB	27975	11/14/05 17:52	Not Recovered	40.6	Sporadic	ARGOS				Transmitted until 11/16 at 1035 / Lost at sea
	SLDMBs					30 min	GPS				38712, 43448, 43394, 38863, 38851
Five	SEIE Raft w/ drogue	27956	11/17/05 16:36	11/19/05 18:59	7.6	5 min	GPS	38.1	43.0	32.1	Deflated and overturned when recovered, Backfloat
	SEIE Raft w/ drogue	12022	11/17/05 16:37	11/19/05 19:50	49.4	Sporadic	ARGOS				Deployed with ADISS ARGOS only / no GPS
	SEPIRB	53243	11/17/05 16:40	Not Recovered	None	N/A	N/A	38.1	43.0	32.1	No transmissions received / Lost at sea
	SEPIRB	52341	11/17/05 16:40	Not Recovered	None	N/A	N/A				No transmissions received / Lost at sea
	SLDMBs					30 min	GPS				43444, 38952, 38946, 38669, 43394

Note: m/s to knots (divide by 0.5144)

However, after the GPS data messages for these SEPIRBs were parsed by Oceans, Ltd., the position data quality and density improved significantly (Figure 16). Because these Units did not have an onboard logging capability, the original position data calculated by the ARGOS system were intermittent, with some long time gaps between position records. In addition, due to the difficulties in tracking and recovering the SEPIRBs, these units tended to be deployed for much longer periods of time. For example, SEPIRB 53241 was originally deployed on 30 October at the start of Drift One and was not recovered until 15 November (the end of Drift Four). Despite the long deployment periods, there were at least two SLDMBs that remained in the general vicinity of the drifting SEPIRBs (Figure 15). Though some SEPIRBs deployed were capable of internally logging GPS data during Drifts Three, Four, and Five, none of these units were recovered, and the only data provided by these units were the sporadic ARGOS-calculated positions.

The following sections will provide a more detailed review of each of the five primary Drifts. These sections will focus primarily on the drift targets that were deployed, with less focus on the SLDMBs. A detailed presentation of the SLDMB trajectories will be presented in Section 4.1 where the development of the current vector fields for each of the drift targets is addressed.

### **3.2.1 Drift One**

Two SEIE life rafts (12021 and 12022) and one SEPIRB (53241) were deployed on 31 October. Raft 12021 had a drogue attached to the stern, while raft 12022 was undrogued. Both rafts were recovered on 2 November for a total of approximately two and half days at sea (Figure 10). During this period, the maximum observed five-minute averaged wind speed was 19.6 knots and the peak gust was 22.9 knots (Table 3). Though both rafts were recovered, Raft 12021 was mostly deflated and flooded upon recovery, and provided no useable data due to failure of the GPS data logger. Raft 12022 was also flooded and submerged in the bow when recovered, but the data logger was not damaged and a full GPS data set was acquired from this raft. The SEPIRB remained at sea much longer and was eventually recovered on 15 November. Based on the GPS data transmitted by this unit, a trajectory plot was compiled for SEPIRB 53241 for almost the entire period of this deployment (Figure 16). In addition, as mentioned above, a few of the SLDMBs that were deployed during this drift remained in reasonably close proximity to this SEPIRB.

The SLDMBs that were deployed in close proximity (approximately 1 km apart) to one another at the start of this drift moved in a southerly direction for approximately 10 km before heading in a west-northwesterly direction, and eventually looping back around towards the east (Figure 10). All five of the deployed SLDMBs remained relatively close to each other through most of Drift One when two of the units (43358 and 43442) began to follow a more northerly track. SEIE Raft 12022 moved off in a similar manner to the SLDMBs, though it traveled a much shorter distance to the west, before turning north, and then moved rapidly to the east. At the time of recovery, it was almost 20 km away from the closest SLDMB (Figure 10).

### **3.2.2 Drift Two**

Two SEIE life rafts (12020 and 12022) and one SEPIRB (53242) were deployed on 9 November. Raft 12022 was drogued and also included the bottom-mounted ADCP, while Raft 12020 was not drogued. Both rafts remained at sea for approximately one full day and were recovered in

good condition. The maximum five-minute averaged wind speed was 32.5 knots with a peak gust speed of 36.7 knots. Complete GPS data sets were recovered for both rafts, and the on-board ADCP data were also recovered from Raft 12022. SEPIRB 53242 transmitted ARGOS position data sporadically until 23 November; however, it could not be located and was not recovered. Based on the ARGOS data track, this SEPIRB eventually ended up more than 100 km southeast of the original deployment location (Figure 15). Although GPS data messages were transmitted by this SEPIRB, it appears as if the on-board GPS receiver failed because none of the GPS messages provided useable position data. The only position data available from this SEPIRB are the sporadic ARGOS data. Because its data return was sporadic, particularly during Drift Two, SEPIRB 53242 data is not included in the data sets used for leeway coefficient determination that are shown in Figure 16.

Both rafts stayed on similar tracks, initially moving due south for approximately 10 km before turning southeast, and then back to the north (Figure 11). As would be expected, the undrogued raft (12020) traveled somewhat farther to the south and then also to the north, than the drogued raft (12022). The four SLDMBs for Drift Two were initially deployed approximately 5 km to the west, north, east, and south of the main drift target deployment location. Though each of the SLDMBs showed the same general southwestward trend before moving off to the northeast, they all moved at different speeds during different portions of the drift period. In addition, SLDMB 38952 had a much greater eastward component than any of the other SLDMBs (Figure 11).

### **3.2.3 Drift Three**

Drift Three was initiated concurrently with the recovery of the Drift Two targets in order to take advantage of a high wind event, also due to some concerns about future ship availability. Because of the high wind conditions and concerns about recovery of the targets, only one drogued SEIE Raft (4512) and one SEPIRB (27980) were deployed for this drift. In addition, the GPS data enclosure was removed from the raft and it was deployed with only a SmartCat ARGOS beacon for position data. The SEIE raft was eventually recovered on 14 November for a total of four days at sea. A peak wind gust of 41.1 knots occurred during Drift Three, while the maximum five-minute averaged wind speed was 38.6 knots (Table 3).

After a fairly lengthy data gap at the start of the deployment, relatively dense ARGOS position data were available for most of the period that the raft was in the water (Figure 12). The SEPIRB never transmitted any data via ARGOS after it was deployed and was not recovered. A total of six SLDMBs were used during Drift Three, four of which were previously deployed for Drift Two and two that were deployed at the start of Drift Three. Four of the six SLDMBs tracked primarily to the south and then slightly to the southeast (Figure 12). Based on the ARGOS positions, the life raft tracked initially to the north, then headed back toward the south, and finally turned to the southeast at the end of the drift run.

### **3.2.4 Drift Four**

Two SEIE life rafts (12020 and 12022) and two SEPIRBs (53243 and 27975) were deployed on 14 November. Raft 12022 was drogued and also included the bottom-mounted ADCP, while Raft 12020 was not drogued. Raft 12022 was recovered on 16 November after approximately three days at sea. The maximum five-minute averaged wind speed for Drift Four was 34.6 knots, while the peak observed gust was 38.7 knots. Raft 12020 was not recovered and was presumed lost at sea. Based on the transmitted ARGOS positions that were received before this raft was lost, this raft tracked rapidly to the east (Figure 13). SEPIRB 53243 was recovered on 16

November after approximately three days at sea. The other SEPIRB (27975) transmitted sporadically until 16 November; however, it was not recovered and was eventually lost at sea. SEPIRB 27975 transmitted sporadically during Drift Four (Figure 15), so its data were not used for leeway coefficient calculations.

Five SLDMBs were deployed during Drift Four. Initially, all five SLDMBs followed the same drift trend, drifting towards the southeast and finally moving in a more southerly direction. The one exception was SLDMB 38863, which was deployed to the east of the drift objects. After drifting southwest, it headed to the northeast for a short time, ultimately drifting to the southwest. The two life rafts initially tracked southeast; the drogued raft continued on this southeast track, while the non-drogued raft drifted to the northeast. The movements of SEPIRBs 27975 and 53243 closely mirrored those of adjacent SLDMBs 43394 and 38712 (Figure 15).

### **3.2.5 Drift Five**

Two SEIE life rafts (12022 and 27956) and two SEPIRBs (53241 and 53243) were deployed on 17 November. Due to a lack of remaining GPS loggers, Raft 12022 was deployed with only an ARGOS transmitter. Both rafts were equipped with drogues attached at the stern and were recovered in close proximity to one another on 19 November after approximately three days at sea. The maximum five-minute averaged wind speed for Drift Five was 38.1 knots, while the peak observed gust was 43.0 knots. Raft 27596 was found deflated and overturned upon recovery, though the data logger recorded a short data set (presumably before it turned over). The track for SEIE 27596 shown in Figure 14 is therefore short and does not show its recovery location. Based on the ARGOS data for Raft 12022, the rafts initially moved in an east-northeast direction, then turned and drifted in a southeast direction until recovery. Though the SEPIRBs were examined and tested prior to deployment, both failed to transmit any data after they had been deployed.

## **4.0 LEEWAY DATA ANALYSIS**

Data analysis involved three primary elements: 1) reduction of the drift target and SLDMB position data to produce the final trajectories; 2) determination of the surface current field at each drift target location by the direct or indirect means; and 3) computation of downwind and crosswind leeway coefficients for each drift target type (e.g., drogued SEIE raft, undrogued SEIE raft, and SEPIRB). Because position data calculated by the ARGOS system were at irregular time intervals, all of the analyses described below were conducted only on the drift targets that had acquired reliable GPS position data (Table 3). In conducting the analyses described below, a large number of figures were generated to support and describe the results for each drift target during each drift. To improve the readability of the report, the number of figures is limited to examples illustrating each step of the analysis. Although figures with representative results are included for each of the steps described below, the remaining figures and supporting information have been grouped by drift target type in Appendix A.

### **4.1 Trajectory Analyses**

The trajectory analyses entailed a more detailed review of the drift target and SLDMB motion over ground for each of the successful drift deployments. Initially, time-series east-west and north-south vector components were computed between each two successive GPS positions for each drift target and SLDMB. By convention, eastward and northward vector components were represented as positive values and westward and southward vector components as negative values. The filtering technique described in Section 2.3 was used to replace outliers in the velocity time-series, producing the final vector motion time-series for each drift target data set (e.g. Figure 17).

The eastward and northward components of the vector motion time-series for adjacent SLDMBs were superimposed on the corresponding vector motion series of each drift target (e.g. panels (a) and (b) in Figures 17 for the drogued raft during Drift Two) to provide a perspective of spatial motion patterns in the surface current field around each drift target. Concurrent wind vector components obtained from the CMB were then added (e.g. panel (c) in Figure 17) to provide an indication of how the motion of the drift targets may have been impacted by winds over the course of the drift. The response of the drogued SEIE raft relative to the SLDMBs and the predominant wind direction during Drift Two is shown as an example in Figure 17. In response to both southeastward surface currents (as indicated by the SLDMB motion) and northerly winds, the SEIE raft moved quickly to the south and then the southeast for the first half of this drift run. About halfway through this drift, the winds decreased, veered to the south-southeast, and then began to increase steadily. The SEIE raft responded quickly to this wind shift and began to move off rapidly in a northerly direction. The surface currents were slower to respond to this wind shift, however, as three of the four SLDMBs did not exhibit a northerly drift component until four to eight hours after the wind shift.



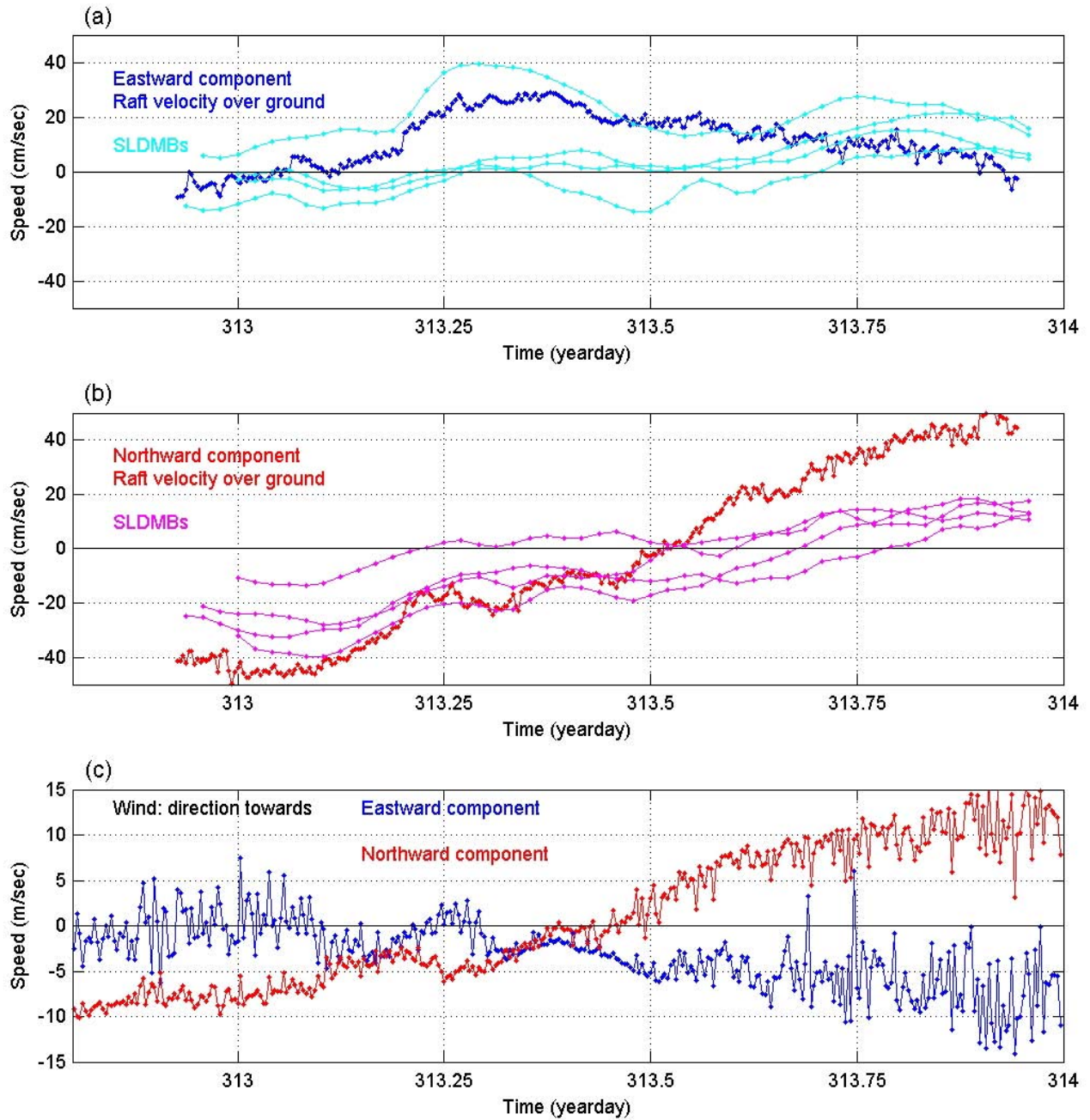


Figure 17. Time-series trajectory plot of the drogued SEIE raft and the SLDMBs during Drift Two. Panels (a) and (b) show the eastward and northward components of the raft and SLDMB velocities over the ground. Panel (c) shows the eastward and northward components of wind velocity in oceanographic notation (i.e., direction that wind is moving towards). The time axis unit is day of year (2005).



During the later part of this drift, the SLDMBs also began to exhibit a more easterly drift component that was also reflected in the motion of the SEIE raft. The behavior of the undrogued raft during this drift was similar to that of the drogued raft, though the responses of the undrogued raft to changes in wind direction and speed, and the total distance covered by this raft were larger.

## **4.2 Surface Current Field Resolution**

The second major element was the resolution of the surface current motion field for each drift, and the development of the specific current motion time-series that would be applied to each drift target. Development of the current motion field was based on either the direct or indirect method. The direct method was applied in those cases during Drifts Two and Four when a raft-mounted downward-looking ADCP was employed to provide a direct measurement of the current field at the drift target. The indirect method was applied in all other cases when a collective analysis of the SLDMB motion data was required to compute the current field at each of the drift targets. Based on the data logging intervals employed for the required data, the direct method resulted in 10-minute current field data and the indirect method resulted in 30-minute current field data; this data interval would be carried through for the subsequent leeway analyses.

### **4.2.1 Direct Current Field Calculations**

ADCP data were used to measure the movement of the drogued rafts relative to the surface waters during Drifts Two and Four. Because the rafts were moving relative to the adjacent surface waters while the ADCP data were being acquired, these data provided a direct measure of the motion of the raft relative to the surface current field. The raw ADCP data were measured at two-second intervals then averaged over a five-minute interval to remove high-frequency motions due to waves, roll, pitch and yaw of the raft, and surface turbulence. The ADCP data at the 0.875 m depth were run through a 20-minute low-pass filter to generate the 10-minute raft motion data that would be used for the subsequent direct leeway analysis computations.

As an example, Figure 18 shows directly measured leeway (raft motion relative to the ocean surface) measured by the ADCP during Drift Two. The drogued raft maintained a small but consistent westward movement relative to the ocean surface throughout the drift (panel (a)). Although the raft itself moved to the east during this drift, it moved more slowly to the east (negative eastward component) than the adjacent surface waters in response to a westward surface wind during the drift. Similarly, the northward component of raft leeway showed an initial southward motion relative to the ocean surface that decreased through the first half of the drift before turning northward and increasing for the remainder of the drift. This reflects that the raft moved somewhat faster relative to the near-surface waters, both initially to the south and then to the north for the last half of the drift. Because the winds shifted from the north to the south over the course of this drift, the response of the northward component in Figure 18 provides a good visual indication of raft leeway. Agreement between the sign (+/-) of the ADCP velocity components in panels (a) and (b) of the figure and winds in panel (c) indicates that the raft is moving downwind relative to the surface current field.

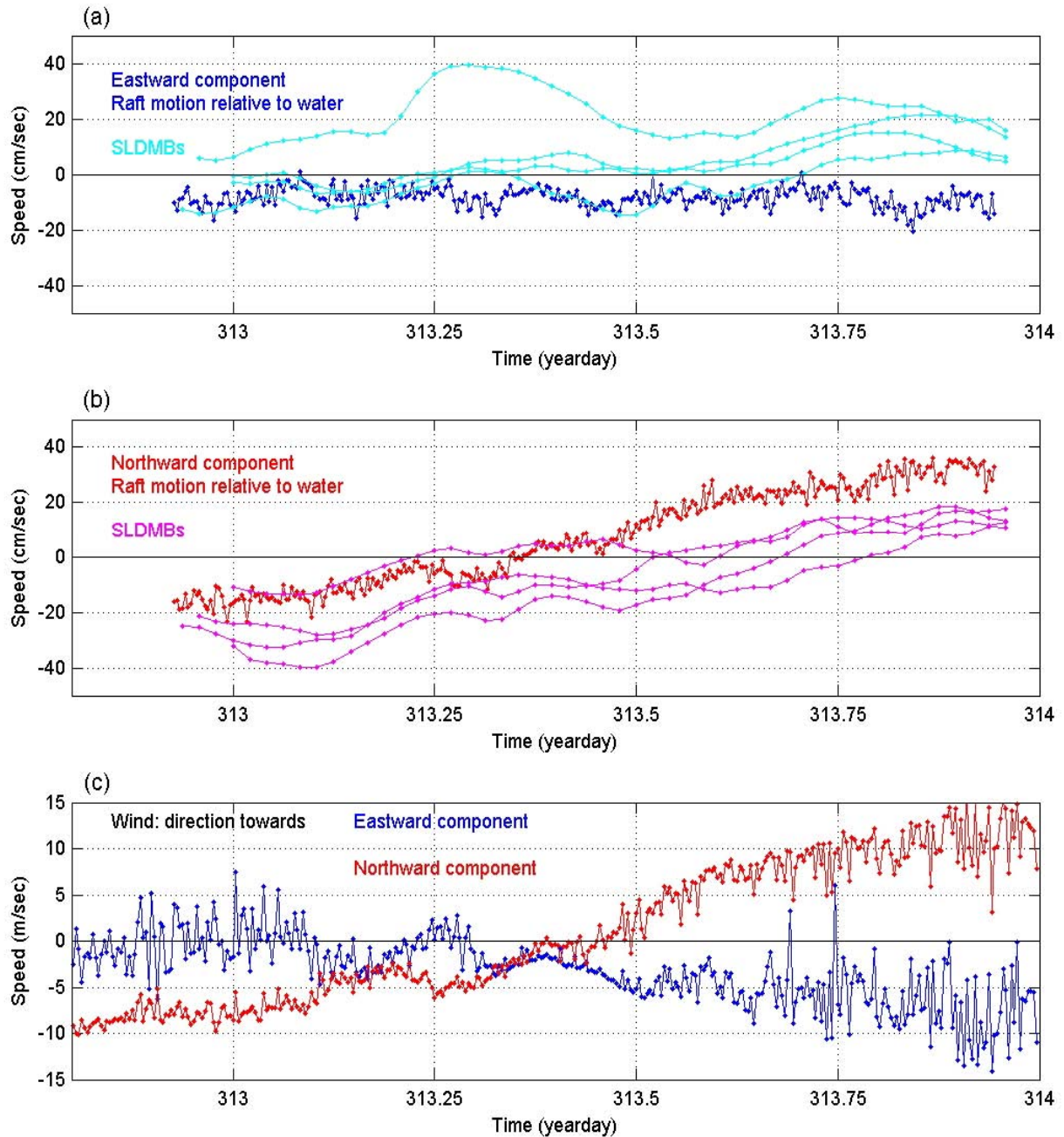


Figure 18. Time-series trajectory plot of the movement of the drogued SEIE raft and SLDMBs relative to the near-surface water and motions of nearby SLDMBs over ground during Drift Two. Panels (a) and (b) depict the eastward and northward components of the raft motion relative to the water surface. Panel (c) depicts the eastward and northward components of the wind vector in oceanographic notation. The time axis unit is day of year (2005).

To examine the accuracy of the averaged ADCP data, the ADCP current vector data were subtracted from the drogued SEIE raft motion for comparison with the motion of adjacent SLDMBs during Drifts Two and Four. Movement of the drogued raft over ground derived from GPS data include the sum of the motion attributable to sea surface currents acting on the raft and leeway due to surface winds. With the leeway component removed by vector subtraction of the ADCP current time-series, the residual will represent the motion of the raft over ground attributable to surface currents. This residual should be consistent with the motion of nearby SLDMBs.

During Drifts Two and Four, the computed SEIE raft motion over the ground compared well with the concurrent motion of the closest SLDMBs. During Drift Two, three of the four deployed SLDMBs moved as a group, but SLDMB 38952 exhibited a disparate eastward motion during the first half of this drift (Figure 19). The eastward component of the drogued SEIE raft motion vector series also differs significantly from the group of three SLDMBs, however, it does agree well with the eastward motion of SLDMB 38952 because this SLDMB was close to the ADCP raft during that part of the Drift. Later in the drift, the trajectories of SLDMB 38952 and the drogued SEIE raft diverge as a result of leeway of the raft, and the similarity of the eastward motions of the raft and SLDMB disappear. The northward motion components of the SLDMBs, and the computed SEIE current field were relatively similar throughout Drift 2. The relatively strong southward motion seen at the beginning of this drift decreased steadily throughout the period, eventually turning northward and increasing during the later portions of the drift. As discussed in Section 4.1 above, a wind shift from the north to the south about halfway through this drift was not reflected in the surface currents until about four-to-eight hours after the wind shift had occurred. The conclusion from this exercise is that the direct leeway measurement technique employed using the ADCP is reasonably accurate, if it can be assumed that the SLDMBs exhibit negligible leeway. Conversely, if the surface current measurement approach is accurate, SLDMBs do exhibit negligibly small leeway.

#### **4.2.2 Indirect Current Field Calculations**

The SI technique (Bretherton, et al., 1976) outlined in Section 2.3 was used to develop indirect current field measurements for this study. The initial step in this analysis was to collectively examine the motions of all SLDMBs over the course of the study in order to decompose the corresponding sea surface current signal into its primary frequency band components. An initial view of the raw time-series SLDMB data clearly showed that forcing processes of varying periods were consistently affecting the SLDMB trajectories (Figures 20 and 21). The time-series filter analyses of these data further revealed that processes in the low- and band-pass frequency ranges had the greatest impact on the SLDMB motion. For these data, low-pass processes were those occurring over periods greater than 24 hours and band-pass processes were those occurring over periods of 10 to 24 hours (or diurnally). The remaining signal components not captured by the low- or band-pass processes were attributed to high-pass frequency processes occurring on periods of less than 10 hours. The vector magnitudes associated with the low-pass processes were sometimes greater than 40 cm/s, while the higher vector magnitudes associated with the band-pass processes were generally less than 20 cm/s. The vector magnitudes associated with the high-pass processes were less than 5 cm/s.

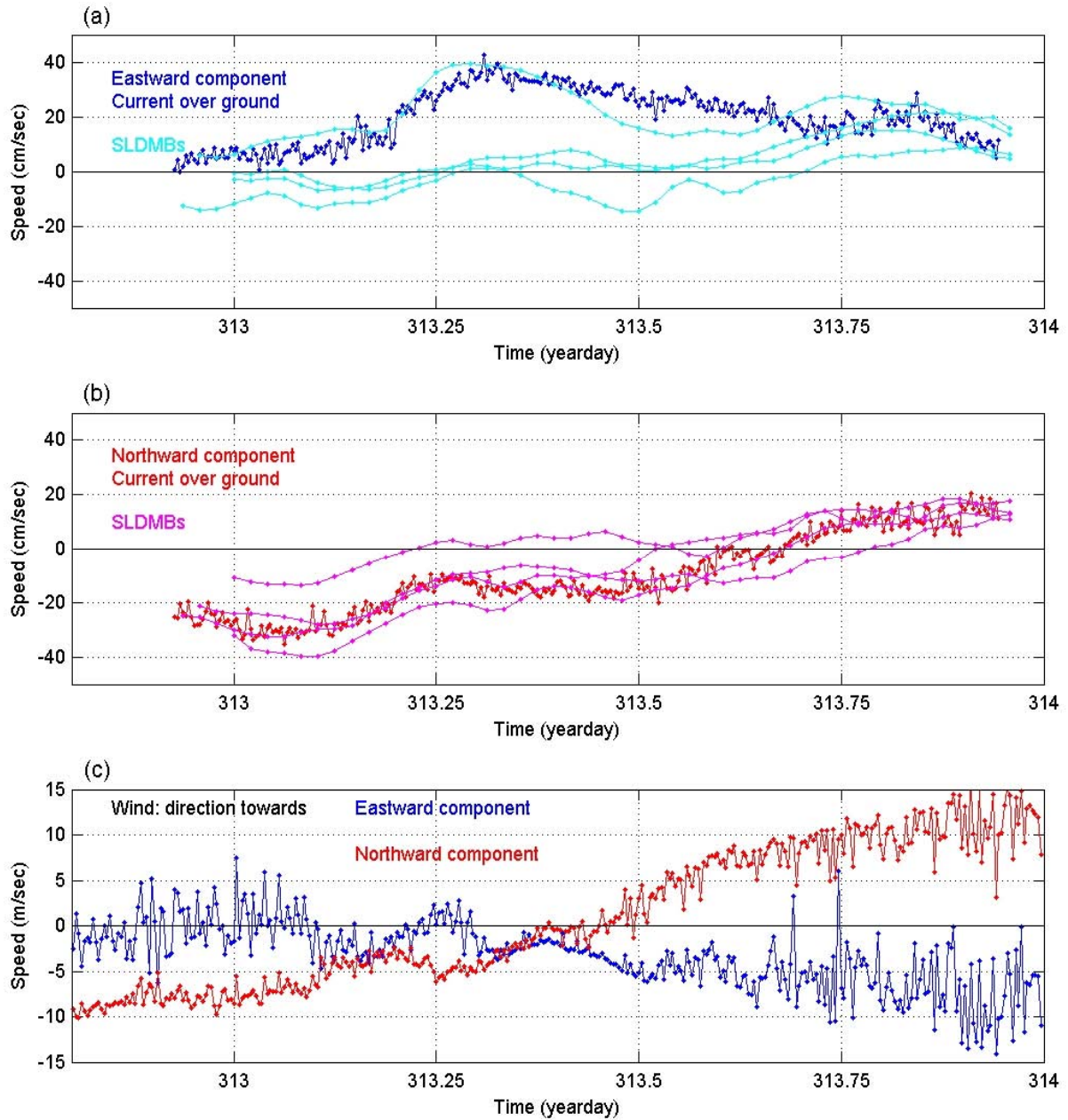


Figure 19. Time-series views of the near-surface current field from drogued raft and SLDMB data during Drift Two. Panels (a) and (b) compare the eastward and northward components of the computed current at the raft with those derived from the SLDMBs. Panel (c) depicts the eastward and northward components of the wind in oceanographic notation. The time axis unit is day of year (2005).



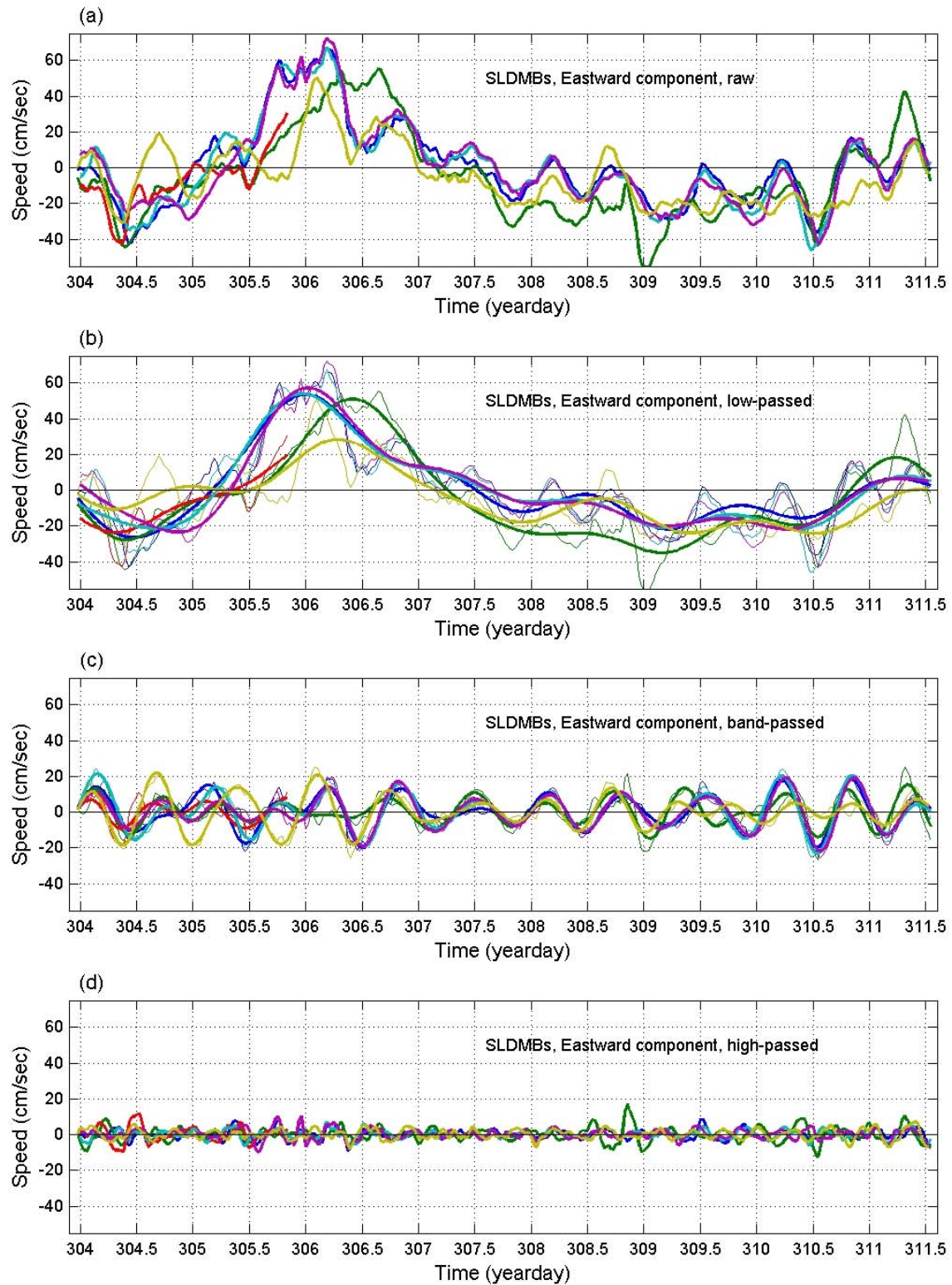


Figure 20. Time-series of the eastward components for SLDMBs deployed during the first 8 days of the field study, as well as the low-pass, band-pass, and high-pass components of the original data

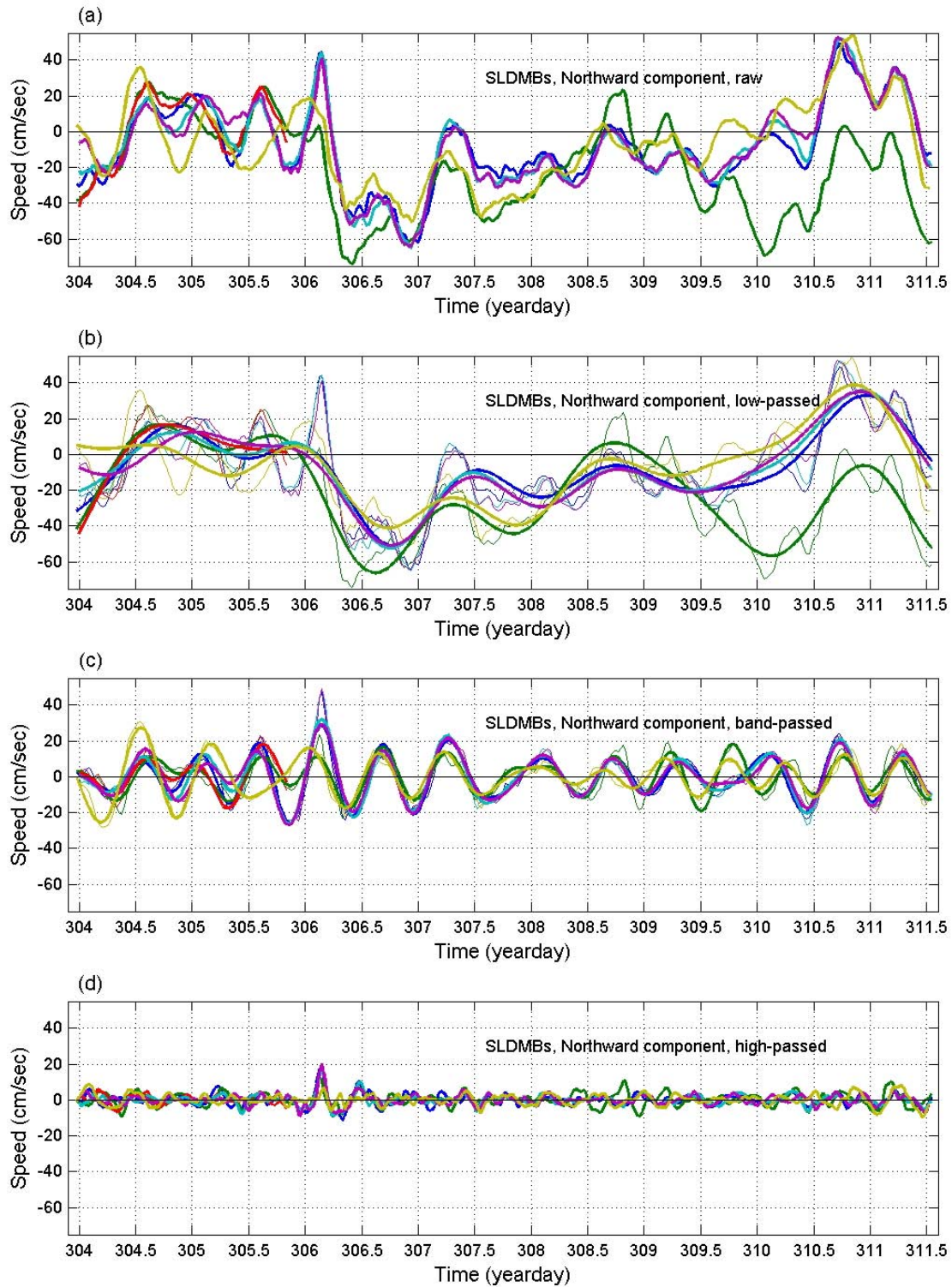


Figure 21. Time-series of the northward components for SLDMBs deployed during the first 8 days of the field study, as well as the low-pass, band-pass, and high-pass components of the original data.

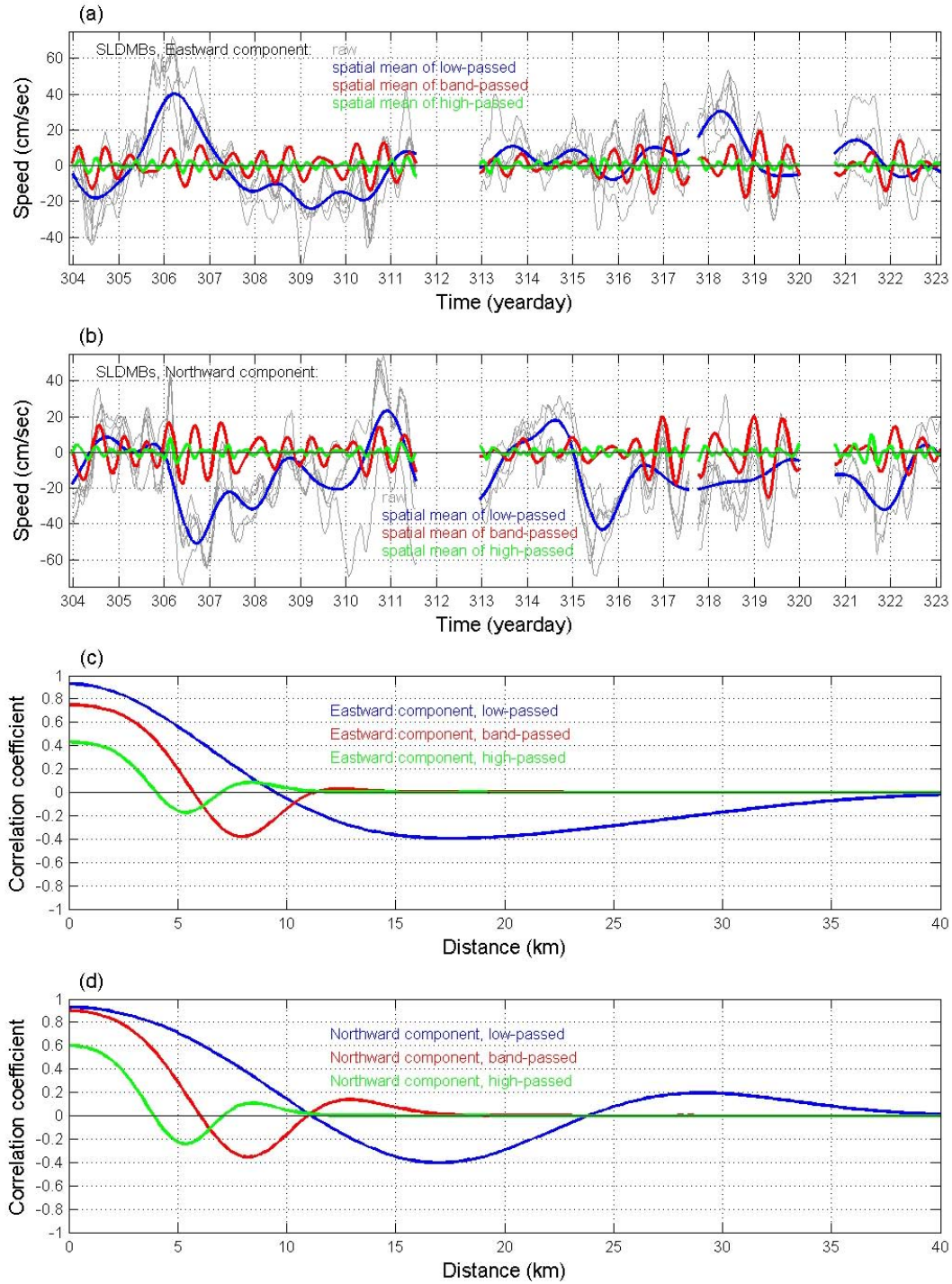


Figure 22. The computed spatial mean current field and spatial correlation functions for each of the three frequency bands derived from the SLDMB data. Panels (a) and (b) show the eastward and northward components of the surface current field; Panels (c) and (d) show the correlation functions for each frequency band as a function of separation distance.



After the SLDMB motion data were filtered into frequency bands, the concurrent data in each band were then combined to create a spatial averaged time-series for the entire study period (Figure 22, panels (a) and (b)). Gaps in these time-series reflect that the SLDMBs and drift targets were not being tracked for short periods. Because SLDMBs that were clustered in close proximity to one another (within 3 km) behaved similarly, the motions of these SLDMBs were first averaged to create a single value at a central location before a spatial average for the entire study area was calculated from the remaining SLDMBs. This spatial average formed the basis for the computation of the surface current field estimate needed for indirect leeway calculations for each of the drift targets.

After each SLDMB trajectory was decomposed into its low-, band-, and high-pass components and the spatially-averaged velocity was computed in each band, the spatial correlations of motions of drifter pairs in each frequency band were then calculated. This was done by initially computing the distance between each of the various SLDMB pairs over the course of the study. For each pair, the eastward and northward vector components within the three frequency bands at each time step were compared in order to generate the correlation relationships. Correlations for all SLDMB pairs were then grouped as a function of separation distance into 1-km bins. All of the vector pair comparisons falling into each 1-km separation bin were then grouped to compute a correlation function for the eastward and northward components for each of the three frequency bands (Figure 22, panels (c) and (d)).

Based on these comparisons, the low-frequency motions were very well correlated within distances of 5 km or less. This positive correlation gradually decreased out to a distance of around 10 km where it became negative. In these cases, a negative correlation reflects the case where the vector components for the SLDMB pair are of an opposing sign (i.e. motions are opposed). The band-pass components were well-correlated within distances of 3 km or less. This positive correlation gradually decreased out to a distance of around 6 km where the correlation became negative. The high-pass components were not as well-correlated even in the near-field, and the correlation became negative at a distance of around 4 km.

Ultimately, the current field estimates for a drift target were based on the computed spatial average that was then adjusted using the measured variance associated with the low-pass, band-pass, and high-pass contribution from each applicable SLDMB. An estimate of the SLDMB variance was based on the measured offset between the observed SLDMB motion and the spatial average for each of the three frequency bands at each increment along the time-series. The extent of the contribution of this measured SLDMB variance to the estimated drift target current field was then based on the correlation functions and the computed distance between the SLDMBs and the drift target. Because of the much stronger correlations, the low-pass and band-pass components were generally the primary factors in the current field measurement. Based on the correlation functions, as the distance between the drift target and each SLDMB increased past 10 km, the potential magnitude of the variance adjustment associated with that SLDMB became quite small. An estimate of the time-series variance was also computed for the current field computations based on the amount of the total variance (as measured between the SLDMBs and the spatial average) that was not recovered by application of the individual SLDMB variances through the applicable correlation functions.



The effectiveness of the SI technique was evaluated by comparing the surface current field measured by ADCP-equipped rafts during Drifts Two and Four with surface currents calculated using the indirect approach for the same rafts. The agreement for Drift Two is generally good (Figure 23). During the middle portion of this drift, the indirect eastward current component estimate was somewhat lower than the directly measured component, primarily because the eastward motion of all but one of the SLDMBs was small; indirect current results for Drift Two are discussed in more detail in the following paragraph. Although the direct and indirect current estimates also compared well for Drift Four, the agreement was not as strong, particularly for the northward current component, because the separation between the raft and the nearest SLDMBs steadily increased to almost 20 km by the end of the drift (Figure 24). In addition, because all of the SLDMBs were to the west of the raft during this period, the computed spatial average was also skewed in this direction and did not necessarily reflect conditions at the raft. The largest observed separation between the direct and indirect current estimates during both Drifts Two and Four occurred when the observed direct current magnitudes were greater than any of the measured SLDMB magnitudes. With the SI technique, the estimated indirect current field will always fall within the bounds of those measured from the SLDMB trajectories. These comparisons between the direct and indirect current estimates helped to demonstrate the general applicability of this technique, as well as the implications related to the spatial relationships between the SLDMBs and the drift target.

An example of the application of the SI technique for the undrogued SEIE raft is discussed below for Drift Two. Panels (a) and (b) in Figure 25 show the time-series of eastward and northward velocity components for the SLDMBs (light gray series), the spatial average current field for all three frequency ranges (dark blue line) from the SLDMB data, and the adjusted estimate of the current field (and variance) at the location of the undrogued raft (red lines). Panel (c) presents a plan view of trajectories. Throughout most of this time-series, the computed spatial average showed only a small eastward component that was controlled by three of the four SLDMBs. The fourth SLDMB had a larger eastward velocity during the first half of the drift, and this SLDMB was much closer to the raft during this time. Use of the SI approach resulted in a higher estimate of the eastward vector component at the drift target that compared well with the current estimate made for the ADCP raft located in this same general area during Drift Two (Figure 19). Because the observed eastward velocity components have greater range during this drift, the eastward variance estimates are noticeably higher.

A result where the distribution of SLDMBs is less favorable is shown in Figure 26 for the undrogued SEIE raft from Drift One. As above, panels (a) and (b) show the eastward and northward time-series motion of the SLDMBs, with the computed spatial average (dark blue line) from these SLDMBs, and the adjusted estimate of the current field (and variance) at the drift target (red lines). During the first part of Drift One, the winds steadily decreased from a period of relatively strong and consistent northerly winds to a period of generally light and variable winds throughout the remainder of the drift. The SLDMBs were deployed within 1 km of the drift target deployment site for this drift, and the SLDMBs remained in close proximity to one another during the drift. The raft, however, moved quite differently than the SLDMBs, and by the end of this drift, it was about 18 km southeast of the closest SLDMB. Because its separation distance from the SLDMBs was larger, the error estimate for the surface current field at the SEIE raft during Drift One, particularly its eastward component, was much larger than

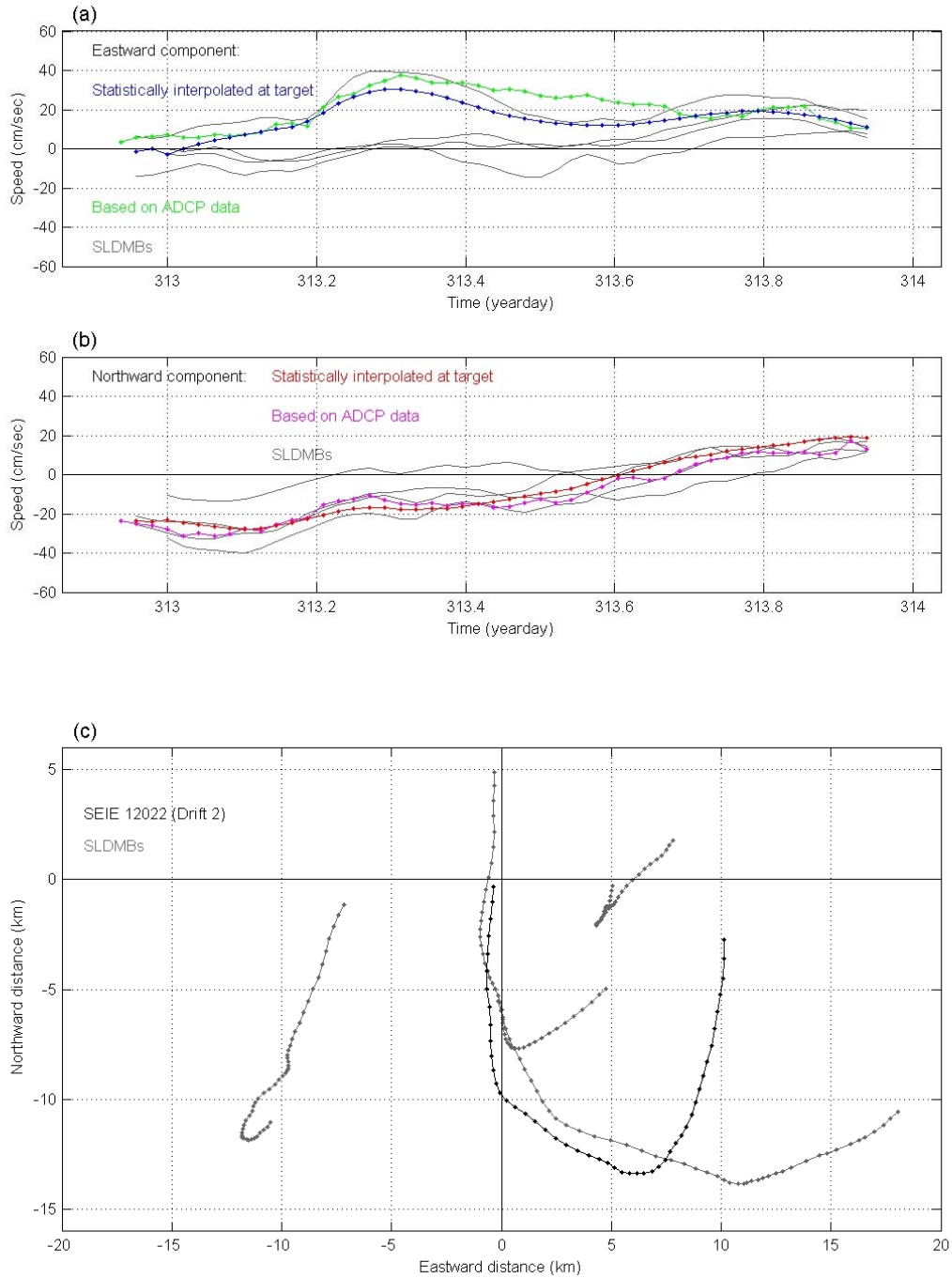


Figure 23. The computed direct and indirect near-surface current field at the drogued raft during Drift Two (panels (a) and (b)). Panel (c) shows a plan view of the raft and SLDMB tracks over the course of the drift. The CMB is located at the origin of the axes.

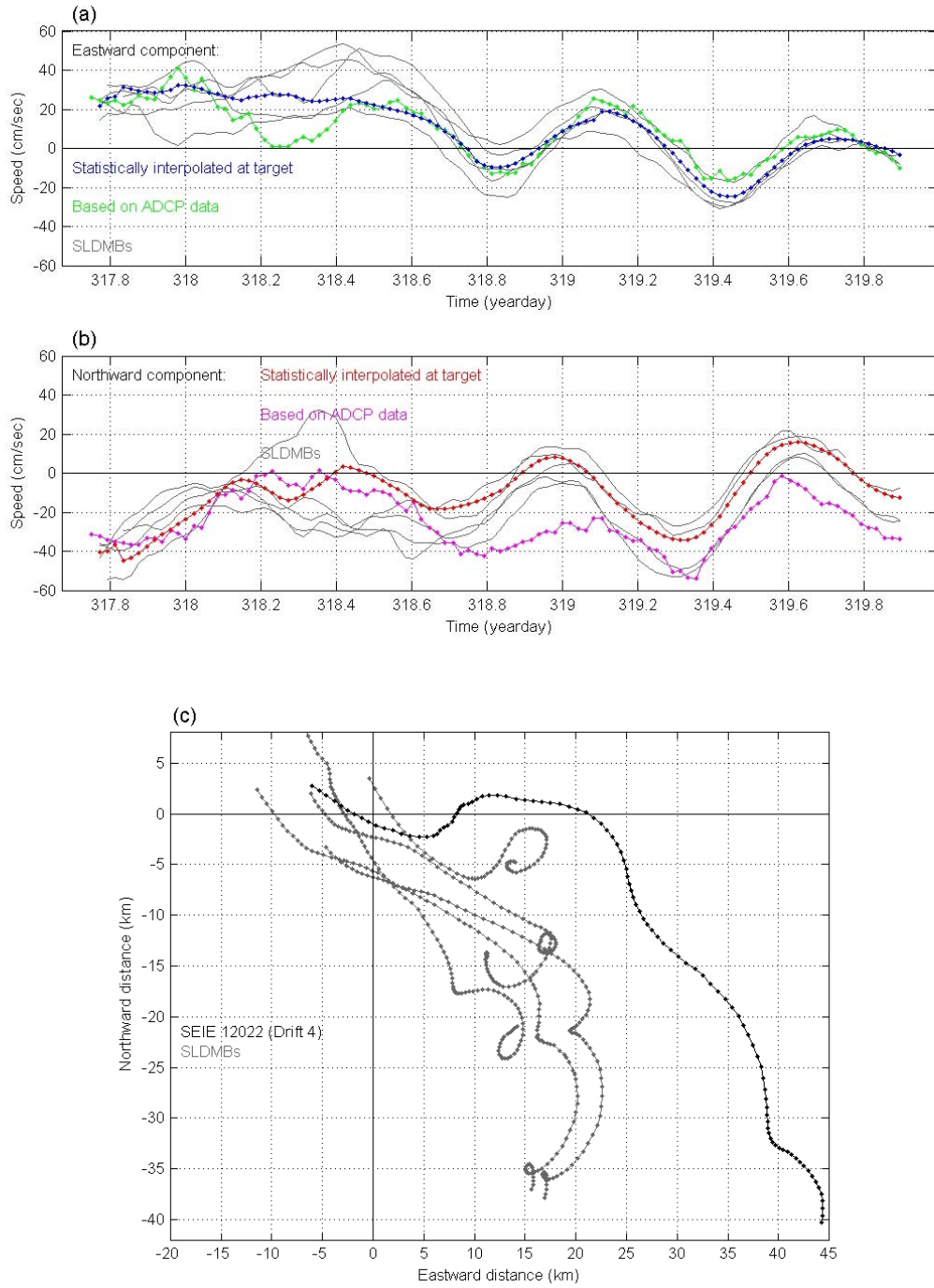


Figure 24. Time-series of the vector components of the computed direct and indirect near-surface current field at the drogued raft during Drift Four (panels (a) and (b)). Panel (c) shows a plan view of the raft and SLDMB tracks over the course of the drift. The CMB is located at the origin of the axes.

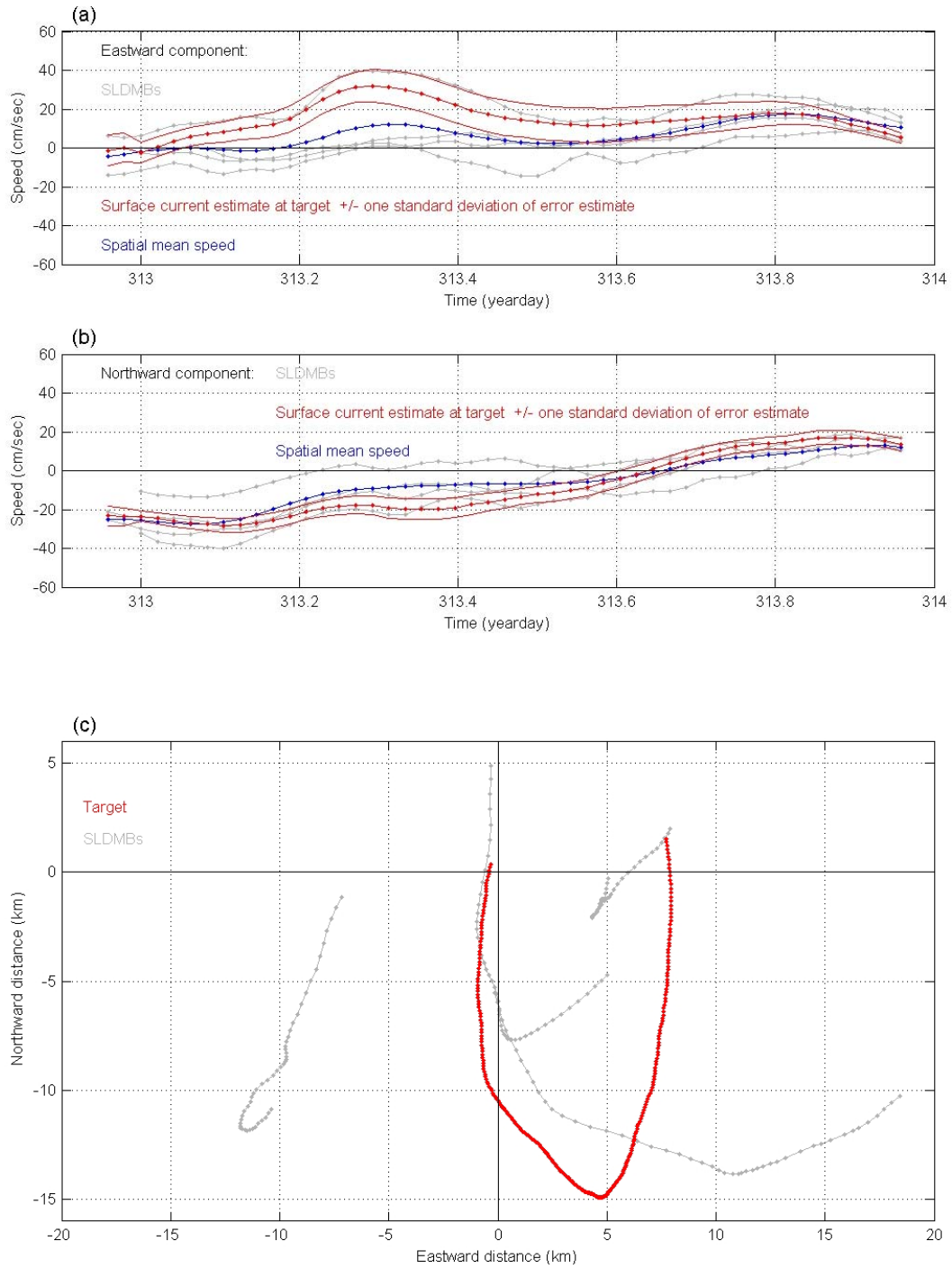


Figure 25. Time-series of the vector components of the computed near-surface current field (bounded by  $\pm 1$  standard deviation of the error) at the undrogued raft during Drift Two (panels (a) and (b)). Panel (c) shows a plan view of the raft and SLDMB tracks over the course of the drift. The origin of the axes is at the location of the CMB.

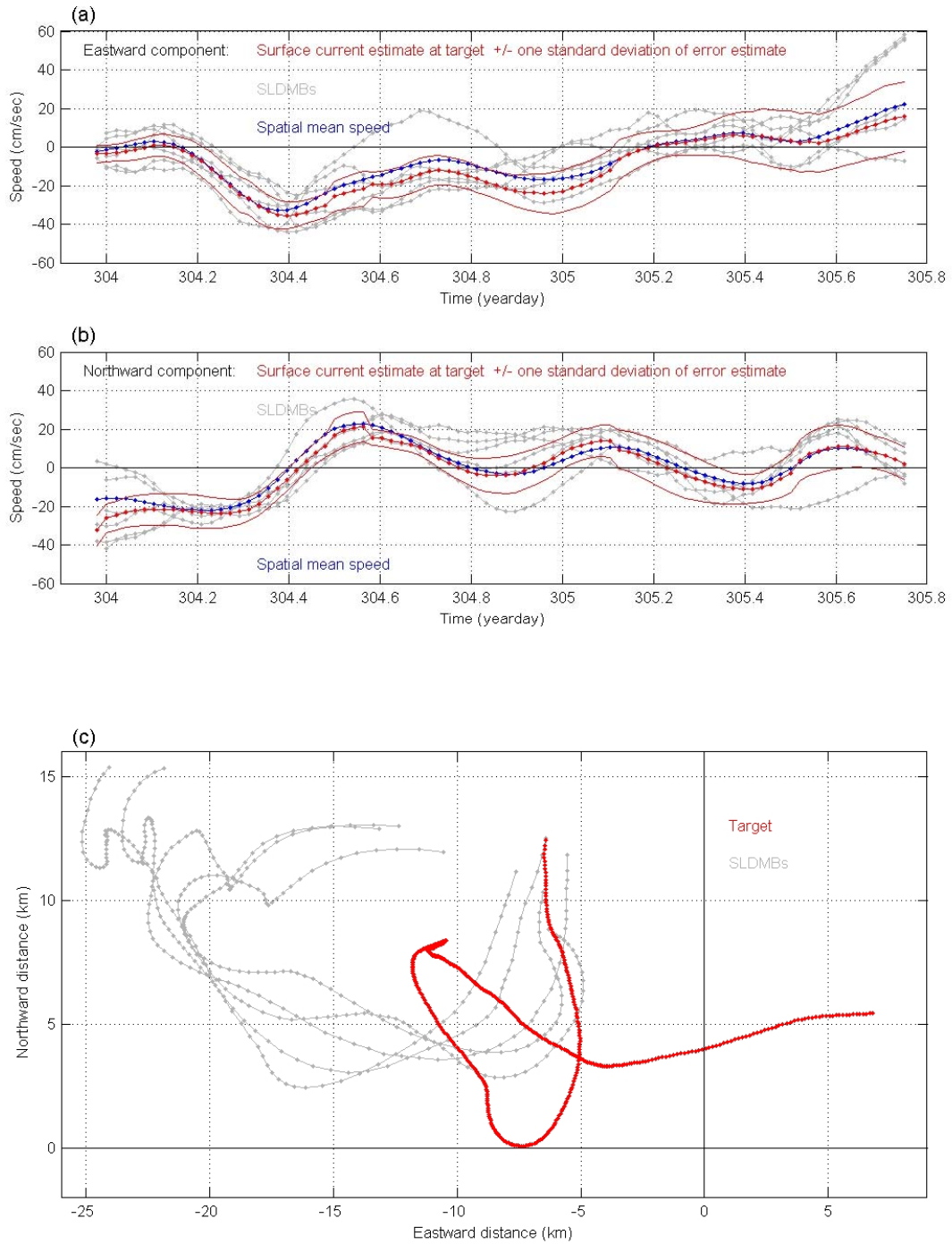


Figure 26. Time-series of the vector components of the computed near-surface current field (bounded by  $\pm 1$  standard deviation of the error) at the undrogued raft during Drift One (panels (a) and (b)). Panel (c) shows a plan view of the raft and SLDMB tracks over the course of the drift. The origin of the axes is at the location of the CMB.

for Drift Two. The surface current estimate for the raft converges on the spatial mean vector, and the error estimate increases (Figure 26) because the magnitude of the spatial correlation coefficient decreases with increasing distance.

### **4.3 Leeway Calculations**

The final analysis element was the computation of the downwind and crosswind leeway coefficients for each of the drift targets. During the course of the data reduction and analyses addressed above, separate and comprehensive data files were developed for each of the drift targets from each of the drifts. The primary elements in these data files were the filtered GPS time and position data for the drift target, its computed vector motion, the applicable wind speed and direction data from the CMB, and the computed current motion field that was developed for that drift target. Data files based on direct current measurements were spaced at a 10-minute intervals and those based on indirect current measurements were spaced at 30-minute intervals.

As addressed previously, the direct method was used for the drogued ADCP rafts that were deployed during Drifts Two and Four, while the indirect method was used for the undrogued rafts in Drifts One and Two, and the SEPIRBs in Drifts One and Four (Table 3). For the direct computations, the computed motion of the raft relative to the water surface was correlated against the recorded wind speed and direction data. For the indirect computations, the computed current vector motion was subtracted from the drift target vector motion to obtain an estimate of the raft motion relative to the water surface. These estimated leeway time-series were then correlated to the recorded wind speed and direction data. Progressive vector diagrams were generated for each of the six drift target data sets to illustrate the relative movement of the target in the downwind and crosswind directions over time. The data were then used to compute the downwind and crosswind leeway coefficients for each drift target from each drift. The following discussion will be focused around the results for each of the three drift target types (e.g., drogued SEIE raft, undrogued SEIE raft, and SEPIRB). Though each drift target was analyzed individually to develop leeway coefficients for each drift, these results were eventually grouped together to compute averaged coefficients for each drifter type. Results of the average leeway computations for each drift target, as well as the correlation statistics are summarized in Table 4. Results and supporting figures for the individual leeway computations are provided in Appendix A.

#### **4.3.1 Leeway of Drogued SEIE Rafts**

Leeway coefficients for the drogued raft (12022) are based on ADCP data acquired during Drifts Two and Four. As discussed in Section 4.2.1, the processed ADCP data were used to directly quantify the movement of the raft relative to the water surface. The progressive vector diagrams for both of these drifts showed that the rafts moved more or less consistently to the right (or in the positive cross-wind direction) of the wind (panel (a) in Figure 27). In general, the leeway drift was more consistent during Drift Four than for Drift Two. The winds during Drift Four were more uniform and blew from the north-northwest at speeds above 7 m/s for much of the period. As discussed previously for Drift Two, the initial northerly winds decreased through the first half of the drift, veered to the south-southeast, and then began to increase steadily towards the end of the drift. The progressive vector diagram for Drift Two shows that the raft made a series of four separate course changes relative to the downwind component. Each of these

Table 4. Summary of the calculated leeway coefficients and relevant statistics. Unless otherwise noted, units are in m/sec.

Model Parameter	Leeway Method	n	Leeway and Correlation Coefficients (m/s)												Wind Speed
			Unconstrained Linear Regression Model						Constrained Linear Regression Model						Range (knots)
			Y	slope	Sy/x	Bias	r	r <sup>2</sup>	Y	slope	Sy/x	Bias	r	r <sup>2</sup>	5-min Average
<b>Drogued SEIE Life Raft</b>															
Downwind Component	Direct	458	0.039	0.017	0.042	0	0.797	0.635	0	0.021	0.044	0.004	0.797	0.635	3.2 - 31.8
Positive Crosswind	Direct	399	0.057	0.000	0.033	0	0.009	0.000	0	0.005	0.038	0.006	0.009	0.000	3.2 - 31.8
Negative Crosswind	Direct	59	-0.034	0.001	0.022	0	0.176	0.031	0	-0.002	0.025	-0.004	-0.176	0.031	3.2 - 31.8
<b>Undrogued SEIE Life Raft</b>															
Downwind Component	Indirect	64	-0.039	0.033	0.042	0	0.937	0.878	0	0.028	0.045	-0.007	0.937	0.878	3.5 - 28.8
Positive Crosswind	Indirect	43	0.070	0.005	0.057	0	0.310	0.096	0	0.012	0.064	0.012	0.310	0.096	3.5 - 28.8
Negative Crosswind	Indirect	21	-0.062	0.001	0.036	0	0.034	0.001	0	-0.010	0.039	-0.005	0.034	0.001	3.5 - 28.8
<b>SEPIRB</b>															
Downwind Component	Indirect	247	-0.018	0.004	0.060	0	0.264	0.070	0	0.002	0.060	-0.003	0.264	0.070	2.7 - 32.3
Positive Crosswind	Indirect	145	0.061	0.000	0.046	0	0.019	0.000	0	0.006	0.051	0.008	0.019	0.000	2.7 - 32.3
Negative Crosswind	Indirect	102	-0.046	0.000	0.046	0	0.034	0.001	0	-0.005	0.051	-0.011	0.034	0.001	2.7 - 32.3

Key:

N: Number of sample points included in the regression model.

Y: y-axis intercept.

Slope: slope of the regression.

Sy/x: Standard error of the estimate computed from the scatter of the data about the regression line.

r: Correlation coefficient of the regression.

Bias: Measure of the bias introduced by the constrained estimate.

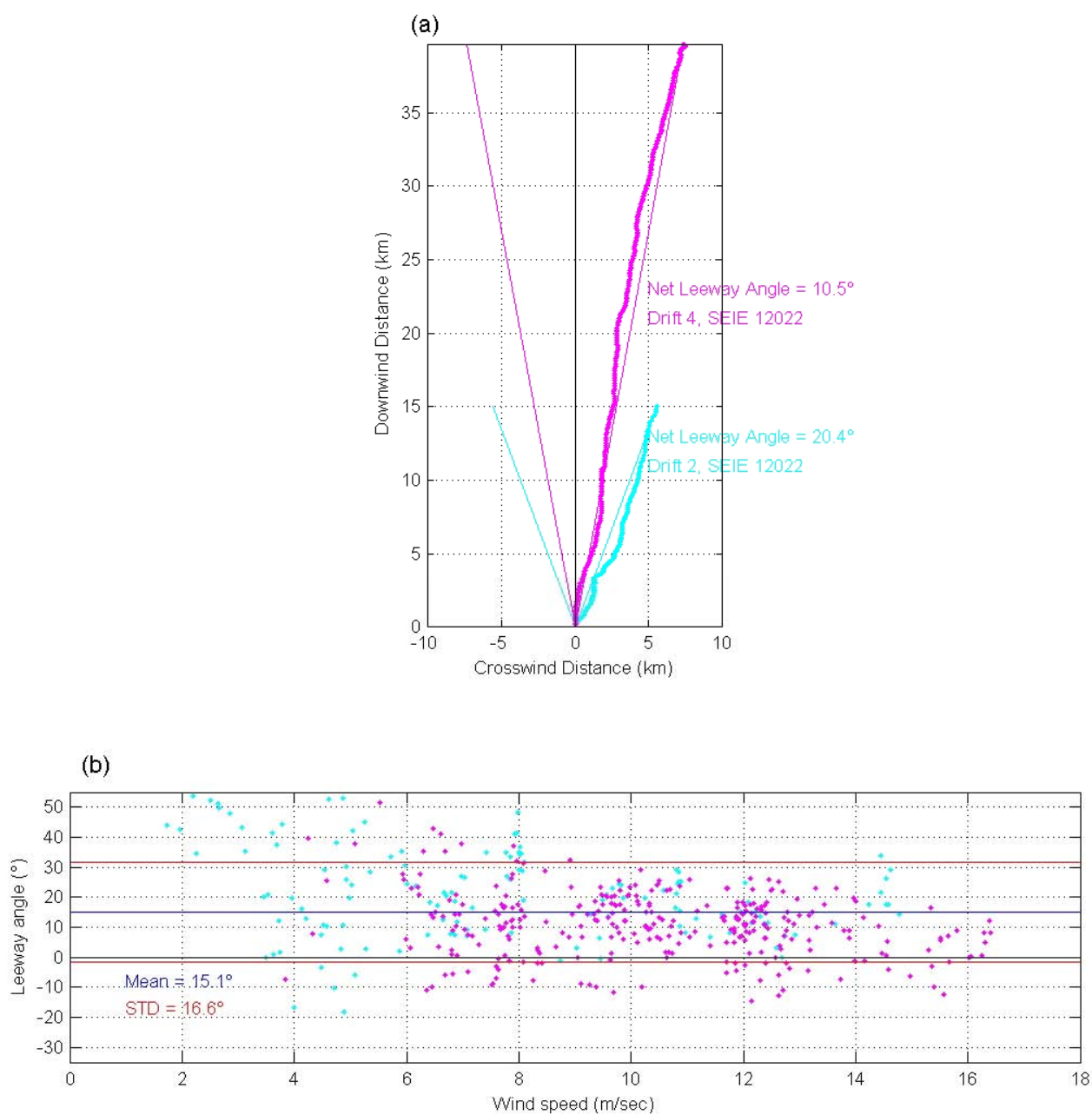


Figure 27. Progressive vector diagrams and leeway angle scatter plots for the drogued rafts from Drifts Two and Four. Panel (a) shows progressive vector diagrams for the drogued rafts; Panel (b) is a scatter plot of the computed leeway angle relative to the observed wind speed, as well as the computed mean and standard deviation of the leeway angle.



changes produced a noticeably different apparent leeway angle. These changes occurred during the early and middle stages of the drift when the winds were becoming light and variable, and surface currents were changing in a direction opposite to the change of wind direction. During the last half of this drift, the agreement improved, with the computed leeway angles closer to the Drift Four results.

The relationship between leeway angle and wind speed for the drogued raft configuration is shown in panel (b) of Figure 27. The mean leeway angle over all winds speeds is 15.1 degrees. The drift speed of the drogued raft was 2.2 percent of the local 10-m wind speed. As the figure illustrates, the comparison was less variable at wind speeds above approximately 7 m/s. This may reflect the variability wind direction during periods of “light and variable” winds, as well as the potential for other forcing processes such as surface currents to influence drift target motion during these same conditions. Although the correlation coefficient of the regression would be improved by using only the data acquired during the higher wind periods, the leeway coefficients are based on all of the data acquired.

The leeway data from Drifts Two and Four were combined for constrained and unconstrained regression calculations of the downwind and crosswind leeway coefficients (Figure 28). The units for both axes in this figure are m/s. For the downwind component, the constrained leeway slope was 0.021 and the unconstrained slope was 0.017 with an intercept of 0.039 m/s. The correlation coefficient ( $r^2$ ) of the downwind leeway data for the drogued raft was 0.635. The mean deviation of the data from the regression line ( $Sy/x$ ) for the unconstrained case was 0.042 m/s. For the positive crosswind component, the constrained leeway slope was 0.005 and the unconstrained slope was 0.0 with an intercept of 0.057 m/s. The constrained leeway slope of the negative crosswind component data was -0.002; the unconstrained slope was 0.001 with an intercept of -0.034 m/s.

#### **4.3.2 Leeway of Undrogued SEIE Rafts**

Leeway coefficients for the undrogued rafts were developed by the indirect method from data collected during Drifts One (12022) and Two (12020). As discussed in Section 4.2.2, in the indirect case, the movement of the raft relative to the water surface was derived from the difference between the raft trajectory over the ground and the current field at the raft. The progressive vector diagrams for both of these drifts show that the leeway of the undrogued rafts (panel (a) in Figure 29) was somewhat more variable than it had been for the drogued rafts. The combination of generally light and variable winds during the drift and the larger error associated with the surface current estimate caused by its larger separation distance from the SLDMBs produced greater leeway uncertainty for the undrogued raft during Drift One. In addition, as addressed in Section 3.2.1, the undrogued raft from Drift One was recovered flooded and submerged at the bow at the end of the drift. Though it is not clear when the raft flooded, the progressive vector data show that the track of the raft shifted noticeably about eight hours into this drift. Due to the raft condition and the greater uncertainty in the results, only the first eight hours of the Drift One undrogued raft data are used for leeway calculations.

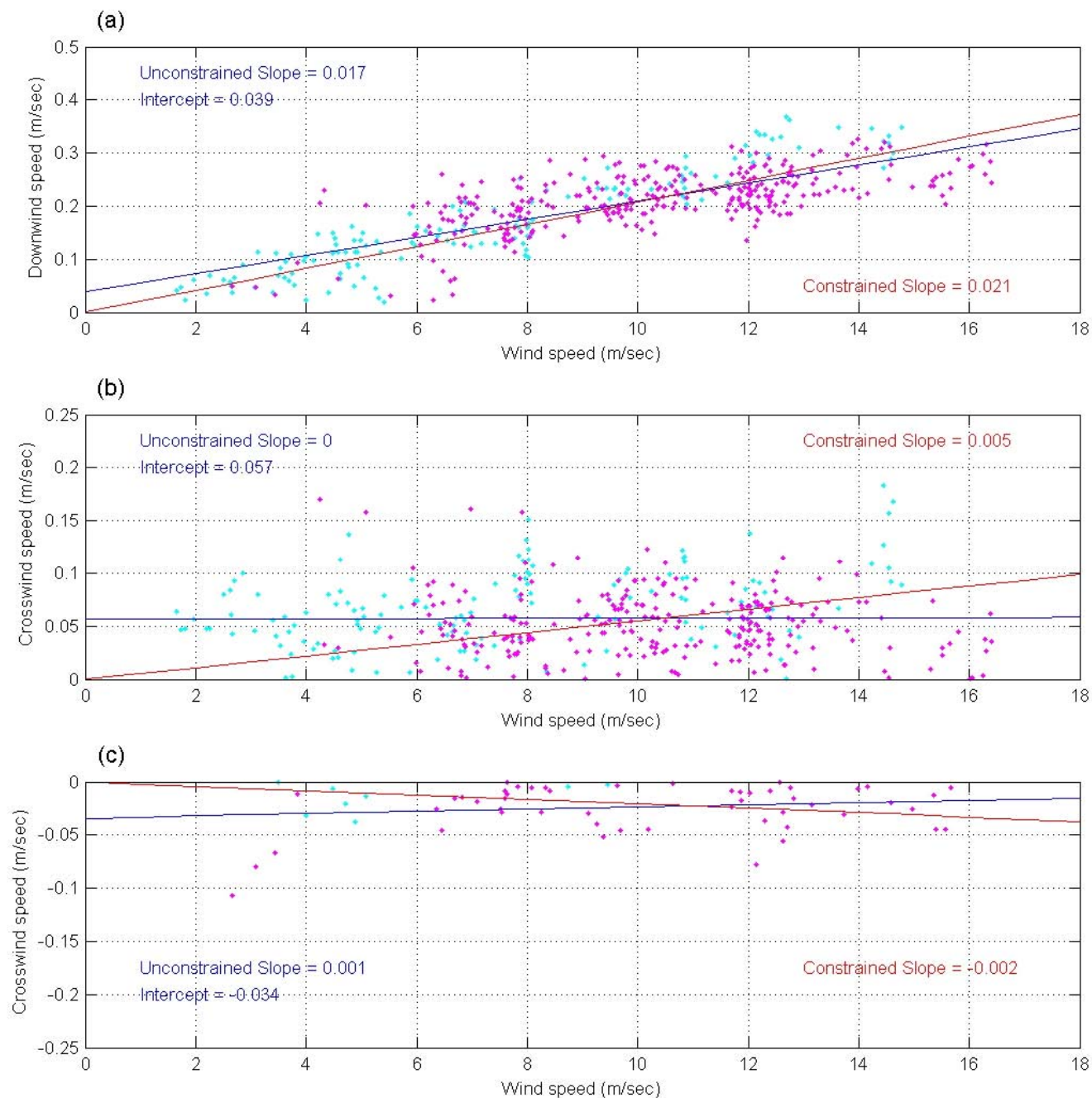


Figure 28. Unconstrained downwind and crosswind (positive and negative) leeway components computed for the drogued rafts from Drifts Two and Four.

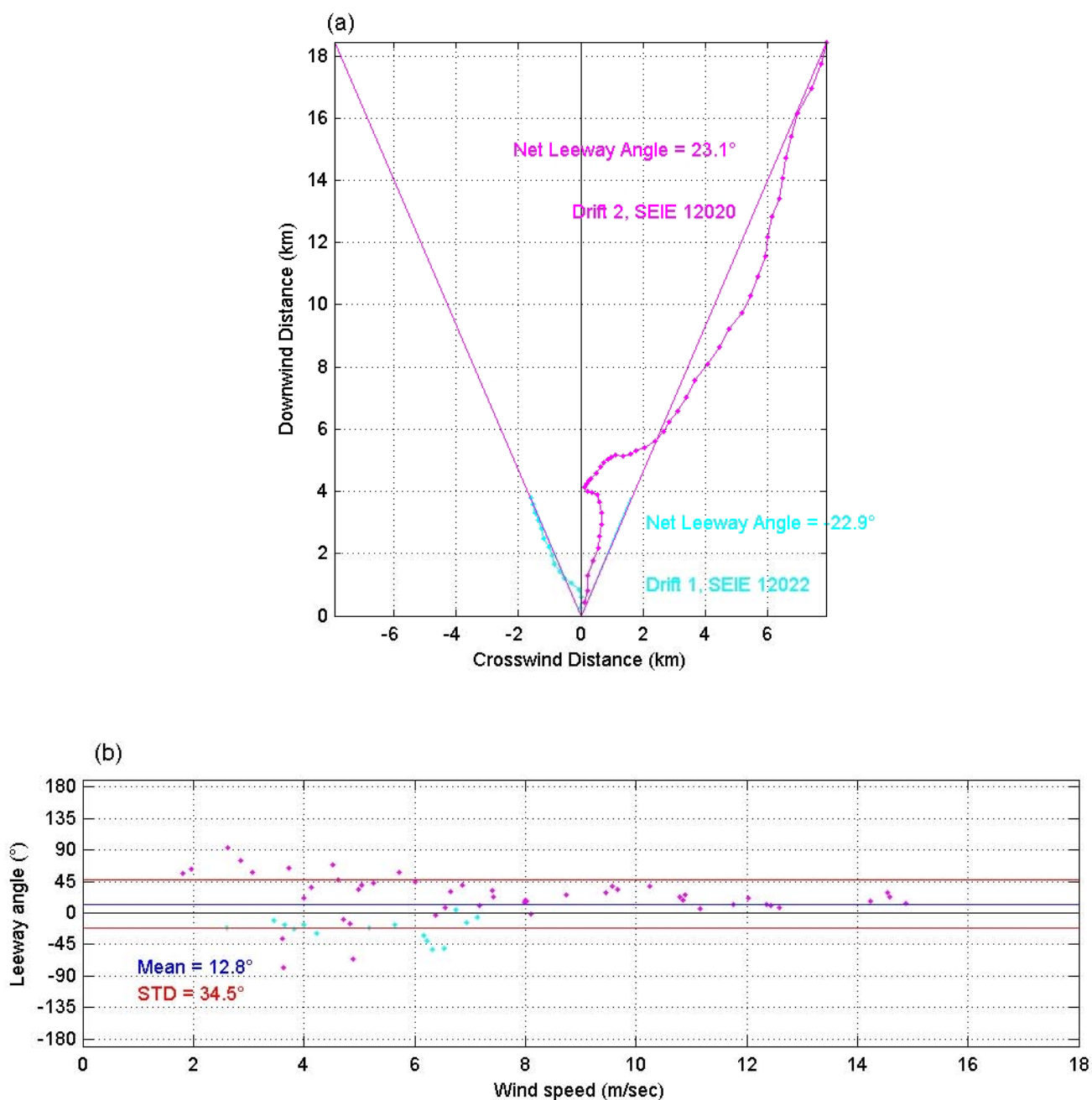


Figure 29. Progressive vector diagrams and leeway angle scatter plots for the undrogued rafts from Drifts One and Two. Panel (a) shows progressive vector diagrams for the undrogued rafts from Drifts One and Two; panel (b) shows leeway angle relative to the observed wind speed, as well as the computed mean and standard deviation of the leeway angle measurement.

As discussed in Section 4.3.1 above, environmental conditions during Drift Two were not as favorable as they had been during Drift Four, but they were still better than the conditions encountered during Drift One. During Drift Two the initial northerly winds decreased through the first half of the drift, veered to the south-southeast, then built steadily toward the end of the drift. Similar to the progressive vector diagram for the drogued raft, the progressive vector diagram for the undrogued raft for Drift Two also showed that the raft made a series of small, short course changes relative to the downwind component and that each of these changes resulted in a noticeably different apparent leeway angle (Figure 29, panel (a)). Again, these course changes occurred during the early and middle stages of the drift when the winds were becoming light and variable and the surface currents were rotating in an opposite direction to the wind. During the last half of this drift, the results were more consistent and the computed leeway angles were more similar to results observed with the drogued raft. Over essentially the same time frame during Drift Two, the undrogued raft moved approximately 18 km downwind and 8 km crosswind, while the drogued raft moved approximately 15 km downwind and 6 km crosswind.

The leeway angle relative to the recorded wind speed is shown with the progressive vector diagram in panel (b) of Figure 29. The mean leeway angle for the combined Drift One and Drift Two data over all winds speeds is 12.8 degrees to the right of the wind, however when the drifts are considered separately, the leeway angles are approximately 23 degrees to the left and right of the wind for Drifts One and Two, respectively. The drift speed of the undrogued raft was 3.0 percent of the local wind speed. The leeway angle is 23 degrees. As with the drogued rafts, the leeway angle was more consistent at wind speeds above approximately 7 m/s. As discussed above, this was most likely the result of the greater variability of wind direction during periods of change when winds were “light and variable”, and to the influence of other forcing during these conditions. The exclusion of much of the Drift One data from the leeway analysis limited the number of lower wind speed data points used for leeway calculations.

The usable leeway data from both drifts were then merged to compute average leeway coefficients in both the downwind and crosswind directions for both the constrained and unconstrained cases (Figure 30). (Again, the axis units are in m/s). For the downwind component, the constrained leeway slope was 0.028 and the unconstrained slope was 0.033 with an intercept of -0.039 m/s. The correlation coefficient of the downwind leeway data for the undrogued raft was 0.878, which was higher than the correlation for the drogued raft downwind data; however, the mean deviation of the data from the regression line in the unconstrained case ( $S_y/x$  of 0.042) was almost identical to that for the drogued raft. The constrained leeway slope of the positive crosswind component was 0.012, and the unconstrained slope was 0.005 with an intercept of 0.070 m/s. The constrained leeway slope of the negative crosswind data was -0.010, while the unconstrained slope was 0.001 with an intercept of -0.062 m/s (Table 4).

### 4.3.3 SEPIRB Leeway

Leeway coefficients for the SEPIRBs were based on indirect data acquired during Drifts One and Four. As discussed in Section 4.2.2, for the indirect case the processed GPS SEPIRB trajectory data were used to calculate the northward and eastward components of its velocity over the ground. The computed current field at the SEPIRB based on adjacent SLDMB motions was subtracted from the SEPIRB motion over ground to estimate its leeway. This process was

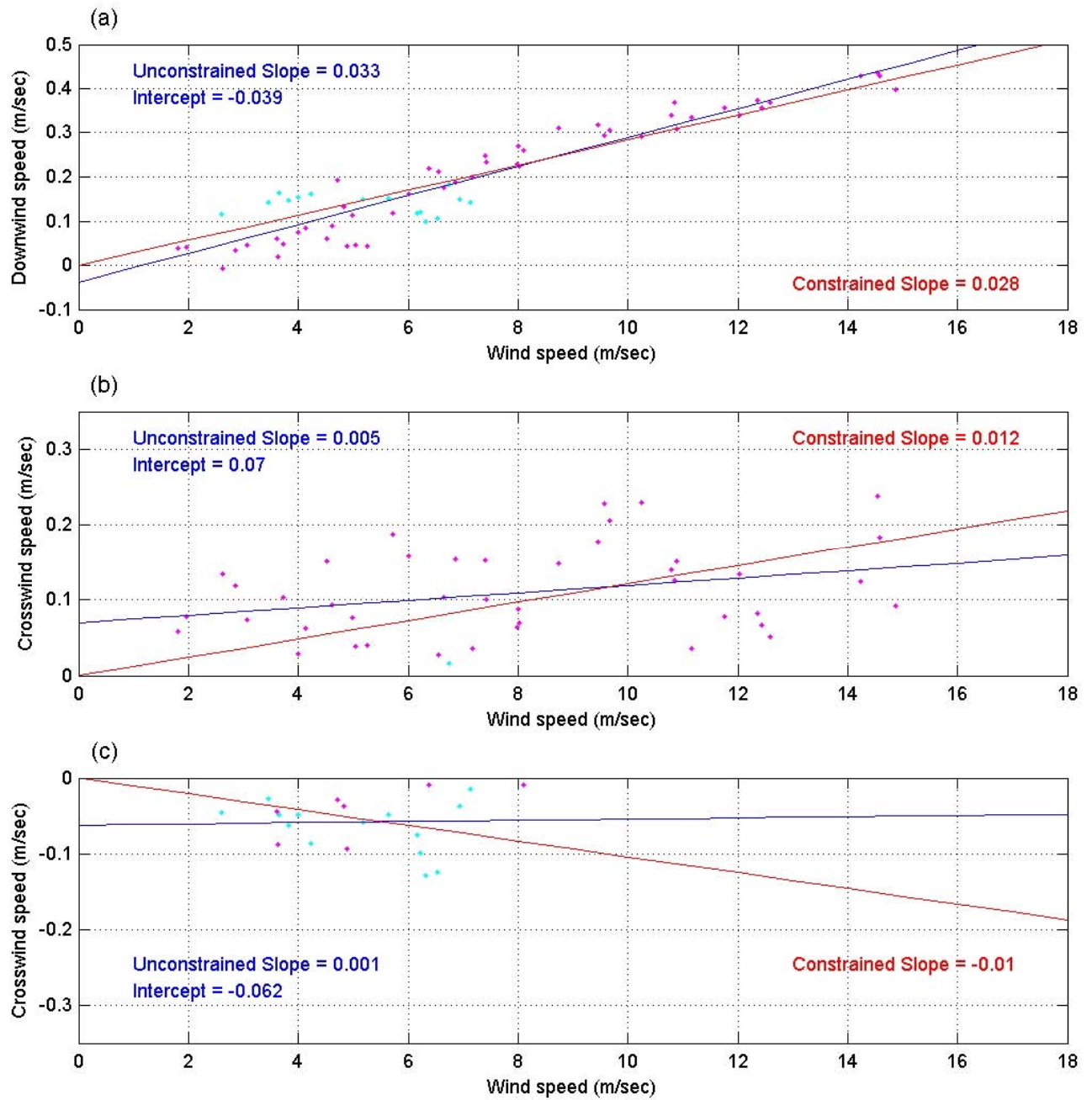


Figure 30. The constrained and unconstrained downwind and crosswind (positive and negative) leeway components computed for the undrogued rafts from Drifts One and Two.

hindered by the sometimes intermittent nature of the SEPIRB GPS data that was transmitted via ARGOS. The data returned from SEPIRB 53241, which was deployed during Drift One covered nearly two weeks. This data set was intermittent, however, with gaps in the position data that were too long to interpolate across (Figure 16). During this drift, SEPIRB 53241 traveled more than 80 km from the CMB and also became separated from most of the SLDMBs. As a result, only data from the first week of this drift were used to calculate leeway coefficients.

The SEPIRB is basically a long cylinder extending vertically in the water column with little above-water surface presentation, so its motion was largely defined by the surface currents. During Drifts One and Four, the motion of the SEPIRBs was very similar to those of nearby SLDMBs that were deployed at the same time (Figure 16). Given that the leeway of the SLDMB is negligible and the SEPIRB movement is very similar to that of the SLDMB, it follows that leeway of the SEPIRB is also zero. As expected, the progressive vector diagrams in panel (a) of Figure 31 for both SEPIRB drifts showed that the SEPIRBs showed little motion in either the downwind or crosswind directions. Though the progressive vector diagrams did show some leeway motion, the movement was inconsistent and minor relative to the total distance covered by the SEPIRB during the course of the drift. Leeway angle as a function of wind speed in panel (b) of Figure 31 shows no consistent relationship between wind speed and SEPIRB leeway angle. The available information indicates that leeway motion of the SEPIRBs was due to random error in the estimate of the indirect surface current field and turbulent fluctuations in the current field.

The SEPIRB data from both of these drifts were merged to compute leeway coefficients in both the downwind and crosswind directions (Figure 32). Both the constrained and unconstrained regressions are shown in the figure. The constrained leeway slope for the downwind component was 0.002 and the unconstrained slope was 0.004 with an intercept of -0.018 m/s. The correlation coefficient of the downwind component of leeway was very low at 0.070 and the mean deviation of the data from the regression line was 0.060 m/s. The constrained leeway slope of the positive crosswind component was 0.006 and the unconstrained positive crosswind slope showed no relation to wind (zero slope), with a y-intercept of 0.061 m/s. The constrained slope of the negative crosswind data was -0.005; the unconstrained negative crosswind slope also showed no relation to wind (zero slope), with a y-intercept of -0.046 m/s.

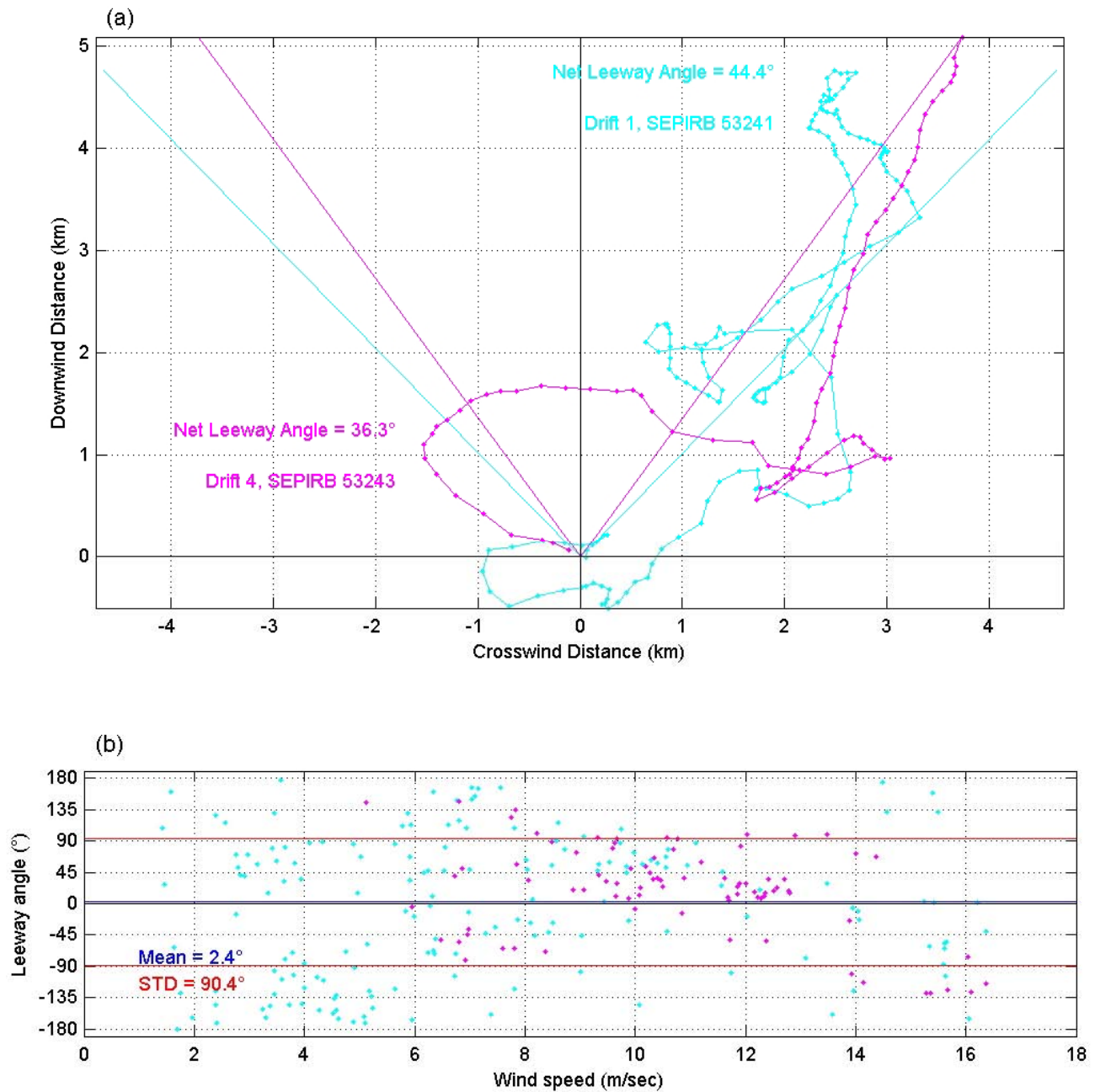


Figure 31. Progressive vector and leeway angle scatter plots for the SEPIRBs from Drifts One and Four. Panel (a) show the SEPIRB progressive vector diagram relative to the downwind direction. Panel (b) shows the scatter plot of the computed leeway angle relative to the observed wind speed along with the computed mean and standard deviation of the leeway angle.



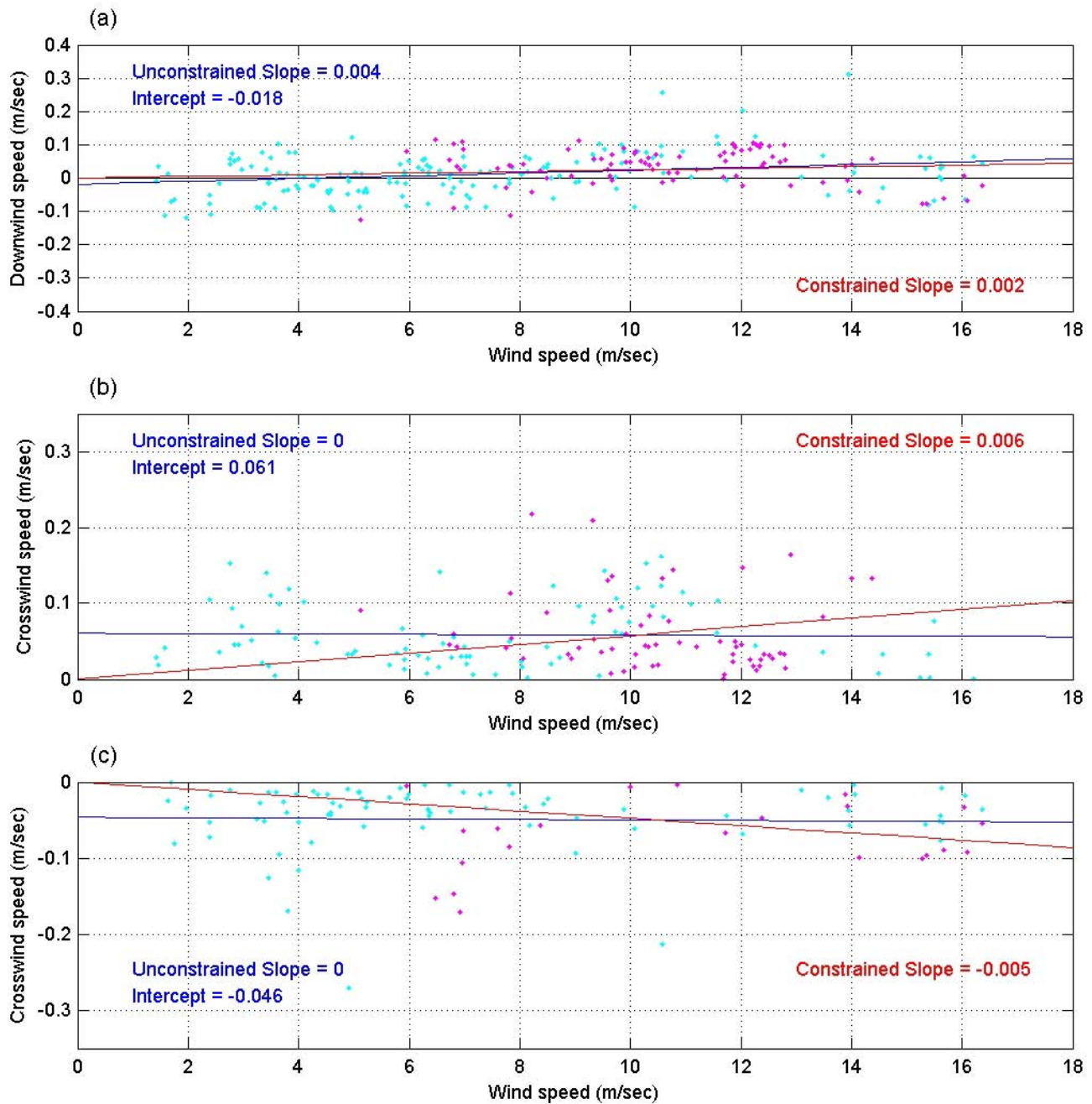


Figure 32. The constrained and unconstrained downwind and crosswind (positive and negative) leeway components computed for the SEPIRBs from Drifts One and Four.



## 5.0 CONCLUSIONS

Direct leeway computations for the drogued SEIE rafts based on two separate drifts showed that the drogued rafts moved at an average net leeway angle of 15 degrees to the right of the downwind direction at 2.2 percent of the local wind speed. The leeway-angle relationship became less consistent at wind speeds below 7 m/s, though the regression results were not similarly affected. The constrained regression slope for the downwind leeway component was 0.021. The computed correlation coefficient of the downwind leeway data for the drogued raft was 0.635 and the mean deviation of the data from the regression line for the constrained case was 0.044 m/s. Because the rafts moved primarily to the right of the wind during both drifts, most of the crosswind component data points were positive. The constrained regression slope for the positive crosswind leeway component was 0.006, while the slope of the negative crosswind leeway component was -0.002. The unconstrained slope for the downwind leeway component was 0.017 with a y-intercept of 0.039 m/s.

Indirect leeway computations for the undrogued SEIE rafts based on the best drift case showed that the raft moved off the downwind direction at an average angle of 23 degrees. As with the drogued rafts, the relationship between the leeway angle and the wind direction was less consistent at wind speeds below about 7 m/s. As would be expected, the magnitude of leeway was larger for the undrogued raft, 3.0 percent of local wind speed. During one drift that included both a drogued and an undrogued raft, the undrogued raft moved approximately 18 km downwind and 8 km crosswind, while the drogued raft moved approximately 15 km downwind and 6 km crosswind. The constrained regression slope for the downwind leeway component was 0.028. The computed correlation coefficient of the downwind leeway component for the undrogued raft was 0.878 and the mean deviation of the data from the regression line in the constrained case was 0.045 m/s. The unconstrained slope for the downwind leeway component was 0.033 with a y-intercept of -0.039 m/s. The constrained regression slope for the positive crosswind leeway component was 0.012; the negative crosswind leeway component slope was -0.010.

Indirect leeway computations for the SEPIRBs based on two separate drifts showed that the SEPIRBs exhibited little leeway motion in either the downwind or crosswind direction. Based on the inconsistency and small magnitude of the downwind and crosswind components, there were no statistically meaningful leeway trends evident in the data. During the two drifts, the motion of the SEPIRBs was very similar to the motions of adjacent SLDMBs. Based on this data; the leeway coefficients for the SEPIRB are zero. This conclusion makes sense because the SEPIRB is basically a long cylinder extending vertically in the water column with little above-water surface presentation. Its motion is therefore essentially identical to the local surface current field. The SEPIRB therefore provides a reasonable estimate of the near-surface current field.

The combination of indirect current field and wind measurements introduced some level of uncertainty and inconsistency into the computation of leeway coefficients. This inconsistency was most noticeable during periods of generally light winds (less than 7 m/s) and was most likely the result of the greater variability associated with the measurement of “light and variable” winds combined with the greater variability in the drift target motion during these same conditions.

The leeway coefficients reported here are based on all of the data considered suitable. An alternative approach would be to compute the leeway coefficients based only on data acquired when the observed wind speeds were greater than 7 m/s. In addition, rather than forcing the regression through zero (a constrained solution), another slope could be computed to define the straight line between zero and the 7 m/s value. This would essentially define a light-wind slope that would not affect the accuracy of slope that was computed for and based upon the more important higher wind periods.

Problems were encountered in maintaining SEIE raft buoyancy during this study. Each of the six SEIE rafts used developed some type of air leak. Air leaks occurred from the flotation bladder, the manual inflation tube, and from the threaded CO<sub>2</sub> canister connections. The air bladder and inflation tube leaks were patched. The leaks from the threaded CO<sub>2</sub> canister connection were stopped by unscrewing the CO<sub>2</sub> canister, wrapping Teflon® tape on the threads and reconnecting the canister to the inflation valve assembly. The Velcro® seal on the canopy flap failed in high winds, so the intervention of a human passenger would be needed to keep the flap closed. Opened flaps combined with losses of buoyancy due to air leakage resulted in raft flooding and data losses.

The raft flap closure problem was corrected by field modifications, as were the air leaks. Before subsequent deployments were made, the field crew modified the instrument package configuration to further minimize loss of buoyancy and potential change of leeway characteristics. A two-inch thick sheet of closed-cell foam flotation was attached between the bottom of the instrument mounting board and the floor of each raft to maintain buoyancy and displace water that entered through the canopy or bottom of the raft. Grommets were also added to the canopy flaps so that the Velcro® seal could be laced shut with line. A small submersible pump in was also installed in the ADCP raft to keep water from accumulating.

Following the end of the study, all of the rafts returned from the study were examined in detail by NSMRL and R&DC staff. The rafts were re-inflated and leakage points identified. The examination concluded that all bladder leaks occurred on the inside of the rafts and in locations that were consistent with abrasion from components of the instrument package and ballast installed in the rafts. In some cases, the leaks were accompanied by visible signs of abrasion.

The SEPIRBs employed for this study had been modified to operate similarly to an SLDMB and thus were capable of transmitting periodic time-stamped GPS data messages via ARGOS. Actual SEPIRBs are designed to repeatedly transmit only the initial position that is recorded when the unit is first deployed; this position would presumably represent the location of a disabled submarine. As the SEPIRB is moved away from the initial deployment location by local currents and winds, it would be helpful if the present position for the SEPIRB location would also be transmitted. This SEPIRB drift information would be particularly useful in the event that personnel have evacuated the submarine and are adrift in the ocean (perhaps in a SEIE raft). As this study has demonstrated, the drift behavior of a SEPIRB is similar to an SLDMB and moves with the local surface current field.

The SLDMBs were used to measure the near-surface current field in the vicinity of each drift target deployment. The SLDMBs generally performed reliably, though there were some sporadic issues with both the time stamp and the position accuracy in several of the data sets.

These errors could be resolved through the time-series analysis and filtering routines performed on the SLDMB position and trajectory data. For most of the drifts, SLDMBs were deployed approximately 5 km to the east, west, north, and south of the drift target deployment location. Despite the relative close proximity of the SLDMBs, they sometimes behaved (or moved) quite differently from one another during the course of a drift. It is assumed that this was a result of spatial variability in the surface current field, so all adjacent SLDMB data were used to compute indirect surface current estimates. There was no indication that the cause of the observed differences in SLDMB motion may have been due to problems (e.g., failure of the panels, etc.) or inconsistencies with the SLDMBs.

Estimating the drift target current field to calculate the indirect leeway coefficients was the most challenging aspect of this study. A statistical interpolation technique was adopted by SAIC to estimate the surface current field. Initially, all of the SLDMB data were examined collectively to decompose the current signal into low-pass (days), band-pass (10 to 24 hours), and high-pass (1 to 10 hours) motions. After these frequency components of SLDMB motion were determined, data from each SLDMB were combined to create a spatially uniform average surface current within each of the bands over the duration of the study. This spatial average formed the basis for the spatially-varying current field estimate for each of the drift targets calculated by the SI method.

Spatial correlation functions were then generated for each frequency band as a function of separation distance between each pair of SLDMBs deployed during the study. Ultimately, the current field measurements for a drift target at any point in time were based on the computed spatial average that was adjusted based on the measured variances associated with the low-pass, band-pass, and high-pass contribution from each of the applicable SLDMBs. An estimate of the SLDMB variance was based on the difference between the observed SLDMB motion and the spatial average vector at each time step in each of the three frequency bands. This difference from the spatial mean motion in each frequency band was then multiplied by the magnitude of the correlation function at the computed distance between each SLDMB and the drift target. The magnitudes of the low-pass and band-pass correlation functions were generally larger at a given separation distance, so these frequencies were typically the major contributors to the current field estimate. Based on the correlation functions, as the distance between the drift target and each SLDMB increased past 10 km, the potential magnitude of the variance adjustment associated with that SLDMB became quite small.

Estimates of the indirect surface current field could be improved by the increased use of SLDMBs (or other surface current data source). During most of this study, SLDMBs were initially deployed in a 5 km grid around the drift target deployment area. The SLDMBs and the drift targets often moved in much different ways, and over longer time periods (more than a day) the SLDMBs may have remained clustered in close proximity to one another, but increasingly far away from the drift targets. In these cases, the computed spatial average based on the SLDMBs was likely not reflective of the surface waters around the drift target, and without any SLDMBs in the vicinity (within 10 km) of the drift targets there was limited recovery of the variance through application of the SI spatial correlation functions. One possible way to improve the indirect surface current estimate would be to establish four near-surface current meter moorings in a grid spaced at perhaps 50 km around the primary deployment area. This longer-term and more spatially spread surface current data would greatly improve the

applicability of the spatial average over the entire deployment area. SLDMBs would still be deployed in the vicinity of the drift targets to measure the near-field variances in the surface currents.

## **6.0 RECOMMENDATIONS**

The leeway coefficients developed from this study are recommended for incorporation by the U.S. Navy into its search planning tools for recovering the crew of a disabled submarine on the ocean floor. This same information should also be incorporated by the CG into its current and next generation tools for search planning. Because forcing and leeway should go to zero along with the wind speed, use of the constrained slopes is recommended for leeway drift calculations. Based on observed relationships between the wind and concurrent drifter motions during this study, the non-zero intercepts calculated by the unconstrained linear regression appear to result from motions of the sea surface of drift targets that were not correlated with the wind. The constrained regressions using only data corresponding to wind speeds greater than 7 m/s would then appear to provide the best estimate for search planning use.

## 7.0 REFERENCES

- Allen, A.A. and J.V. Plourde, 1999. Review of Leeway; Experiments and Implementation. U.S. Department of Transportation, U.S. Coast Guard, CD-D-08-99, Washington D.C.
- Bretherton, F. P., R. E. Davis, C. B. Fandry, 1976. A technique for objective analysis and design of oceanographic experiments applied to MODE-73. *Deep-Sea Research*, vol. 23, pp 559-582.
- Department of National Defence (DND) and Canadian Coast Guard (CCG), 1985. National Search and Rescue Manual. Department of National Defence and Canadian Coast Guard, B-GA-209-001/FB-001, Ottawa.
- Emery, W.J., Thomson, R.E., 2004. *Data Analysis Methods in Physical Oceanography*. Pergammon Press, Oxford.
- Fitzgerald, R. B., D.J. Finlayson, J.F. Cross, A. Allen, 1993. Drift of Common Search and Rescue Objects – Phase II. Publication prepared for Transportation Development Centre, Transport Canada, Montreal, TP# 11673E.
- Fitzgerald, R., D.J. Finlayson, and A. Allen, 1994. Drift of Common Search and Rescue Objects – Phase III. Publication prepared for the Canadian Coast Guard. Transport Canada, Pub. No. TP 12179, Ottawa.
- National Defense/Fisheries and Oceans Canada/Coast Guard (DFO), 1998. National Search and Rescue Manual, B-GA-209-001, DFO 5449.
- National Search and Rescue Committee, 2000. United States National Search and Rescue Supplement to the International Aeronautical and Maritime Search and Rescue Manual. Washington, D.C.
- SAIC, 2005. Leeway Testing and Analysis Project Study Plan, October 2005. Prepared for the U.S. Coast Guard Research and Development Center.
- Smith, S.D., 1988. Coefficients for the sea surface stress, heat flux, and wind profiles as a function of wind speed and temperature. *J. Geo. Res.*, 93, C12, pp 15467-15472.

(This page intentionally left blank.)

## **Appendix A – Supporting Drift Target Results**

Results are grouped first by target configuration, then by Drift.

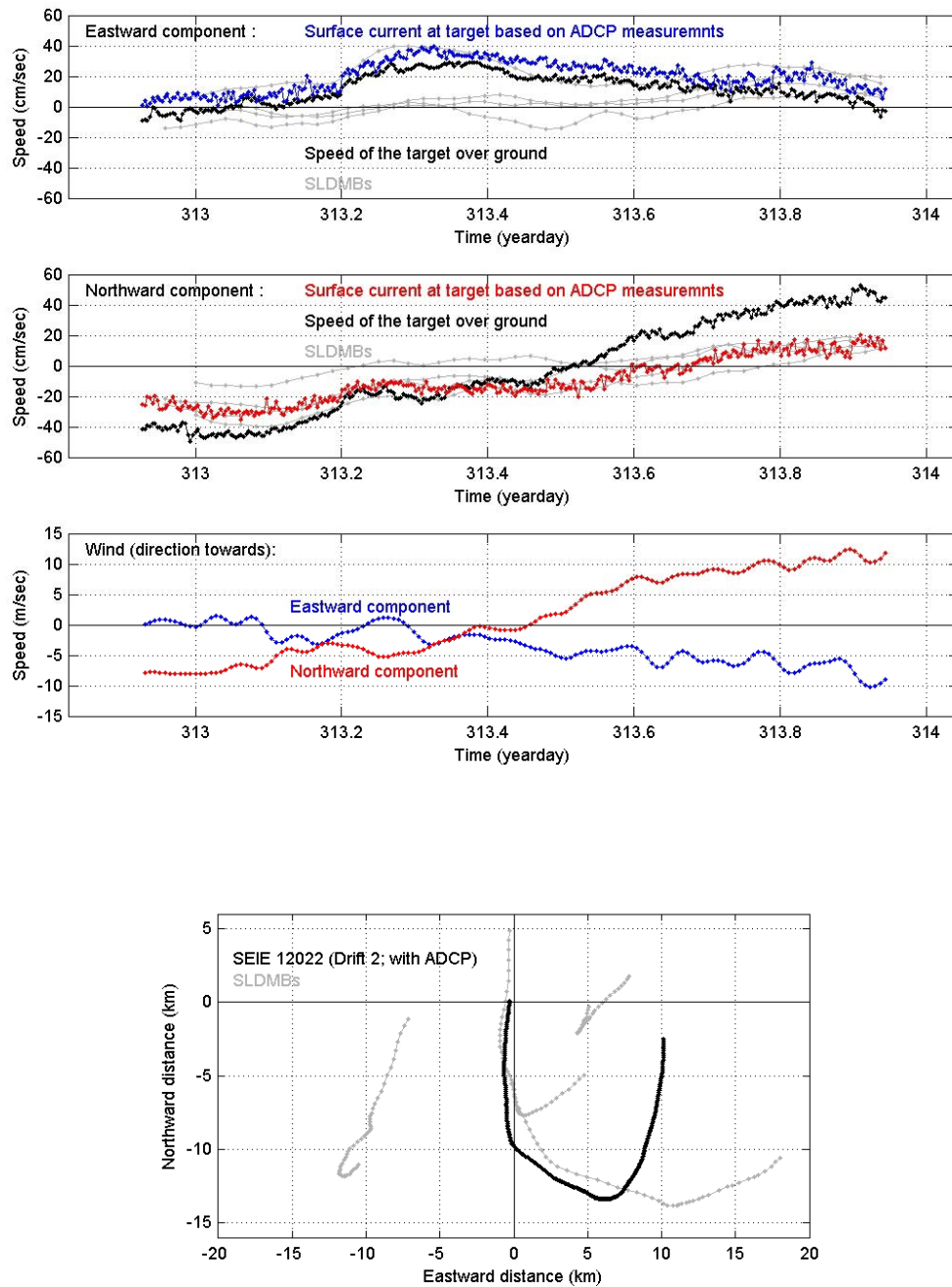


Figure A-1. Time-series vector plot of the movement of the drogued SEIE raft over the ground and also the computed direct current field during Drift Two.



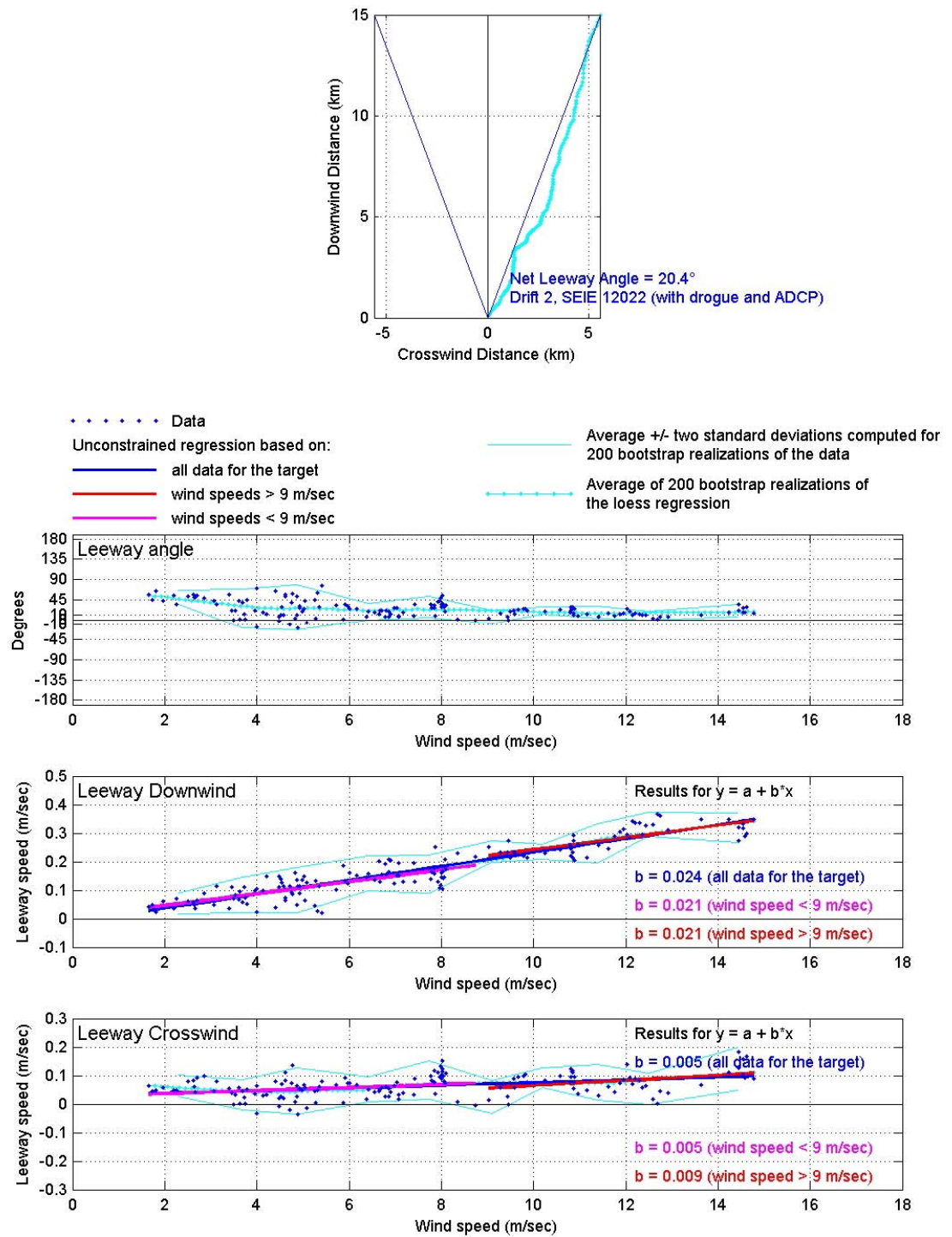


Figure A-2. Progressive vector diagrams and constrained and unconstrained downwind and crosswind (positive and negative) leeway components computed for the drogued raft from Drift Two.

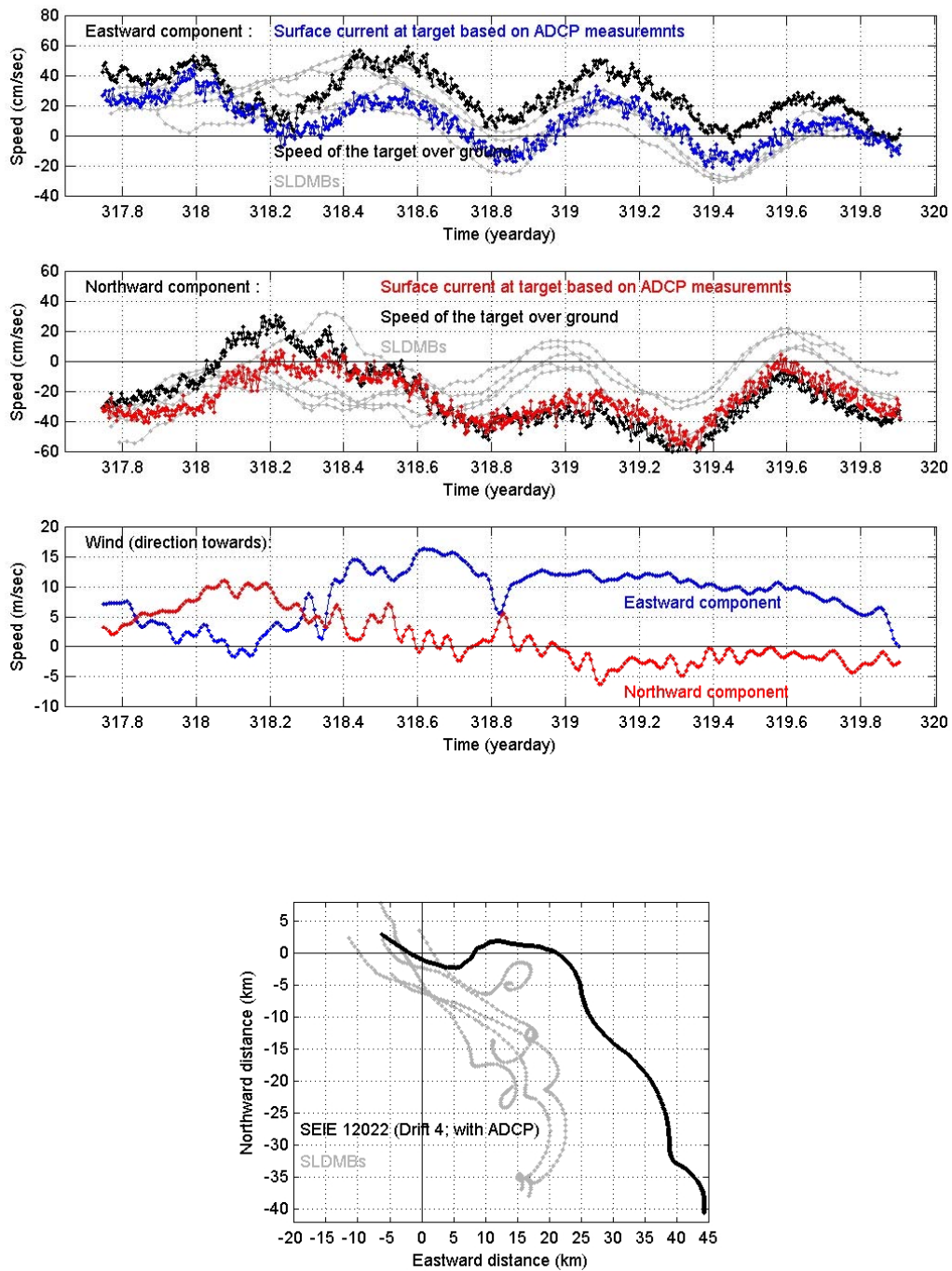


Figure A-3. Time-series vector plot of the movement of the drogued SEIE raft over the ground and also the computed direct current field during Drift Four.

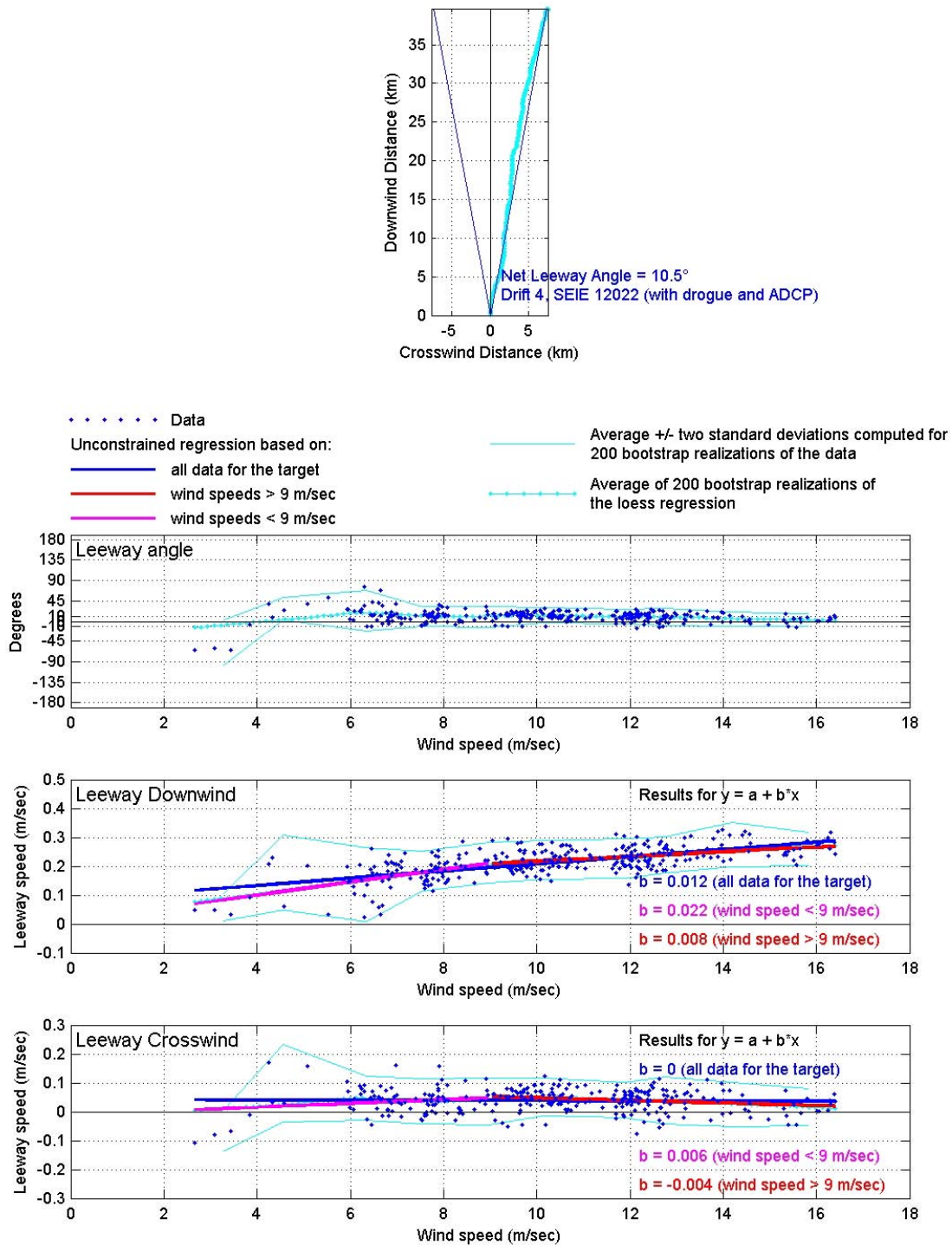


Figure A-4. Progressive vector diagrams and constrained and unconstrained downwind and crosswind (positive and negative) leeway components computed for the drogued raft from Drift Four.

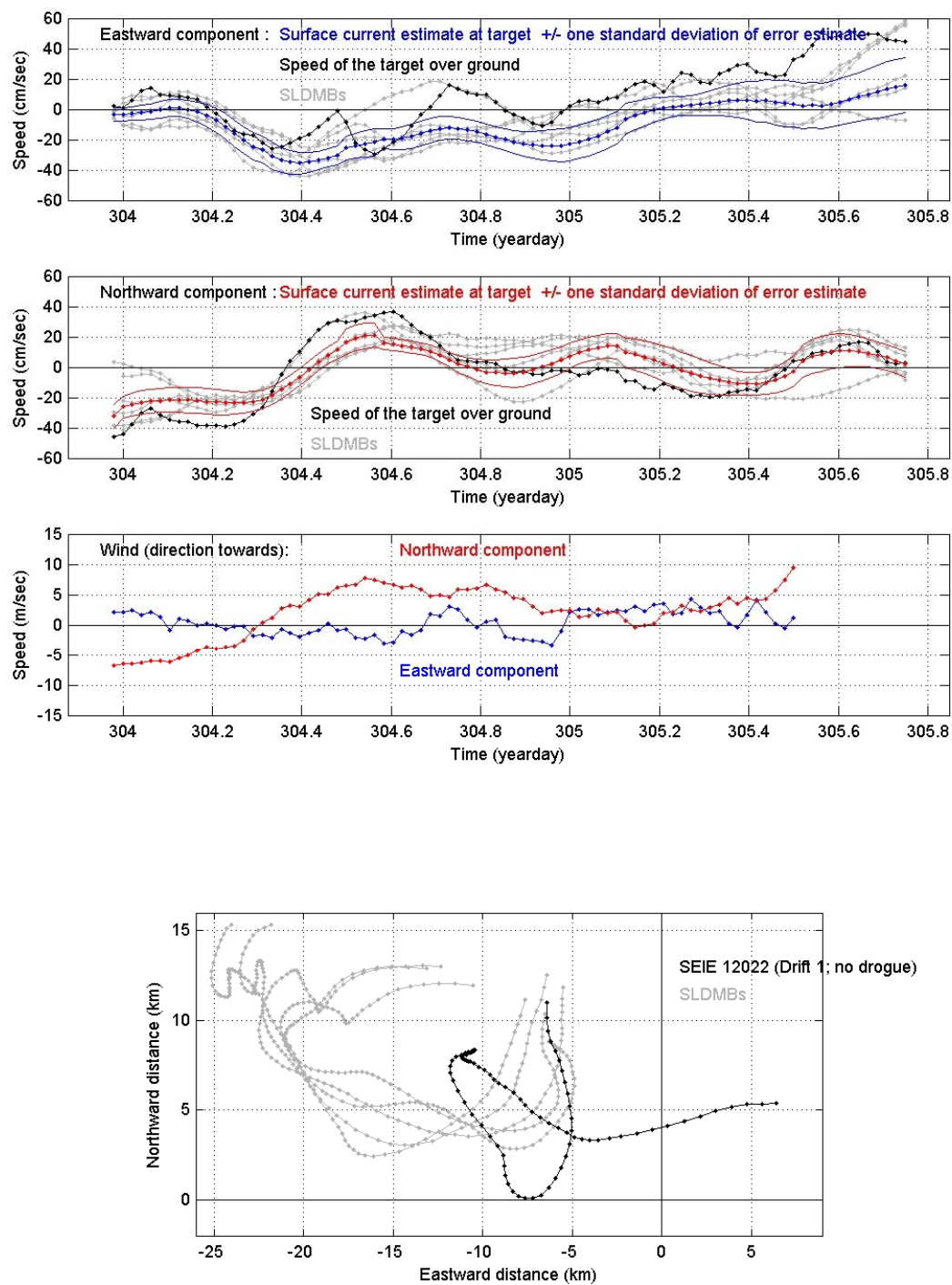


Figure A-5. Time-series vector plot of the movement of the undrogued SEIE raft over the ground and also the computed indirect current field during Drift One.



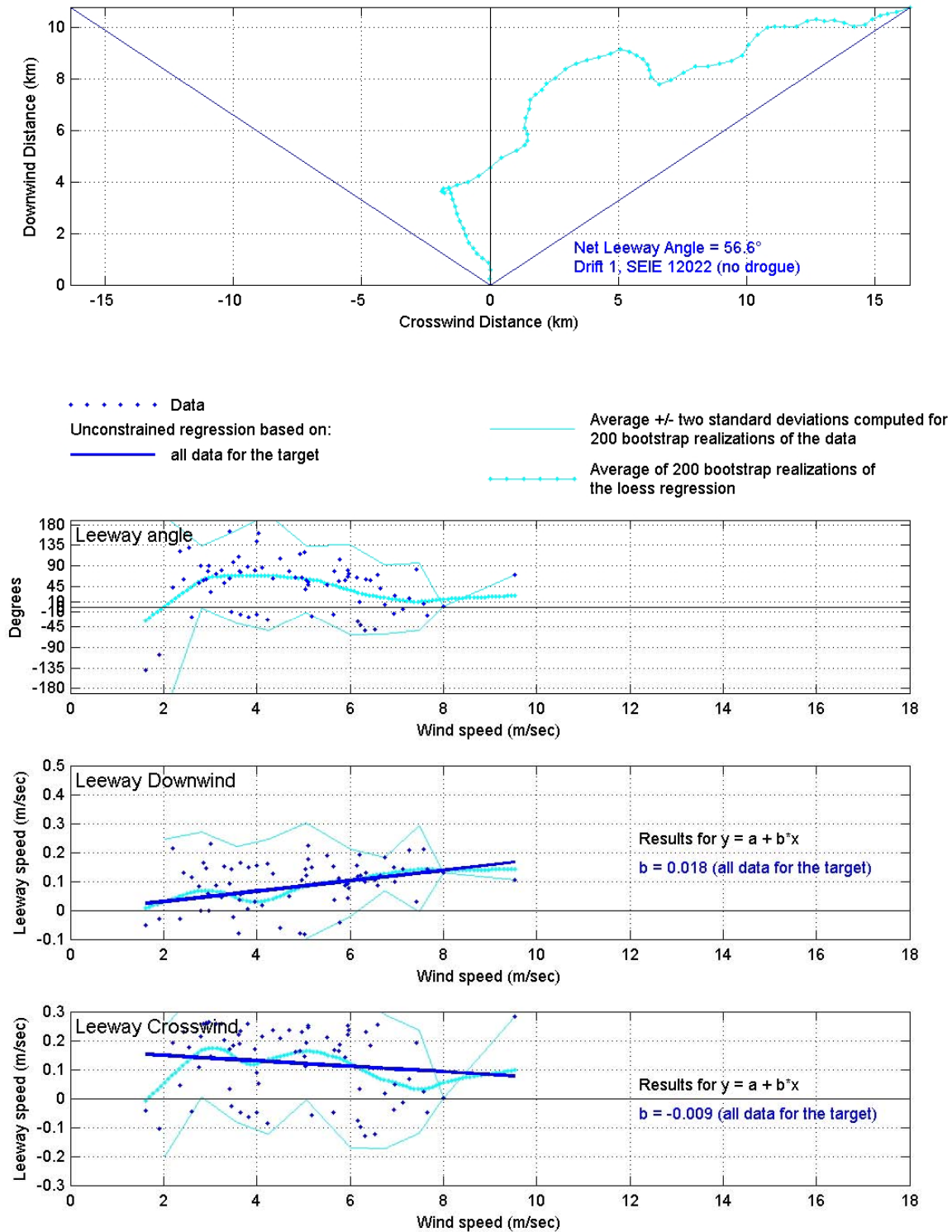


Figure A-6. Progressive vector diagrams and constrained and unconstrained downwind and crosswind (positive and negative) leeway components computed for the undrogued raft from Drift One.

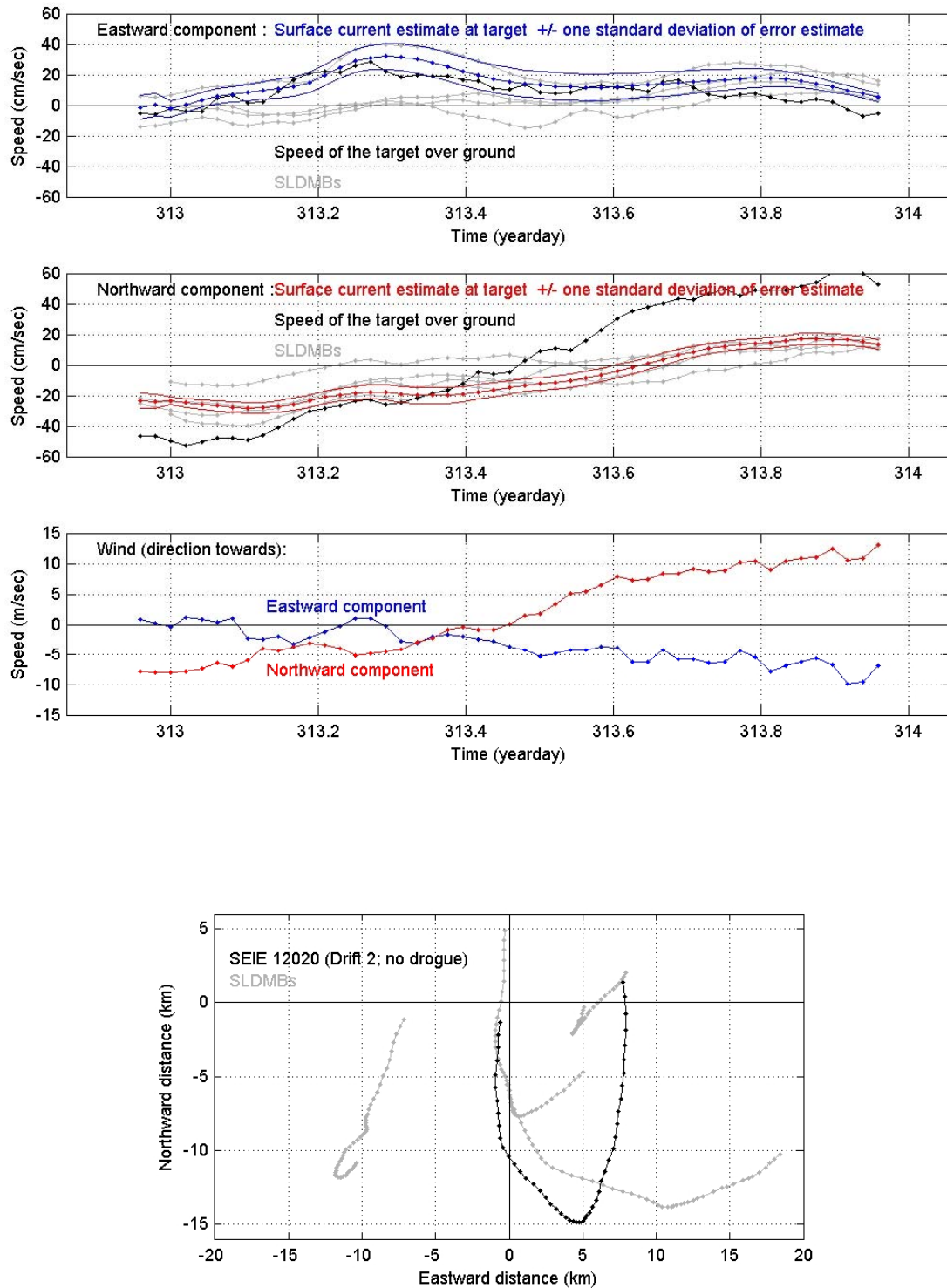


Figure A-7. Time-series vector plot of the movement of the undrogued SEIE raft over the ground and also the computed indirect current field during Drift Two.

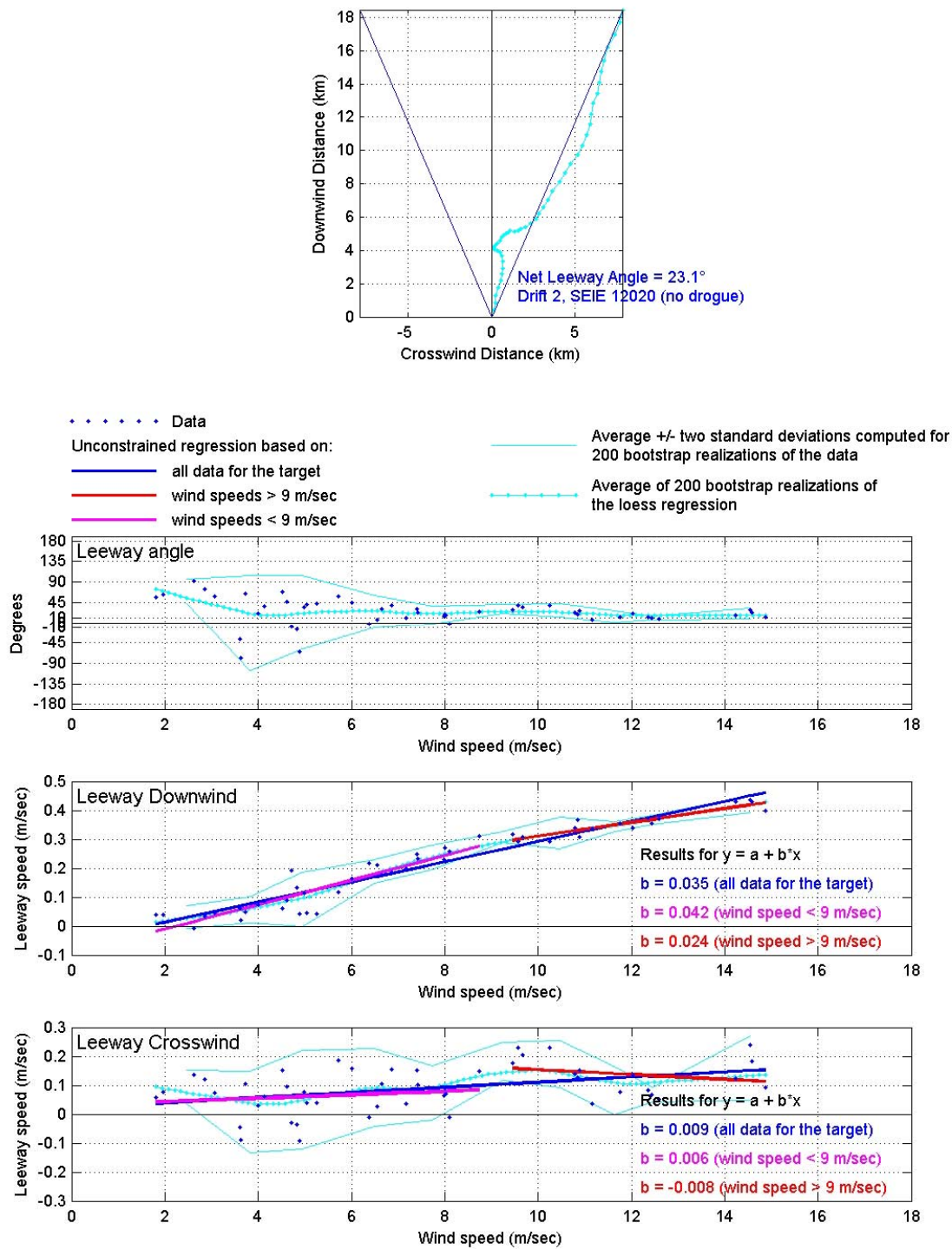


Figure A-8. Progressive vector diagrams and constrained and unconstrained downwind and crosswind (positive and negative) leeway components computed for the undrogued raft from Drift Two.

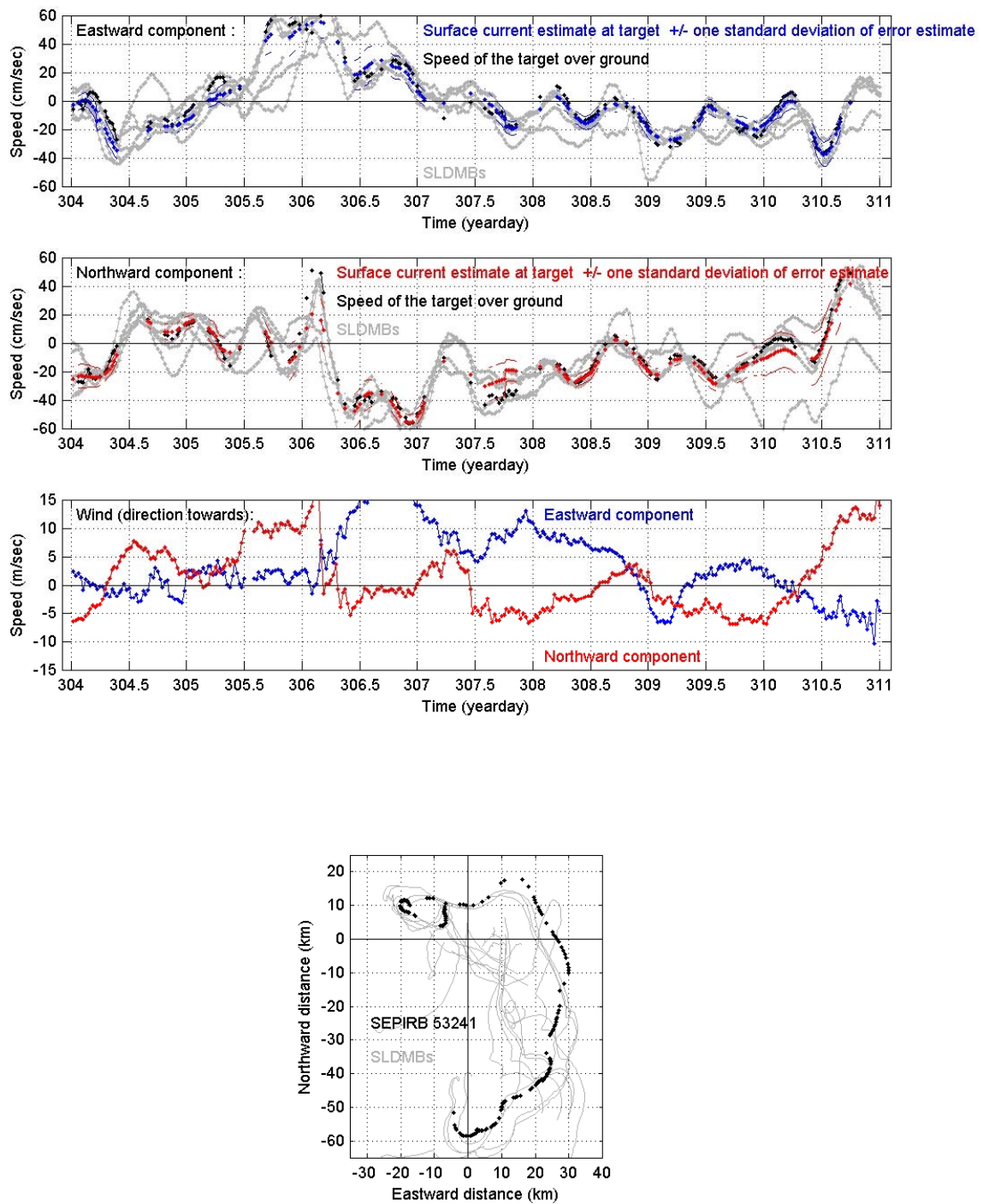


Figure A-9. Time-series vector plot of the movement of SEPIRB 53241 over the ground and also the computed indirect current field during the course of the drift from 31 October through 15 November.



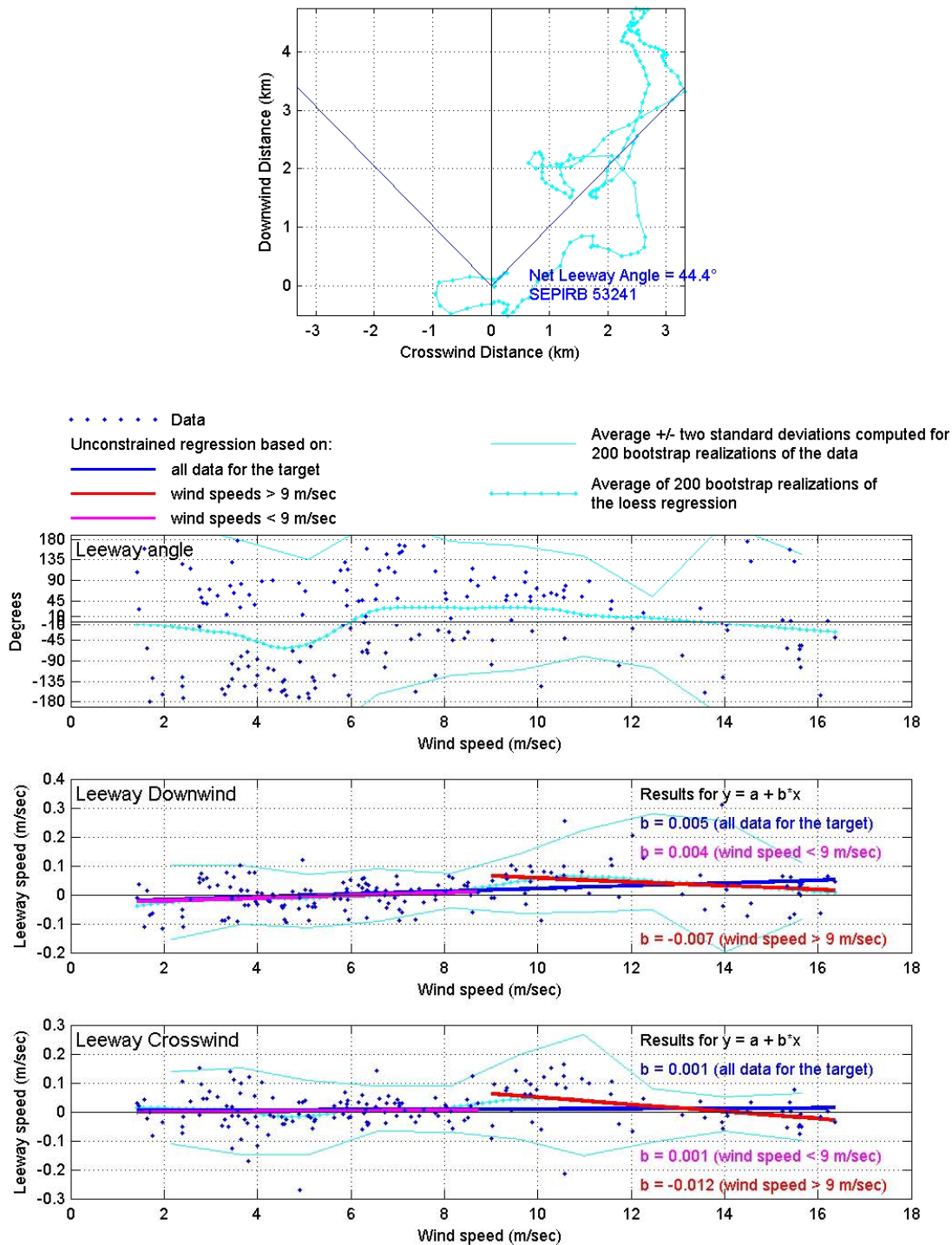


Figure A-10. Progressive vector diagrams and constrained and unconstrained downwind and crosswind (positive and negative) leeway components computed for SEPIRB 53241.

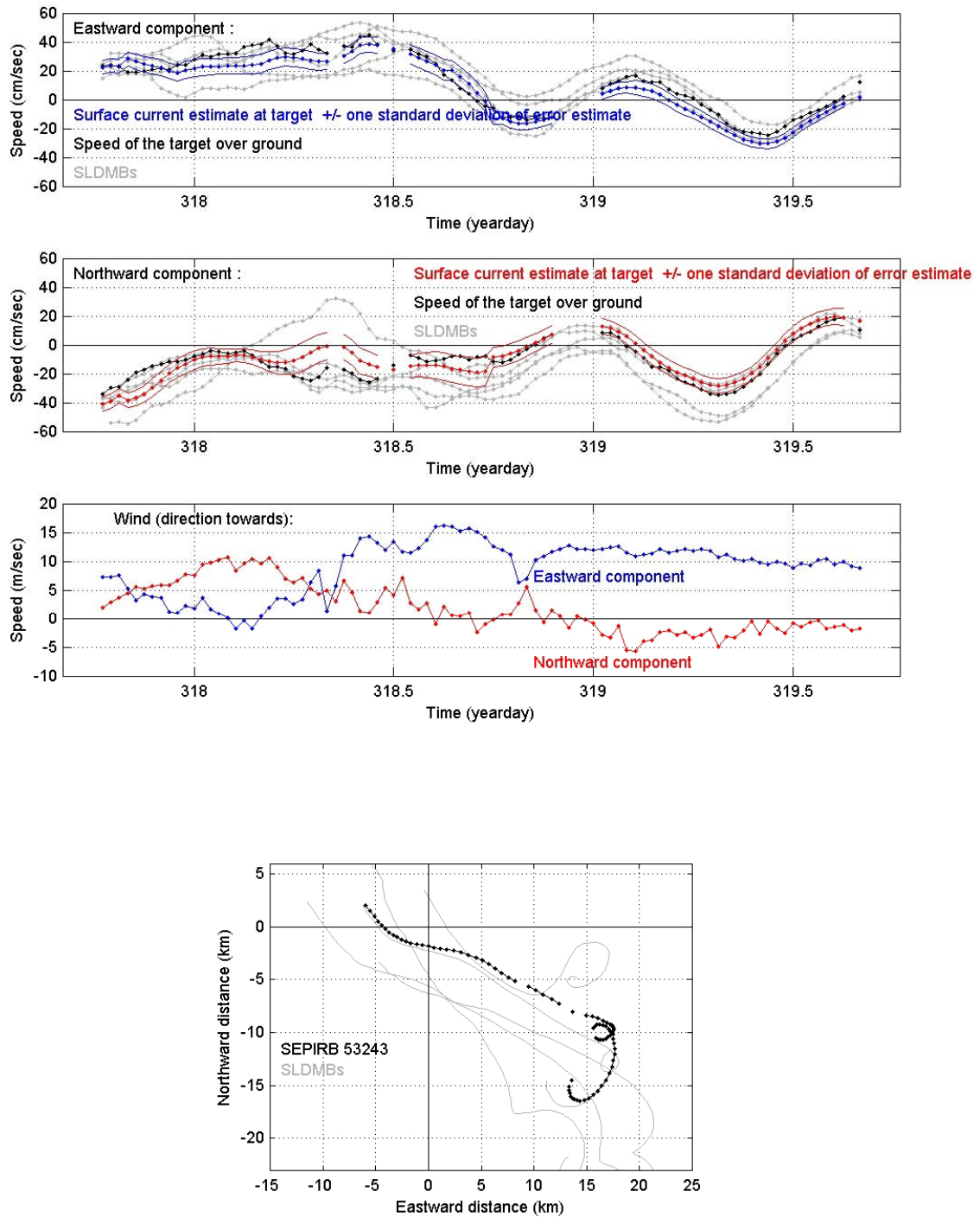


Figure A-11. Time-series vector plot of the movement of SEPIRB 53243 over the ground and also the computed indirect current field during the course of the drift from 14 November through 16 November.

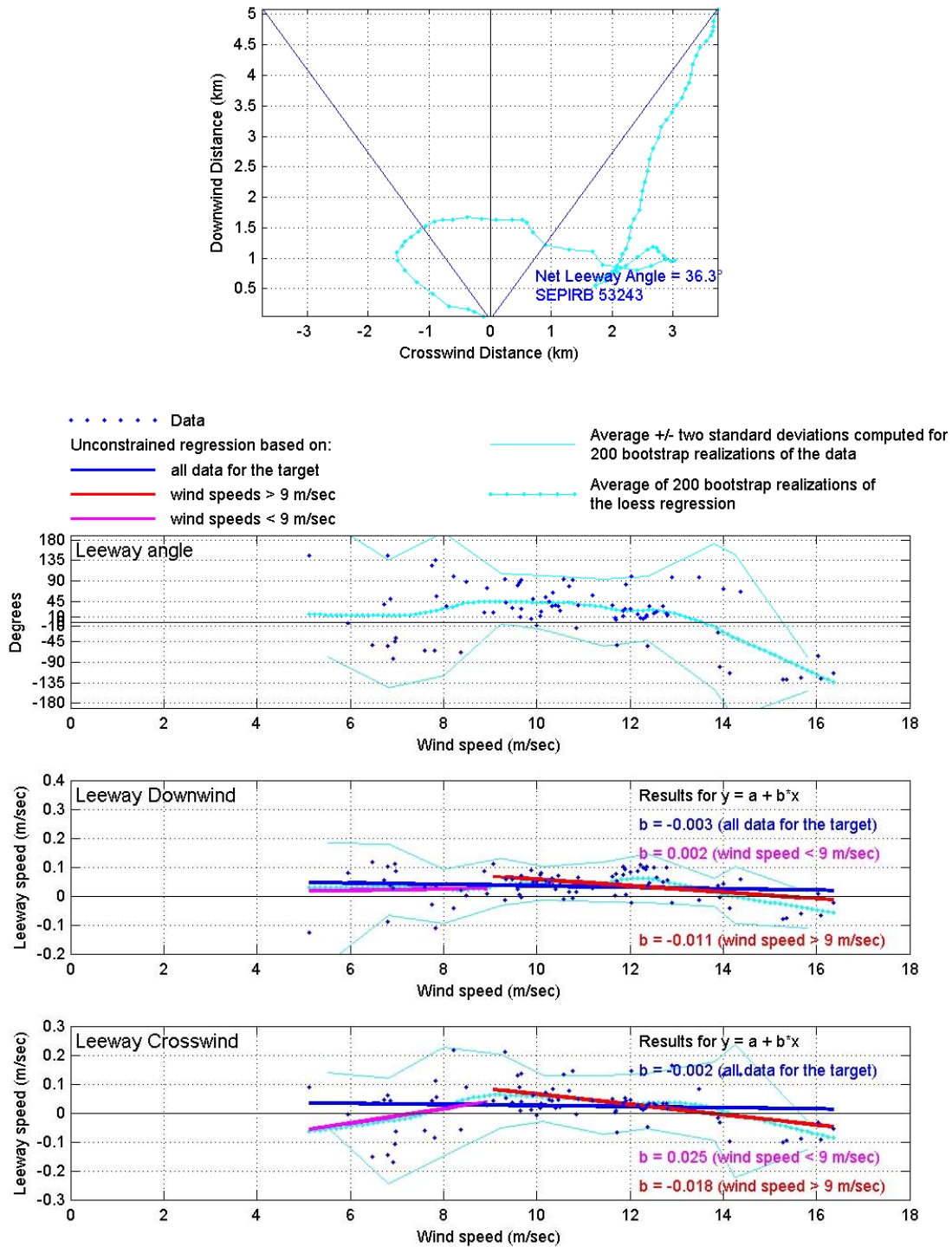


Figure A-12. Progressive vector diagrams and constrained and unconstrained downwind and crosswind (positive and negative) leeway components computed for SEPIRB 53243.